# SOFT X-RAYS FROM THE LARGE MAGELLANIC CLOUD AND THE GALAXY - IMPLICATIONS ON THE ORIGIN OF THE DIFFUSE X-RAY BACKGROUND

Thesis by

Knox Stedman Long, Jr.

In Partial Fulfillment of the Requirements

for the Degree of

Doctor of Philosophy

California Institute of Technology

Pasadena, California

1975

(Submitted October 1, 1975)

# ACKNOWLEDGEMENTS

Without the help of many individuals this dissertation would not have been written. In Australia, the Sounding Rocket Division of Goddard Space Flight Center, in particular D. Shrewsberry, T. Budney, R. Drury and M. Windsor, ensured the successful launches of the payload. Range support at Woomera was provided by the Weapons Research Establishment of the Australian Government. Under adverse conditions, T. C. Vu maintained the experiment electronics. At Caltech, fellow graduate students F. Cordova and W. Priedhorsky served above and beyond during window fabrication and pre-flight calibrations. Additional technical support was supplied by J. Coulson and A. Barclay. My special thanks go to W. E. Moore for his practical pre-flight advice and aid as well as for many post-flight discussions both here at Caltech and at the University of Cambridge, where we enjoyed the hospitality of the Institute of Astronomy. Finally, I would like to thank G. Garmire who has provided insight and advice at every stage while still permitting an inexperienced graduate student to make most of his own decisions.

This research has been supported in part by NASA grants NGR 05-002-284 and NGL 05-002-207. I would also like to acknowledge the support of a NDEA fellowship during my first three years as a graduate student.

# ABSTRACT

Observations of Southern Hemisphere X-ray sources are reported, obtained on two attitude-controlled sounding rocket experiments launched from Woomera, Australia on 1 and 8 November 1973. The X-ray luminosity of the Large Magellanic Cloud was observed to be $10^{38}$ ergs $s^{-1}$ between 0.4 and 1.5 keV. An upper limit on the extragalactic diffuse X-ray flux of 250 photons $(cm^2\ s\ keV\ sr)^{-1}$ at 0.215 keV was derived, based on the lack of modulation of soft X-rays by neutral interstellar matter in the direction of the Large Magellanic Cloud. Spectra of three extended soft X-ray regions are reported. Two of the regions, in Eridanus and in Gemini-Monoceros, are of Galactic origin. The third lies in a direction of very low neutral hydrogen column density and hence its spatial origin cannot be unambiguously established. The volume emissivity required in Galactic enhanced regions, which are interpreted as plasmas with temperatures of several million degrees, does not differ greatly from what is required to generate the soft X-ray background. An anomalously high X-ray flux between 0.4 and 1.5 keV was observed in the direction of Cen X-3 in the 5° x 10° detector on both flights 1 and 2. However, this emission does not originate from Cen X-3 as reported by Bleeker _et al_. (1973) or from $\eta$ Car as suggested by Hill _et al_. (1972). A possible energy dependence in the pulsed flux fraction from Cen X-3 is discussed.

# TABLE OF CONTENTS

# FOREWORD

This dissertation consists of results obtained on two X-ray sounding rocket experiments which took place in November 1973 from Woomera, Australia. In many ways, the data obtained did not reflect our pre-flight hopes, particularly in terms of the actual surface brightness of the sources which we selected to observe. Nevertheless, we have used these data to arrive at a number of conclusions which were not previously known and which we feel are useful:

(1) Between 0.4 and 1.5 keV, the X-ray luminosity of the Large Magellanic Cloud is $\sim 10^{38}$ erg $s^{-1}$. The X-ray spectrum of the LMC at these energies is consistent with an extrapolation of the spectrum observed above 1.5 keV.

(2) The observed X-ray flux between 0.15 and 0.28 keV in the direction of the LMC exhibits little or no modulation by cool interstellar matter in the LMC and the Galaxy. Based on a simple model, we conclude that no more than 9% of the observed flux is extragalactic in origin. This corresponds to an upper limit to the extragalactic flux incident on the Galaxy of 250 photons $(cm^2\ s\ keV\ sr)^{-1}$ at 0.215 keV. This limit is the strongest upper limit derived thus far based on modulation by interstellar matter.

(3) We report the first spectra of two soft X-ray enhancements in the Southern hemisphere, as well as confirm the spectrum of another enhancement in Gemini-Monoceros. The spectra of the three enhancements are found to be similar, consistent with emission from plasmas with

temperatures of several million degrees, exhibiting little or no absorption due to neutral hydrogen.

(4) Cen X-3 is not, as previously reported, a strong soft X-ray source. On the other hand, a soft X-ray source does, we feel, exist nearby whose spectrum peaks near 0.7 keV. Grain scattering cannot account for apparent decrease in the pulsed fraction of Cen X-3 near 2 keV.

# CHAPTER I

# THE SOFT X-RAY BACKGROUND PROBLEM

## I. Introduction

Above 2 keV, the diffuse X-ray sky has been found to be remarkably isotropic. Even a Galactic plane bulge has been 90% accounted for by known sources (Cooke and Pounds 1971). Since Galactic absorption above 2 keV is small, the observed isotropy implies an extragalactic or extended spherical halo origin for the high energy isotropic flux.

At 0.25 keV, however, the diffuse X-ray sky exhibits considerable anisotropy. Unidentified sources account for the bulk of the observed flux, which exceeds an extrapolation of the observed power law above 2 keV by a factor of 3 to 7. The fundamental nature and origin of the 0.25 keV flux remains today an unanswered question. The experiments described in this thesis do not answer the question, but they place strong limits on the total amount of the flux which can be of extra-galactic origin (Chapter 3). In addition, the X-ray properties of several intensified background regions are described and interpreted in terms of emission from a diffuse hot plasma (Chapter 4). Soft X-ray emission from our nearest neighbor galaxy, the Large Magellanic Cloud, is analyzed (Chapter 2). Finally, the possibility of soft X-ray emission from a well-known hard X-ray source, Cen X-3, is ruled out, contrary to observations of Bleeker *et al*. (1973). An alternative suggestion that a new region of diffuse soft X-ray emission has been located is advanced (Chapter 5).

## II. Determination of the Extragalactic 0.25 keV Flux

At 0.25 keV, absorption effects due to cool interstellar gas are substantial. Hence anisotropy at low energies is expected. If the 0.25 keV flux were extragalactic in origin the observed flux should be greatest near the poles and vanishing near the Galactic equator. Original observations seemed to confirm this model, revealing a strong North Polar excess. Bowyer *et al*. (1968) concluded that the soft X-ray background was simply due to an extension of the extragalactic power law ($\alpha = 1.8$) modulated by neutral gas. However, this first picture proved to be a considerable oversimplification.

Observations by Henry *et al*. (1968) clearly indicated the presence of a substantial flux of 0.25 keV X-rays at the Galactic equator. Bowyer *et al*. had reported that in order to explain the latitude modulation which they observed, the cross section of the interstellar matter must be approximately half the theoretical value, a result which was later interpreted in terms of cloud clumping (Bowyer and Field 1969). However, clumping in the plane is simply not a viable explanation since optical depths at 0.25 keV in the plane of the Galaxy are of order 100. The existence of a plane flux, now well verified, implies a galactic source of emission.

The observed flux at the North Galactic Pole was found by Henry *et al*. to be 600 ± 40 photons $(cm^2\ s\ keV\ sr)^{-1}$ at 0.25 keV. Even when no hydrogen absorption is included, this flux represents an enhancement by a factor of approximately 7 over an extrapolation of the diffuse power law spectrum observed at higher X-ray energies. Fluxes reported by other observers (see Silk 1973), though typically 200-300 photons $(cm^2\ s\ keV\ sr)^{-1}$, consistently have indicated a low energy excess. If the North Polar flux were of extragalactic origin, a total extragalactic flux of 500-800 photons $(cm^2\ s\ keV\ sr)^{-1}$ would be required, assuming theoretical cross sections.

Verification of a low energy excess of extragalactic origin would have important cosmological implications. A hot $10^6$ °K plasma with sufficient density to gravitationally bind the Universe would be largely invisible in other energy bands but would produce approximately the observed 0.25 keV flux (Field and Henry 1964, Field 1972). However, verification of extragalactic origin is difficult because the Galactic contribution to the North Polar flux is not known.

The observational situation today is far from clear. Studies by various groups are difficult to compare, and no group has yet mapped the entire sky,although in the Northern Galactic Hemisphere the basic (10°) features of the sky brightness distribution at 0.25 keV seem agreed upon.

The survey of Davidsen et al. (1972), from a spinning rocket experiment, is a good example of available sky maps (Figure 1.1). The North Polar cap is clearly visible. Apparently the 0.25 keV flux increases away from the plane, consistent with the hypothesis

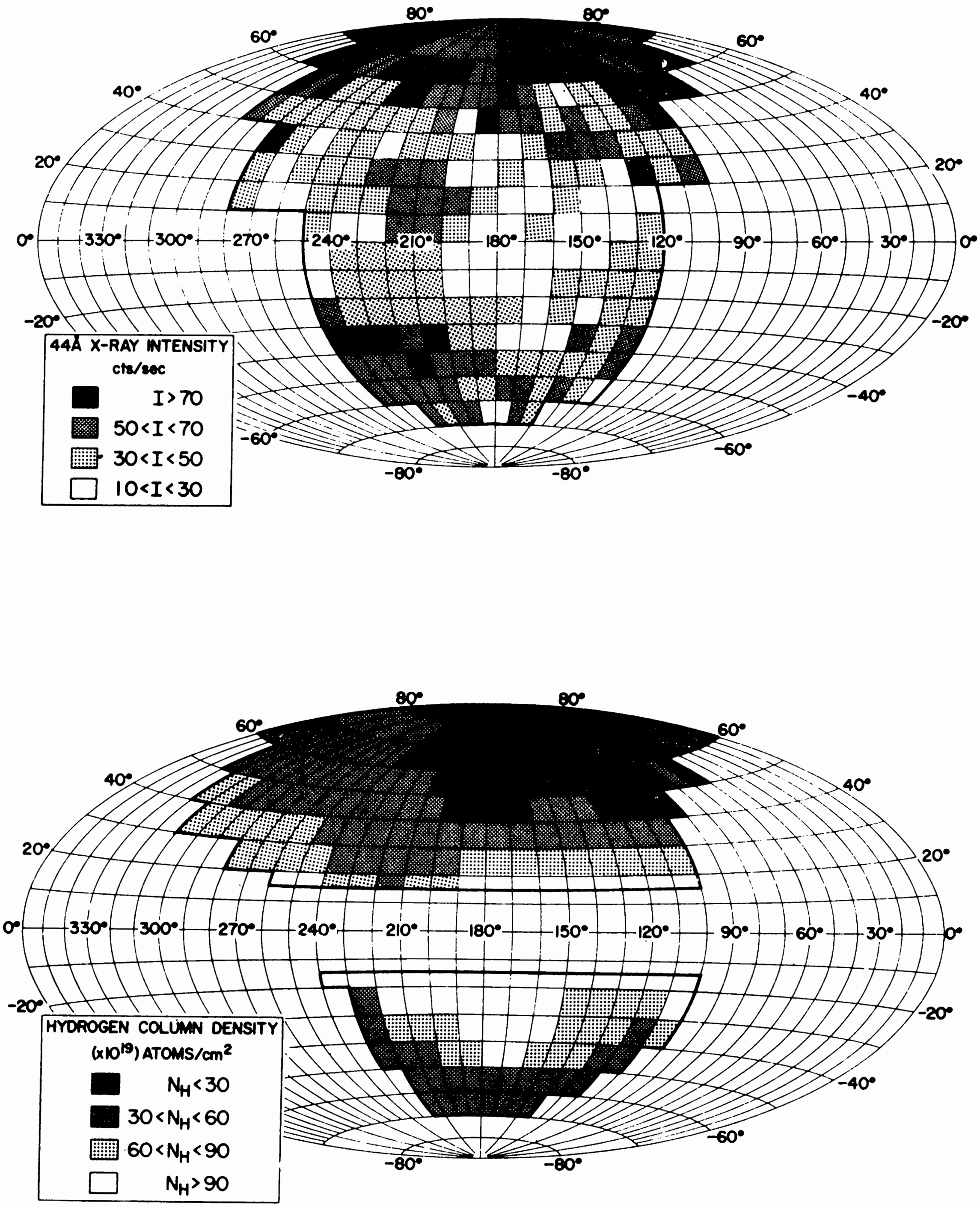


Figure 1.1

This map of the 0.25 keV X-ray background, taken from Davidsen et al. (1972), shows that X-ray intensity correlates only in a gross sense with the total hydrogen column density. The North Polar cap is clearly evident. Both maps are in New Galactic coordinates.

that much of the flux is extragalactic, although the lack of detailed correspondence with the hydrogen column density as well as the observed plane flux shows the importance of Galactic emission.

Davidsen et al. attacked the pivotal problem of separation of the extragalactic and the Galactic flux phenomenologically. They assumed that Galactic emissivity is proportional to the hydrogen density. In this case the intensity along a given line of sight is given by

$$I = I_{EX} \exp(-\sigma N_H) + I_G(1 - \exp(-\sigma N_H)) \qquad (1.1)$$

where $I_{EX}$ and $I_G$ are the extragalactic and local fluxes respectively, $\sigma$ is the effective cross-section and $N_H$ is the hydrogen column density. $I_{EX}$, $I_G$ and $\sigma$ were regarded as free parameters. Although there is considerable scatter in the data points from best fit values, presumably due to the patchy nature of emission, the general shape of the average latitude dependence of the radiation in the 0.28 and 0.68 keV windows corresponds moderately well to their model. Excessive clumping of the gas is not needed as the theoretical cross section falls within the acceptable range of cross sections. The ratio of $I_{EX}/I_G$ is approximately 4.

The fundamental criticism which can be made of all studies of a type similar to Davidsen et al. is that coverage of the sky is not even, and that the model is basically constrained by the excess of the North Polar flux over the plane flux. If the North Polar flux were strongly contaminated by a local source, then arguments about the extragalactic excess are in serious jeopardy. There are two considerations which make this likely:

(1) New observations by Williamson *et al*. (1974) of the South Galactic Pole region do not reveal nearly as bright a polar cap as in the North although total hydrogen column densities are similar. (A phenomenological analysis similar to that of Davidsen *et al*. would be useful but has not yet been reported.)

(2) The brightest emission regions of the Northern Galactic Hemisphere seem to correlate fairly well with an enhanced radio continuum structure, the North Polar Spur, which extends from about 10° above the plane in the direction of the Galactic Center to within 10° of the North Galactic Pole (Bunner *et al*. 1972, de Korte *et al*. 1974). Fluxes of 300 ± 150 photons $(cm^2\ s\ keV\ sr)^{-1}$ have been reported by Bunner *et al*. and are approximately the same order of magnitude as the total pole flux measured by Davidsen *et al*.

A much better understanding of the extragalactic flux seems to require an understanding of Galactic emission mechanisms which produce enhancements which are on the order of brightness of the Polar enhancement itself. Observations are, however, dominated by negative rather than positive results.

## III. A Point Source Origin for Galactic Emission?

Strong limitations on the possibility that discrete point sources create the diffuse X-ray background come from two sources--the observed small scale homogeneity of the diffuse X-ray background and direct observations of candidate stellar populations.

Gorenstein and Tucker (1972) analyzed 0.25 keV X-ray data from the Virgo region using a one-dimensional focusing collector with a total solid angle of 4.5 square degrees. Based on a rms variation of 14% in the observed counting rate and an assumed exponential scale height for the source population, they deduced that the density of the source population in the Galactic plane is less than 1 $pc^{-3}$ and greater than or approximately equal to $10^{-2}$ $pc^{-3}$. The upper limit to the density of sources is not of interest since it exceeds the density of all known stellar systems. Although neglect of the beam shape compromises the lower limit somewhat, the lack of observed granularity is strong evidence that only the densest stellar populations can account for the observed X-ray background.

Vanderhill *et al*. (1975) reported upper limits on the soft X-ray flux (typically 0.6 photons $(cm^2\ s\ keV)^{-1}$ at 0.26 keV) from about 50 stars and concluded that the soft X-ray background was unlikely to be a product of X-ray emission from most types of stars including main sequence stars, giants or dwarfs. However, they note that densities of white dwarfs and M-dwarfs are uncertain and that if densities of these types of stars were as large as the Gorenstein and Tucker lower limit, such stars would not be ruled out by the Vanderhill *et al*. observation. Positive detections of some stars, notably dwarf novae, have been reported (Henry *et al*. 1975, Catura *et al*.

1975); however, stellar densities and observed fluxes of these stars are inconsistent with their being the source of the diffuse X-ray background.

## IV. Hot Plasma Theories

Emission from a diffuse hot plasma is an obvious and attractive alternative to discrete sources, although at non-X-ray wavelengths such a plasma is extremely difficult to study. The reason for a hot plasma's near invisibility is the fact that the emission measure required to produce the observed flux between 0.18 and 0.28 keV of approximately $10^{-8}$ ergs $(cm^2\ s\ sr)^{-1}$ is only $2 \times 10^{-3}\ cm^{-6}$ pc, assuming an emissivity of $2 \times 10^{-23}\ n_e^2 (cm^{-3})$ ergs $(cm^3\ s)^{-1}$ (Tucker and Koren 1971). For comparison, faint H II regions on the Palomar Sky Survey have emission measures of approximately $10\ cm^{-6}$ pc.

The distance corresponding to approximately 1 optical depth at 0.25 keV, approximately 200 pc, and the emission measure imply that $\langle n_e^2 \rangle$ approximately equals $10^{-5}\ cm^{-6}$ and that the average volume emissivity is approximately $3 \times 10^{-28}$ ergs $(cm^3\ s)^{-1}$. Thus $\langle n_e \rangle \sim 3 \times 10^{-3}\ cm^{-3}$ if clumping is small. If the fraction of space occupied by hot gas is near one, rough pressure equilibrium would be maintained between the hot gas and other components of the ISM. The cooling time for the plasma is given by

$$t_c \simeq \frac{3kT}{n_e \Lambda} \simeq 2.7 \times 10^5 \frac{T_6}{n_e} \left( \frac{5 \times 10^{-23}\ erg\ s^{-1}\ cm^3}{\Lambda} \right) \text{years} \quad (1.2)$$

where $\Lambda$ is the radiative cooling coefficient. Thus the upper limit on the cooling time is less than $10^8$ years. To maintain the hypothesized plasma, energy must be resupplied on shorter time scales. The average volume emissivity, a Galactic radius of 15 kpc, and an emission region 400 pc thick (or an exponential scale height of 200 pc) imply that the total Galactic luminosity between 0.18 and 0.28 keV is approximately $2 \times 10^{39}$ erg $s^{-1}$, a result which is of course not at all dependent on having a plasma model.

Proposed mechanisms for heating the gas often involve supernova remnants simply because the energy requirements seem easily satisfied and supernova remnants are known to be bright soft X-ray sources which contain hot plasmas. The emission rate of $3 \times 10^{-28}$ ergs $(cm^3\ s)^{-1}$ requires only $3 \times 10^{48}$ ergs/event, if one supernova occurs every 50 years. $3 \times 10^{48}$ ergs is approximately 1% of the blast wave energy determined from observations of Vela or the Cygnus Loop (Moore 1975, Stevens 1973). The volume heated by $3 \times 10^{48}$ ergs, assuming pressure equilibrium and that the density of the gas is approximately $3 \times 10^{-3}$ $cm^{-3}$ is $7 \times 10^{60}$ $cm^3$ which implies a typical region of space is reheated every $5 \times 10^7$ years. The emission rate required, assuming a lifetime of $5 \times 10^7$ years for the 40 pc radius supernova bubbles, would be $5 \times 10^{33}$ ergs $s^{-1}$. Upper limits on the X-ray luminosity of all known supernova remnants (see Seward _et al_. 1975) lie comfortably above this value, although X-ray emission from known supernova remnants is probably dominated by the shock-created shell (or synchrotron emission) rather than the highly evacuated core which would produce X-ray emission in the old, large diameter remnants. On the other hand, if individual supernova remnant lifetimes are much less than $5 \times 10^6$ years the luminosity required from old supernova remnants to produce the observed 0.25 keV flux would exceed the luminosity of many observed remnants and would seem to be ruled out.

These postulated old (80 pc diameter) supernova remnants would not appear in current lists due to their low predicted surface brightness, approximately $10^{-22}$ W $m^{-2}$ $sr^{-1}$ $Hz^{-1}$ at 1 GHz, a brightness temperature of less than 10°K and the large angular size of nearby remnants (Ilovaisky and Lequeux 1972b). In the same units the sensitivity of the 3C survey at 178 MHz (Bennett 1962) was $3 \times 10^{-21}$ W $m^{-2}$ $sr^{-1}$ $Hz^{-1}$.

Cox and Smith (1974) have pointed out, however, that if the lifetime of supernova bubbles is approximately $4 \times 10^6$ years or longer, a hot network of tunnels is created due to the fact that new supernovae occurring near old bubbles will reheat the diffuse bubble region preferentially to the interstellar medium (ISM) since the shock speed is more rapid in diffuse regions. They calculate that between 14 and 50% of the ISM will be occupied by the hot tunnel regions. Such a tunnel network might explain the large scale height of Galactic X-ray emission by allowing communication with a hot Galactic corona. Cooling considerations imply that the tunnel structure would collapse if the temperature was less than $3 \times 10^5$ °K.

Qualitatively, the hot tunnel network configuration seems to explain the variations in the X-ray background as determined from the two Caltech rocket flights which are described in this dissertation. The soft diffuse X-ray background seems to be dominated by extended features, whose typical angular size is 10° or greater, exceeding the angular size of all known supernovae. In any event, known supernovae would not account for the low energy diffuse background, because the sky would appear much more anisotropic over angular scales of less than 5°.

## V. The Caltech Australian X-ray Experiments

The X-ray data described herein consisted of two X-ray sounding rocket experiments, utilizing the same payload, launched from Woomera, Australia in November, 1973. The experiment description is contained in the Appendix but basically the rocket payload consisted of a bank of four proportional counters whose gross characteristics are listed in Figure 1.2. Counters 1-3 were low energy counters, sensitive between 0.1 and 2.5 keV, while counter 4 recorded X-ray events between 1.5 and 18 keV. Flight 1 was dedicated to an observation of the Large Magellanic Cloud, whose low energy X-ray properties were previously unknown below 1 keV. Flight 2 produced data on a 900 square degree area centered about the constellation of Eridanus, a region known to exhibit strong spatial variations. Both flights included observations of Centaurus X-3, an eclipsing binary X-ray source. Launch times were predicated by the desire to observe this source both in the non-eclipsed and the eclipsed state.

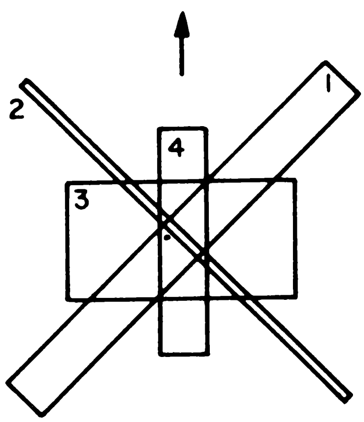


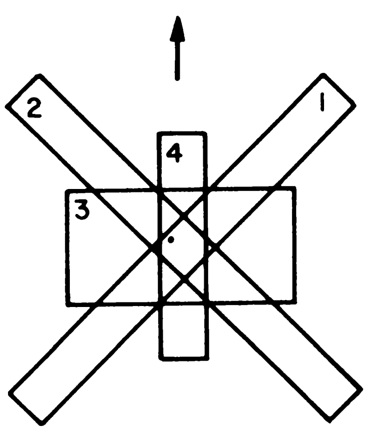


| Counter | Solid Angle | Area ($cm^2$) | Counting Gas |
|---|---|---|---|
| <u>Flight 1</u> | | | |
| 1 | $2^\circ \times 20^\circ$ | 89 | Propane |
| 2 | $0.4^\circ \times 20^\circ$ | 188 | Propane |
| 3 | $5^\circ \times 10^\circ$ | 352 | Propane |
| 4 | $2^\circ \times 10^\circ$ | 350 | P-10 |
| <u>Flight 2</u> | | | |
| 1 | $2^\circ \times 20^\circ$ | 188 | Propane |
| 2 | $2^\circ \times 20^\circ$ | 188 | Propane |
| 3 | $5^\circ \times 10^\circ$ | 352 | Propane |
| 4 | $2^\circ \times 10^\circ$ | 350 | P-10 |

Figure 1.2

Detector characteristics of the Caltech Australian X-ray experiments. The drawing shows the relative orientation and size of the field of view for each counter on each flight as the experiment looked at the sky. The arrow indicates the direction of the nose position of the rocket. (The approximate average position of Cen X-3 during holds on that object, as discussed in Chapter 5, is indicated by the dot near the center of the field of view.)

# CHAPTER II

# SOFT X-RAY EMISSION FROM THE LMC

## I. Introduction

Because the Large Magellanic Cloud (LMC) is our nearest neighbor galaxy it will play an important role in understanding X-ray emission in our own galaxy, despite the obvious morphological differences between the two structures. Although originally designated as an irregular galaxy lacking rotational symmetry by Hubble, de Vaucouleurs has reclassified the LMC as a prototype for barred spirals in which one major spiral arm dominates the spiral structure (de Vaucouleurs and Freeman 1972). The featureless hydrogen-deficient bar, approximately 1° x 3.5°, is the outstanding optical feature of the LMC, and is also visible as a weak 408-MHz continuum radio source (160 flux units, Matthewson and Healy 1963). The bar constitutes approximately 90% of the mass of the LMC and is made up predominantly of Pop II stars (see photograph, Figure 2.1). At one end of the bar is the spectacular 30 Doradus complex (approximately 1° x 3°) which dominates H I profiles of the LMC. Emerging from the other end of the bar the major spiral arm can be clearly seen in ultraviolet photographs of the LMC. Diffuse cluster-rich outer regions and several small arms near 30 Doradus constitute the remainder of the LMC, which has an apparent visual diameter of approximately 6°. At 1410 MHz, emission from the LMC totals 620 flux units, approximately 20% due to discrete sources. Eleven probable supernova remnants have been identified by McGee and Newton (1972). Approximately 55 kpc distant, the LMC has an estimated mass, determined from the 21-cm rotation curve, of about $10^{10}$ $M_{\odot}$, of which from 5 to 9% is thought to be neutral hydrogen (McGee and Milton 1966). These and other optical and radio properties of the LMC have been summarized by Bok (1966) and references therein.

## II. Original X-ray Observations

Emission between 2 and 10 keV from the LMC was first reported by Mark *et al*. (1969). Four sources in the LMC are listed in the 3U catalog and account for more than 90% of the 2-7 keV flux in the direction of the LMC as measured by Uhuru (Leong *et al*. 1971). All of these sources except LMC X-4 were later observed by the Copernicus X-ray telescope (Rapley and Tuohy 1974) and by OSO-7 (Markert and Clark 1975). LMC X-2, LMC X-3, and LMC X-5 (discovered by OSO-7) are known to be variable over a period of months. The source 30 Doradus, whose radio characteristics are similar to those of the Galactic Center, does not appear to be a bright hard source as indicated by earlier low resolution surveys (Price *et al*. 1971). However, the observed sources do appear similar to the high luminosity ($10^{38}$ erg $s^{-1}$) compact sources which dominate the total 2-7 keV emission in our galaxy. Variability in particular is not surprising since over 3/4 of the Galactic 3U sources with maximum fluxes greater

Figure 2.1

Five slow scans were executed over the Large Magellanic Cloud. "Crosses" indicate positions obtained from the star field camera. The solid line represents the estimated aspect assuming that scans continued in great circles from known positions (see the Appendix, Section III). The dashed line encloses the location of a possible source seen in the 0.4° x 20° propane counter (photograph courtesy of Professor P. Hodge, University of Washington).

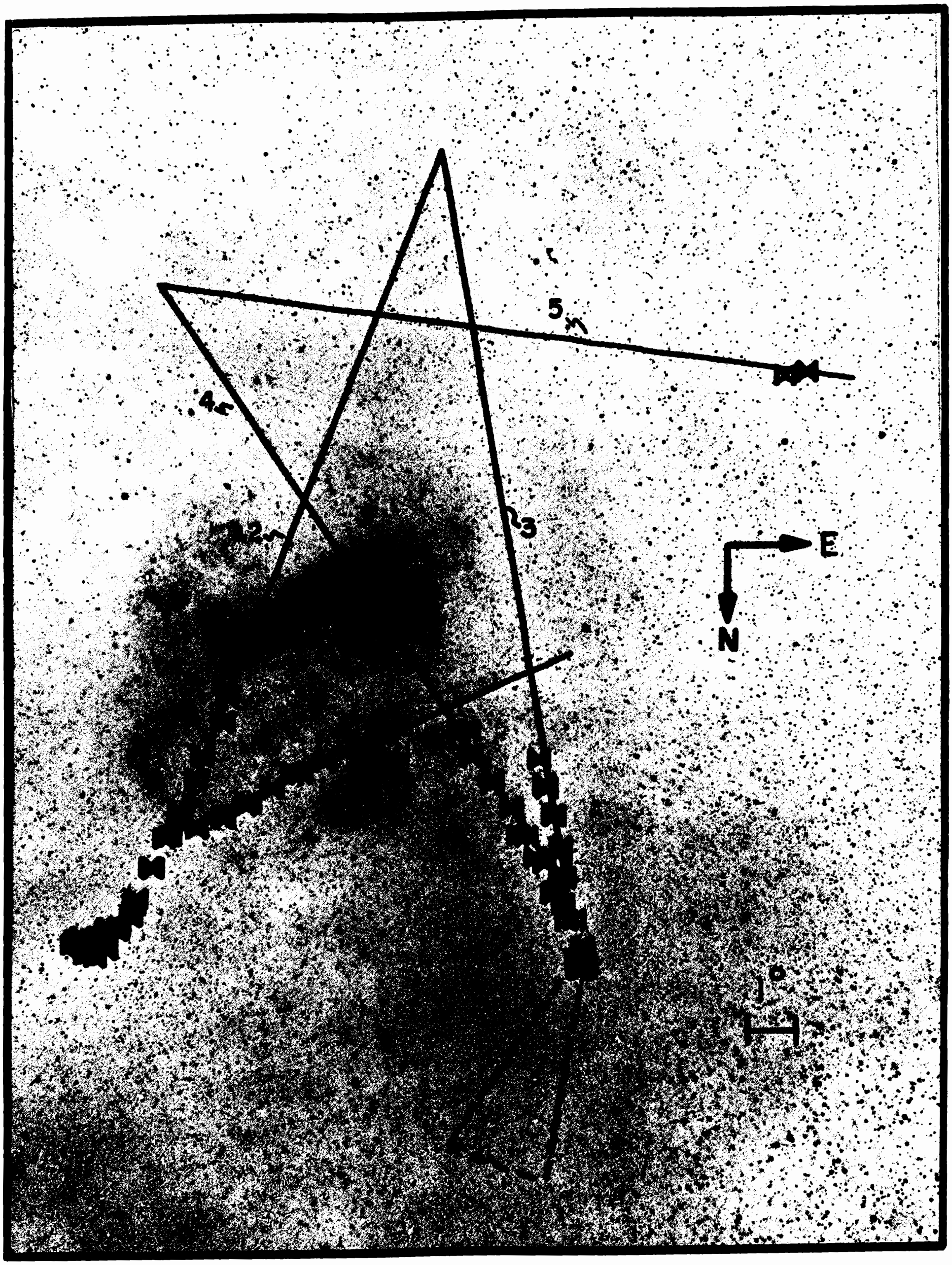
5
4
2
3
E
N
1°

than or equal to 100 Uhuru counts vary by at least a factor of two. Spectra obtained by Uhuru and by OSO-7 are also similar to spectra obtained from compact Galactic objects.

Weaker X-ray point sources in the LMC have not been observed due to source confusion and the lack of detector sensitivity. Determination of the luminosity function of compact X-ray sources should be possible, however, as experiments are improved. Such observations should allow verification of suggestions (Margon and Ostriker 1973) of a luminosity gap at approximately $10^{37.5}$ erg $s^{-1}$ in compact hard X-ray sources.

## III. The Caltech Experiment

Although point source observations of identified Uhuru sources down to energies as low as 0.7 keV had been carried out with the Copernicus focusing collector, no general surveys cf soft X-ray emission from the LMC had been attempted prior to the launch of the Caltech experiment at 17:30 UT 1 November, 1973. Therefore, the scan path was designed so that a two-dimensional sky map of the region could be produced if the LMC proved to be a bright source of soft X-rays. Six slow scans at approximately 0.5° $s^{-1}$ were programmed as the aspect solution of the LMC portion of flight 1 indicates (Figure 2.1).

Between 0.4 and 1.5 keV, X-ray emission from the LMC is clearly visible in the 5° x 10° propane detector (Figure 2.2), although the

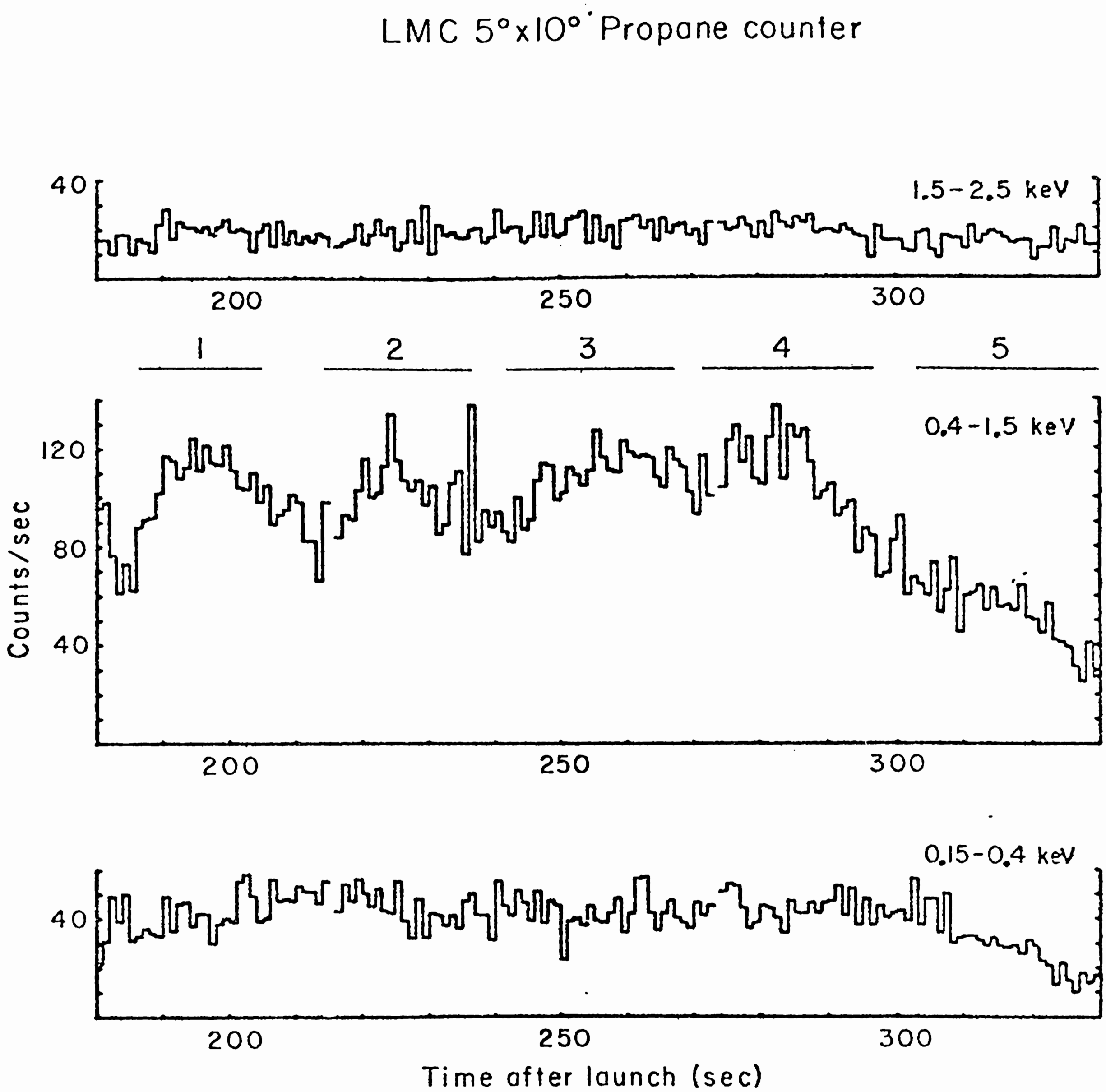


Figure 2.2

Raw counting rates from the $5^{o}$ x $10^{o}$ propane counter during the LMC scans, which are indicated by number, show emission from the LMC between 0.4 and 1.5 keV. The low counting rate during scan 5 is predominantly, but not entirely, due to atmospheric absorption. (The counting rate was arbitrarily put to zero during two voltage calibrations.)

source strength was too low for a detailed sky-brightness map to be produced with the narrow collimators. The incident flux from the LMC in the 0.4 - 1.5 keV band was approximately 0.3 counts $cm^{-2}$ $s^{-1}$. In arriving at this conclusion a diffuse background flux equal to that observed during the fast 5° $s^{-1}$ scan, which the rocket executed between Cen X-3 and the LMC (183-186 s), was subtracted from the flux observed when the collimator was centered over the LMC.

Data from the 0.4° x 20° detector (Figure 2.3) revealed that soft X-ray emission does not appear to have been due to one or two strong point sources. The only significant peak (5σ) in the data from that counter occurred when the collimator bore position was centered at a R.A. = 90.3° and dec = -62.6° at t = 266-269 s. Data from the 2° x 20° detector also indicates an enhanced counting rate. The experiment was executing a fast 5° $s^{-1}$ pitch at this time so that a point source as far as 5° from the center position could explain the observation. The region in which the postulated source lies, based on the assumption that the source was not in the field of view (FOV) before the pitch began, is illustrated in Figure 2.1. The only other time when this region was viewed by the 0.4° x 20° counter was near t = 200 s at which time the rocket was just beginning a fast pitch. Here too the counting rate was anomalously high between 0.4 and 1.5 keV, although there is no convincing evidence of the source above 1.5 keV. If real, the source strength would amount to approximately one-third of the total flux from the LMC.

From the 0.4 to 1.5 keV data of the 2° x 20° propane counter a crude map of the emission region was constructed (Figure 2.5).

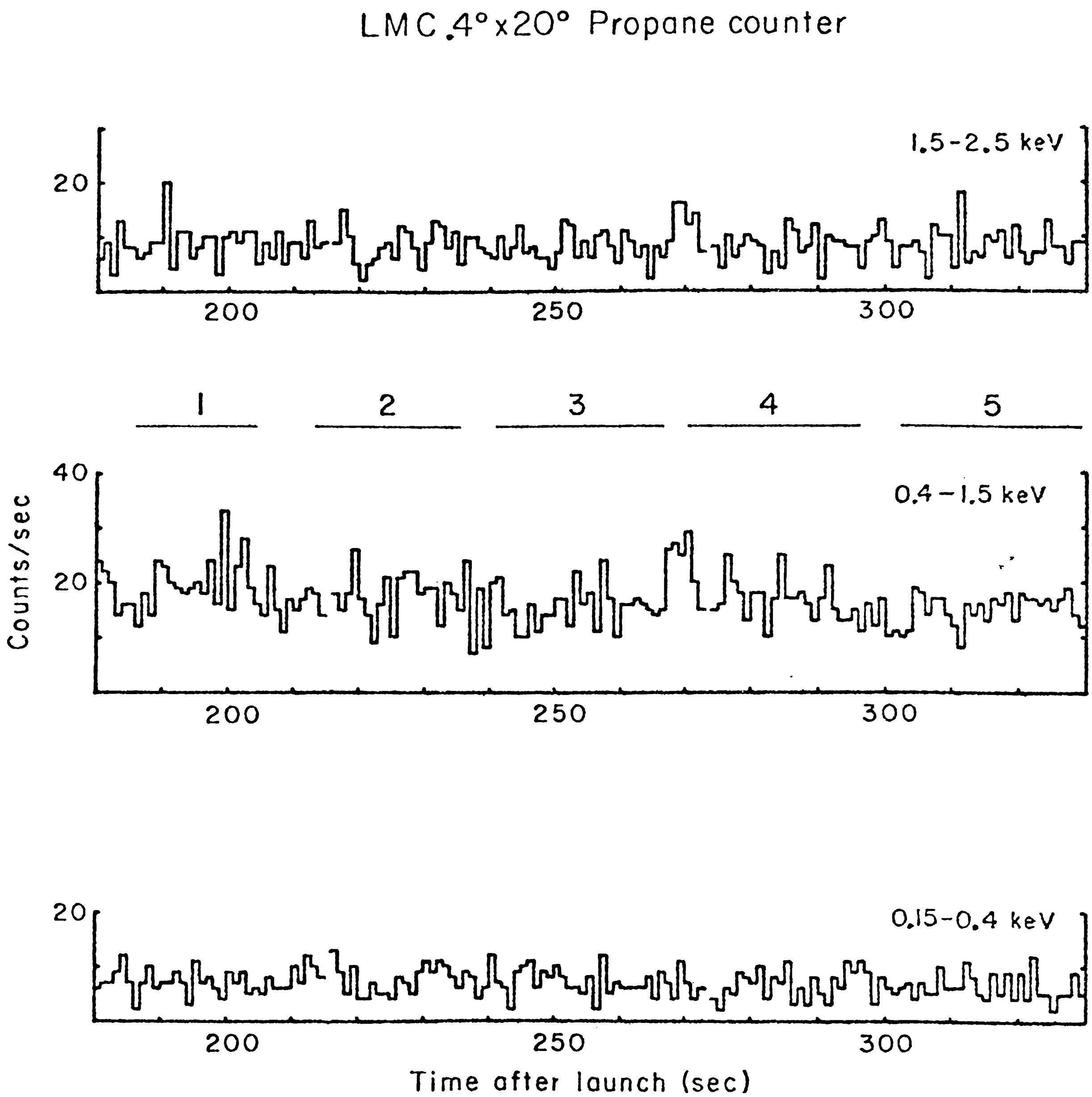


Figure 2.3

Same as Figure 2.2 for the 0.4° x 20° propane counter. A possible source was observed between 266 and 269 seconds.

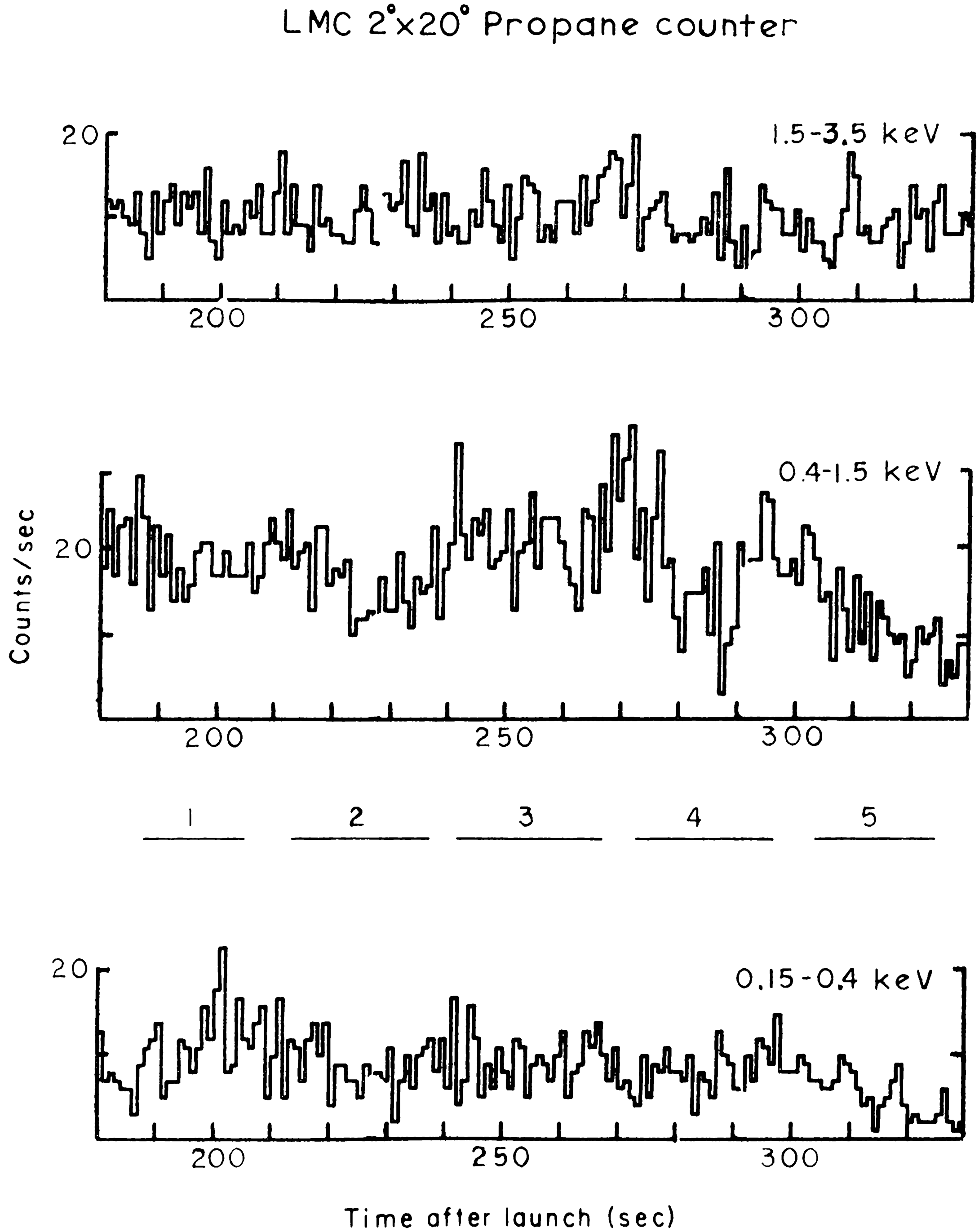


Figure 2.4

Same as Figures 2.2 and 2.3 for the 2° x 20° propane counter.

Figure 2.5

The low signal to noise ratio observed in the 2° x 20° propane counter made creation of a detailed sky map impossible. Nevertheless, a crude indication of the nature of emission from the LMC can be gleaned from the figure. The map was made using 3-second averages of the data between 0.4 and 1.5 keV. Positions in the LMC scans are indicated in which this average counting rate was $< 2$, 2-4, 4-6, and 6-8 $\sigma$ above minimum 3-second averages, which were observed when the entire collimator was off the LMC between scans 2 and 3. (The large size 20° of the collimator, coupled with the low signal to noise, implies, however, that any conclusions drawn from this map should be regarded as tentative.) Both the positions of the spiral arm (ARM) and the optical bar (BAR) are indicated.

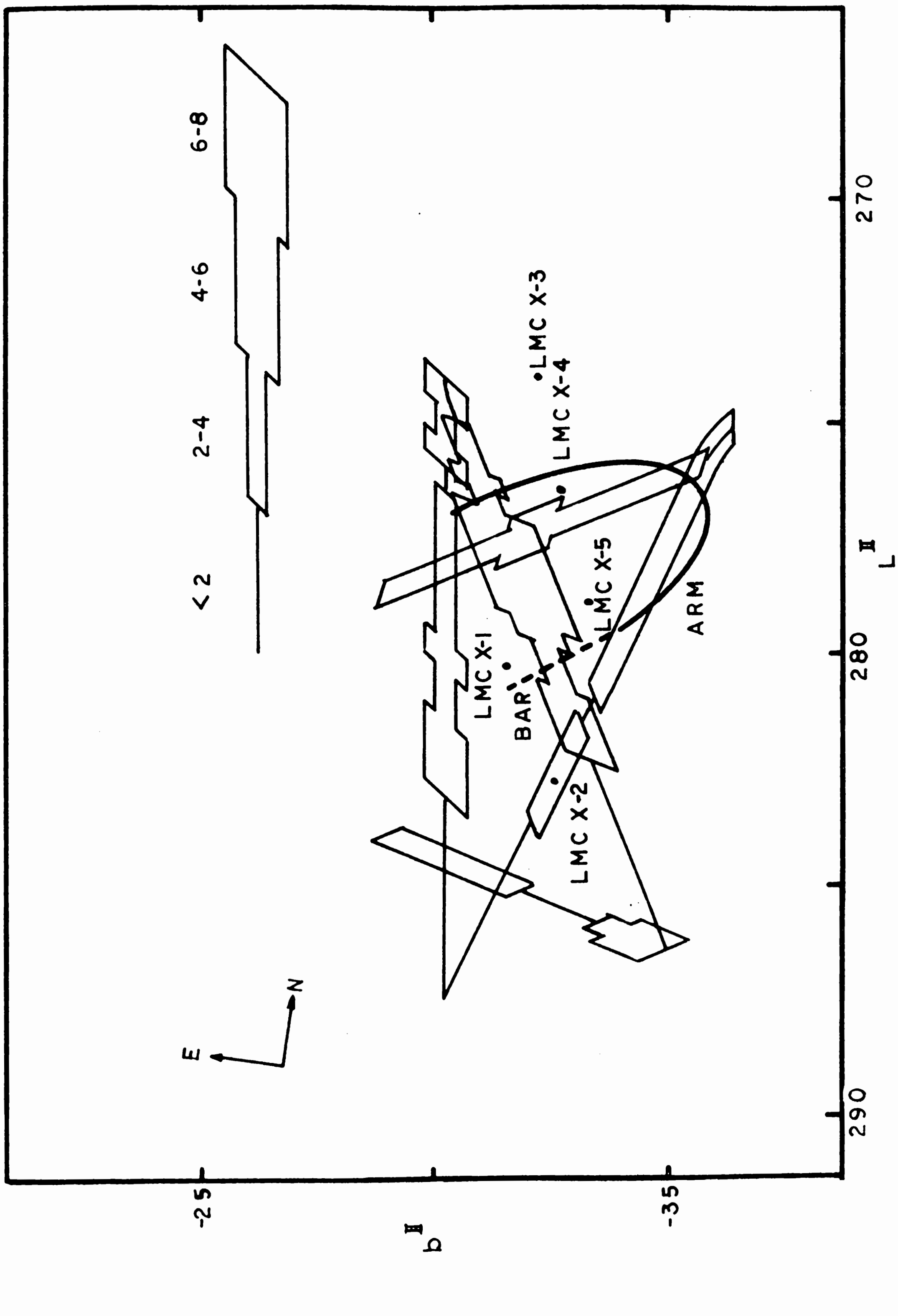

6-8
4-6
2-4
< 2
LMC X-3
LMC X-4
LMC X-5
LMC X-1
BAR
ARM
LMC X-2
N
E
270
280
290
L II
-25
-35
b II

The emission appears to be relatively diffuse, observed throughout most of the optical galaxy. Maximum counting rates were observed when the collimator was centered a few degrees north of the optical bar, either in the region encircled by the major spiral arm of the LMC or centered near the major hydrogen concentrations near 30 Doradus. No strong correlation with known point sources, which would have been in the FOV for approximately 5 seconds, was observed, although the possible contribution of the point source flux is difficult to estimate in view of the rather crowded nature of the region, the extreme length of the 2° x 20° collimator, and, more importantly, the low signal to noise ratio.

## IV. Soft X-ray Spectra and Luminosity

In what may simply be a parameterization of a composite spectrum due to many different types of sources, the observed spectrum of the LMC in the 5° x 10° propane detector (0.15 - 2.5 keV) may be fitted either with a thermal spectrum $0.3 < kT < 0.5$ keV, $0.3 < N_H < 0.9 \times 10^{21}$ atoms cm$^{-2}$ or a photon power law spectrum $1.9 < \alpha < 3.4$, $0.6 < N_H < 1.4 \times 10^{21}$ atoms cm$^{-2}$. The power law spectrum is similar in intensity and slope to a composite spectrum between 1.5 and 12 keV, given by Price _et al_. (1971) of $0.16 \pm 0.04$ counts cm$^{-2}$ s$^{-1}$, $2. < \alpha < 3.$ Such a spectrum suggests that the total luminosity observed (approximately $10^{38}$ ergs s$^{-1}$ for $0.4 < E_x < 1.5$ keV) may be emission from the same sources detected by Uhuru in the 2-6 keV band, although as noted

Table 1.1

FLUX LIMITS ON IDENTIFIED LMC POINT SOURCES*

| Source | Incident Flux (0.4-1.5 keV) cts $(cm^2\ s\ keV)^{-1}$ |
|---|---|
| LMC X-1 | -0.10 ± 0.06 |
| LMC X-3 | +0.09 ± 0.04 |
| LMC X-4 | +0.06 + 0.06 |
| LMC X-5 | -0.05 ± 0.05 |

* Sources scanned by $0.4^o$ x $20^o$ counter only.

Figure 2.6

This LMC spectrum, obtained with the 5° x 10° propane counter, can be fit equally well with thermal continuum or power law models. Within the insets, $\chi^2 + 1$, $\chi^2 + 3$, and $\chi^2 + 5$ contours of the spectral fits are shown.

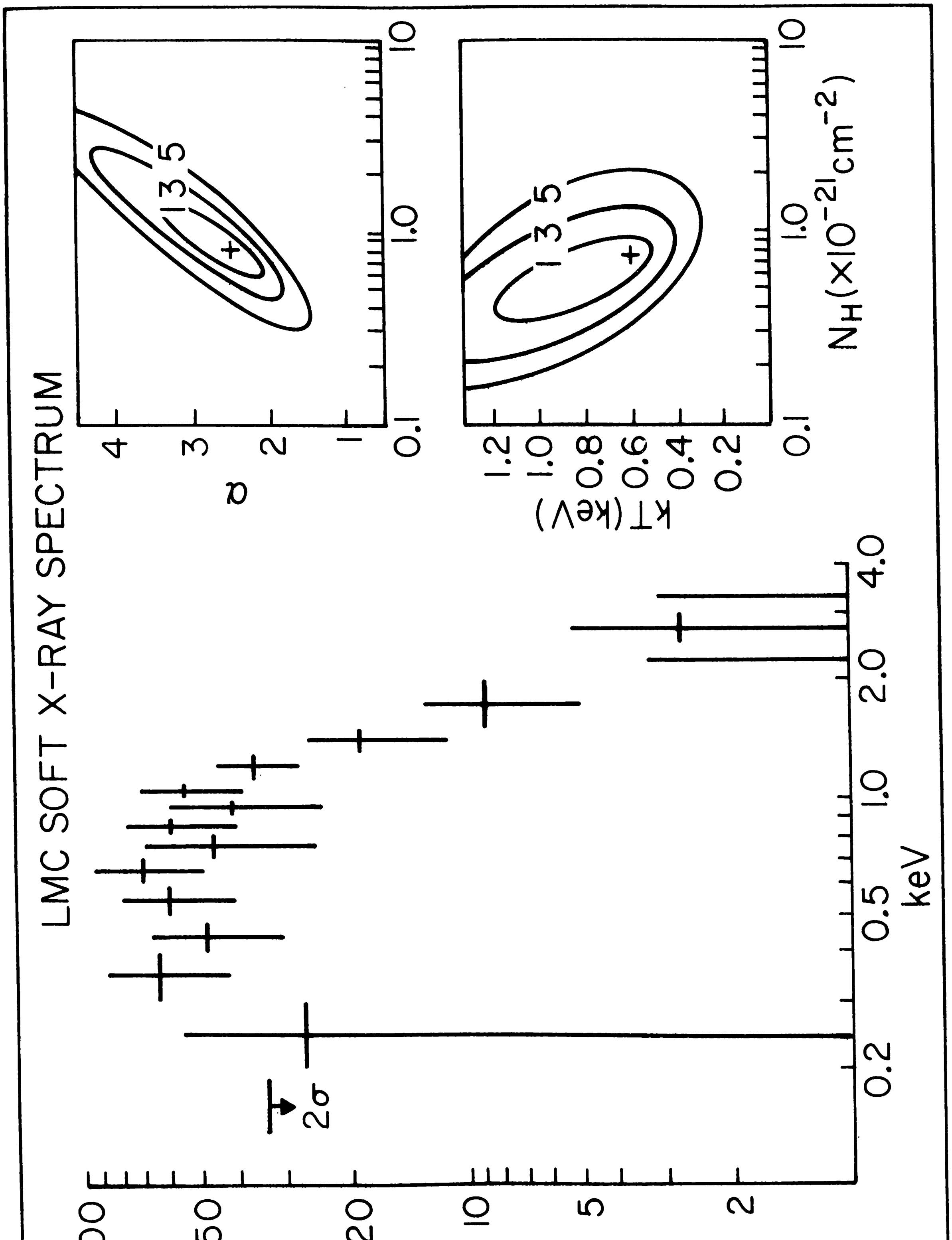

LMC SOFT X-RAY SPECTRUM
counts keV$^{-1}$ sec$^{-1}$
100
50
20
10
5
2
2σ
0.2
0.5
1.0
2.0
4.0
keV
α
4
3
2
1
1 3 5
0.1
1.0
10
kT (keV)
1.2
1.0
0.8
0.6
0.4
0.2
$N_H$ ($\times 10^{-21}$ cm$^{-2}$)

data from counters 2 and 3 seem to indicate diffuse emission.

The fitted spectrum of LMC X-1 obtained by Markert and Clark (1975), which includes a $2\sigma$ upper limit of neutral matter absorption, indicates that about one third of the total flux would be accounted for by that one source. If absorption in the remaining sources was as low, nearly all of the observed flux could be accounted for by the known point sources. Where usable aspect photographs exist to describe the crossing of the $0.4° \times 20°$ collimator over a known source, upper limits to the flux were derived between 0.4 and 1.5 keV (Table 2.1). These upper limits do not exclude the possibility that all the flux arises from the known point sources, but they make it unlikely that one or two sources alone are the dominant contributors to the observed X-ray flux and tend to indicate that a diffuse or many point source emission model may be required.

## V. Emission from the LMC Bar

Evidence for diffuse emission from the bar was presented by Rappaport et al. (1975). A $5\sigma$ source was observed between 0.4 and 1.5 keV when the field of view of the MIT one-dimensional collector was parallel to the optical bar of the LMC. Because the source was not observed on a subsequent scan when the long direction of the collector passed obliquely across the bar an extended, elongated source was postulated. Constraints on the spectrum were derived by assuming a spectral shape consistent with uniform thermal emission within a uniformly absorbing medium, e.g.

$$N(E) = C\, E^{-1} \exp(E/kT) \cdot \exp(-N_G\sigma) \cdot (1-\exp(-N_B\sigma))(N_B\sigma)^{-1} \quad (2.1)$$
$$\text{photons cm}^{-2}\ \text{s}^{-1}\ \text{keV}^{-1}$$

where Galactic hydrogen $N_G$ was taken to be 6 x $10^{20}$ atoms $cm^{-2}$, and hydrogen within the bar $N_B$ was taken to be 15 x $10^{20}$ atoms $cm^{-2}$. Only values of kT $\simeq$ 0.25 keV were found to be consistent with the lack of a detectable flux below the carbon K edge of the detector window, while much larger values of kT were ruled out by the lack of detection by the OSO-7 satellite. Rappaport et al. found that the volume emissivity of the bar, assumed to be approximately 300 pc thick, is 10 to 15 times that of the solar neighborhood. If this result were verified, detailed studies of low energy emission from the LMC would undoubtedly greatly aid understanding of diffuse emission in our own galaxy.

During the second Caltech 0.5° $s^{-1}$ scan, the 0.4° x 20° collimator was positioned within 10° of the orientation of the MIT collector. The LMC bar has an angular extent of approximately 0.75° in the narrow direction. The excess observed by MIT indicated an angular extent of approximately 1.0°; however, the first second of the 3-second excess may have been contaminated by LMC X-1. In view of these considerations, the bar source should have been within the field of view of counter 2 for 2 or 3 seconds.

The narrow 0.4° collimation of the MIT focusing collector is very similar to that of counter 2. The average excess observed by

MIT was approximately 12 counts $s^{-1}$ for 3 seconds. The constant C in the postulated MIT spectrum (Eq. 2.1) was evaluated using the experimental parameters found in Figure 1 of Borken et al. (1972). The effective areas quoted therein were divided by two since on this MIT flight only half the detector was functional due to a faulty pressure regulator. Depending on the extent of contamination by LMC X-1, $16 \lesssim C \lesssim 24$ implying a total incident counting rate of between 0.4 and 0.6 counts $cm^{-2}$ $s^{-1}$ between 0.4 and 1.5 keV. This rate is slightly larger than the total excess observed by the 5° x 10° propane detector.

Convolving the normalized MIT spectrum with the detector response of counter 2 indicates that approximately 17 excess counts $s^{-1}$ should have been observed for at least two seconds between 0.4 and 1.5 keV, of which approximately 13 excess counts $s^{-1}$ should have fallen between 0.4 and 0.9 keV. Given a background rate of 9.5 counts $s^{-1}$ between 0.4 and 0.9 keV, 13 excess counts $s^{-1}$ would be a $3\sigma$ signal, given Poisson statistics. In two seconds a total $5\sigma$ excess should have been observed. CIT and MIT results are compared in Figure 2.7. No source was evident. An excess with a strength half that observed by MIT should have appeared at the $3\sigma$ level in two seconds.

Neither the MIT results nor the Caltech measurement with regard to the bar are extremely compelling, due to the small number of total counts and due to possible source confusion with LMC X-1, which is known to vary by a factor of four within three hours (Tuohy and Rapley

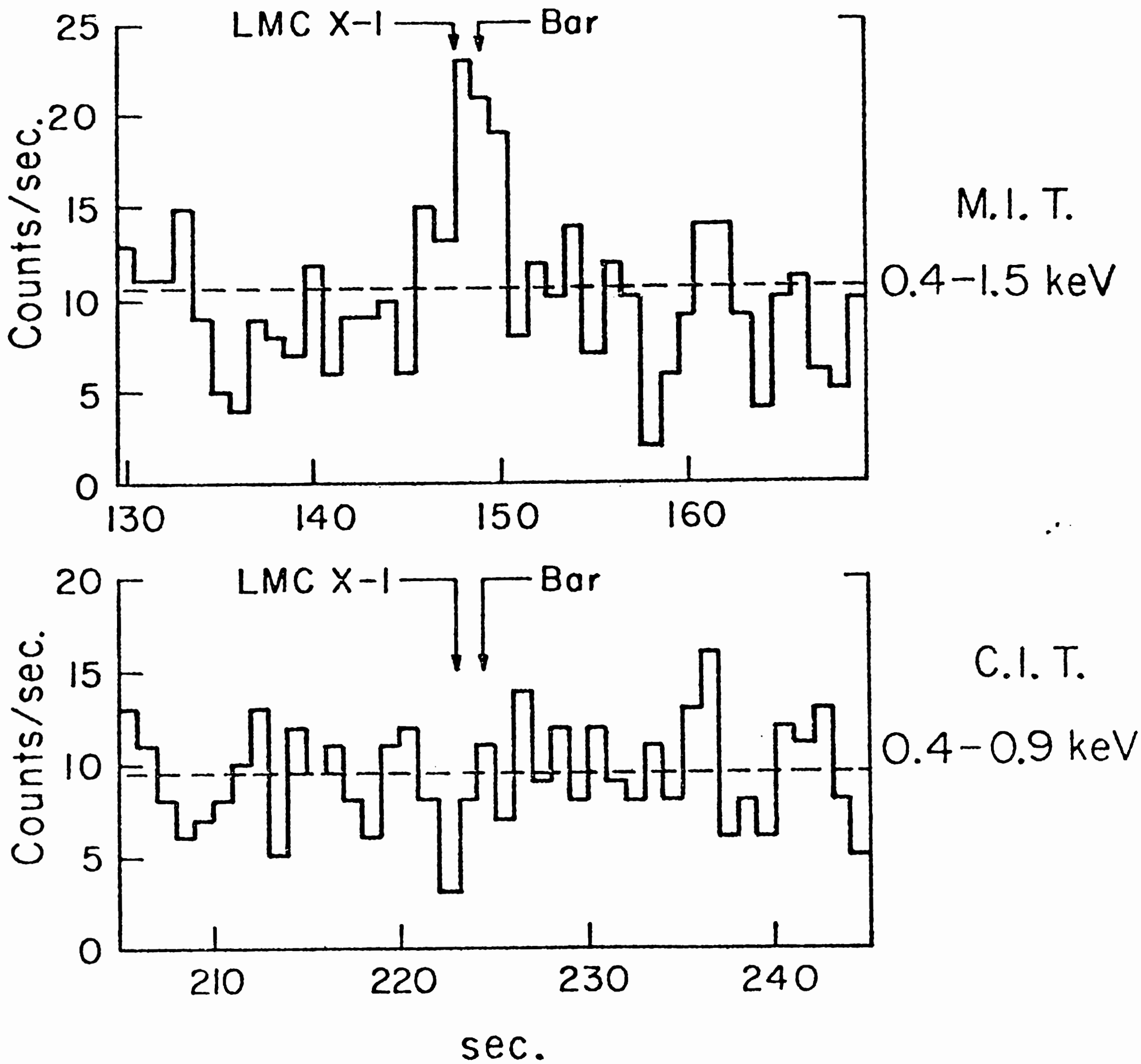


Figure 2.7

A comparison of counting rates of the MIT scan and a similar Caltech scan, both with narrow collimators, did not produce consistent results concerning emission from the LMC bar. The energy interval in the CIT histogram was chosen to maximize signal to noise based on the reported MIT spectrum.

1975). Maps with better spatial detail and better statistics are clearly required to unambiguously determine the spatial distribution of soft X-ray emission within the LMC.

## VI. The LMC and the Galaxy

The luminosity of the LMC between 0.4 and 1.5 keV is approximately $10^{38}$ $ergs^{-1}$. Davidsen et al. (1972) estimated the emissivity of our own galaxy at 0.68 keV to be $2.5 \times 10^{-19}$ photons $(cm^3\ s\ keV)^{-1}$ in the plane. Assuming uniform emissivity in a disc of thickness 400 pc and radius of 15 kpc leads to a crude estimate of the total luminosity of our galaxy between 0.4 and 1.5 keV of about $2 \times 10^{39}$ erg $s^{-1}$. Rapley and Tuohy (1974) have suggested that comparisons involving the X-ray luminosity and the mass of the LMC are naive in view of the dissimilar evolutionary history of the two galaxies, a fact which they find reflected in the relative number of high luminosity sources in the LMC, approximately 25% the number of such sources in the Galaxy. (Note that with only four or five sources this comparison may also be rather naive.). However, the 0.4 to 1.5 keV X-ray luminosities of the two galaxies more nearly reflect the mass ratio, both total mass or hydrogen mass, than the high luminosity X-ray source counts. If further X-ray observations confirm that emission from the bar is not a significant fraction of the total 0.4 to 1.5 keV flux from the LMC, that fact would tend to imply that soft Galactic X-ray emission is not associated with Pop II systems, but rather seems more intimately connected with regions of more recent star formation.

# CHAPTER III

# THE LMC AND THE SOFT X-RAY BACKGROUND

## I. Introduction

If a large fraction of the soft X-ray diffuse flux is of extragalactic origin, cool gas in nearby external galaxies should cast an X-ray shadow, as originally pointed out by Gould and Sciama (1964). Few external galaxies have a sufficient angular size to cast a shadow measurable on a rocket experiment, however. The relatively small area-solid angle-time factor available to a sounding rocket limits observations. Three attempts have been reported. In all cases absorption by the hydrogen within our own galaxy was as important as hydrogen contained in the external galaxy. None of these measurements requires an extragalactic flux in excess of an extension of the power law observed between 2 and 10 keV.

McCammon *et al*. (1972) found that no more than 25% of the flux between 0.12 and 0.28 keV observed in the direction of the Small Magellanic Cloud was extragalactic in origin. The experiment consisted of a slow (0.4° $s^{-1}$) raster scan of the SMC region and utilized a 6° x 10° FWHM P-10 proportional counter.

The on-board camera failed, but aspect information, accurate to within 1.5°, was recovered from magnetometer data and from the observed crossing of SMC X-1. Hydrogen column densities varied from 1 to 4 x $10^{20}$

atoms for the Galaxy and up to 2.5 x $10^{21}$ atoms $cm^{-2}$ for the SMC, although the angular size of the dense regions of the SMC is considerably smaller than the collimator FWHM. Source contamination from the only known source in that region, SMC X-1, was not a problem at 0.25 keV, since SMC X-1 was observed to have a cutoff of $10^{21}$ atoms $cm^{-2}$ corresponding to 1 optical depth at 0.4 keV. McCammon *et al*. report an observed flux of six times an extrapolation of the diffuse 2 - 10 keV X-ray spectrum, taken to be 11 $E^{-1.4}$ photons $(cm^2\ s\ keV\ sr)^{-1}$, even when making no allowance for interstellar absorption. The relevant quantity for both cosmological and comparison purposes, the extragalactic flux limit determined from the experiment, is unfortunately not quoted. From the published scan path, however, the transmission of the Galactic and SMC hydrogen at 0.25 keV is estimated to be 45 ± 5% if $\sigma_{eff} = 0.4 \times 10^{-20}\ cm^2$, which implies that 8 ± 1% of the observed flux could be accounted for by an extension of the power law spectrum observed between 2 and 10 keV. (For reasons explained in Section VII, this transmission is somewhat high; the actual value of a power law is approximately 5%.) The upper limit of 25% of the observed flux which may be extragalactic at 0.25 keV corresponds to a possible enhancement of up to 2 (or 5) times a simple power law extrapolation, e.g., a total flux of approximately 300 photons $(cm^2\ s\ keV\ sr)^{-1}$ at 0.25 keV.

Margon et al. (1974) have reported an upper limit of 52 ± 5% for the observed extragalactic flux fraction between 0.1 and 0.28 keV in the direction of M31. The experiment consisted of a two minute rocket observation of M31 and two nearby background points, one 4° west and one 3° north of M31, and was carried out with a beam that was approximately 2° square (FWHM) and a very thin 85 μg $cm^{-2}$ polypropylene window coated with 35 μg $cm^{-2}$ of colloidal carbon. Neutral hydrogen measurements were made using the NRAO 140-ft. telescope on a grid with points separated by approximately 30 ft. to determine the effective transmission. Grid values of neutral hydrogen obtained varied between $6.1 \times 10^{20}$ and $1.1 \times 10^{21}$ atoms $cm^{-2}$ for the Galaxy and from trace amounts to $1.8 \times 10^{21}$ atoms $cm^{-2}$ for M31.

Models of the soft X-ray background in which the entire flux is of cosmological origin or due to a diffuse Galactic halo are incompatible with their data. To determine an upper limit on the extragalactic flux, Margon _et al_. assume that all of the flux observed at the point of maximum transmission is of cosmological origin. Such an extragalactic flux would account for an average extragalactic flux fraction of 52 ± 5% for the three positions together. The cosmological flux required corresponds to an upper limit on the extragalactic flux of 800-1000 photons $(cm^2\ s\ keV\ sr)^{-1}$ which the authors believe indicates that the upper limit derived is close to the actual value since the upper limit is similar to the value Margon _et al_. infer from polar fluxes. However, the high latitude data are primarily of the North Galactic Pole and are, as noted earlier, undoubtedly contaminated by the existence of the North Polar Spur. There is no compelling reason to believe that the upper limit derived by Margon _et al_. is

Table 3.1

OBSERVED LOW-ENERGY DIFFUSE X-RAY FLUX FRACTIONS

IN EXTRAGALACTIC SHADOWING EXPERIMENTS

| | Object | Observed Local Flux | Observed Halo Flux | Observed Extra-Gal Flux |
|---|---|---|---|---|
| McCammon *et al.* (1971) | SMC | -- | < 100% | < 25% |
| Margon *et al.* (1974) | M31 | > 48 ± 5% | < 52 ± 5% | < 52 ± 5% |
| Rappaport *et al.* (1975) | LMC | > 35% | < 65% | < 30% |
| Current experiment (smooth) | LMC | 90-94% | <9% | < 9% |

any more than an upper limit.

Rappaport et al. (1975) have analyzed one 0.5° $s^{-1}$ scan of their one-dimensional (0.4° x 9.5° FWHM) focusing collector observation of the LMC to determine the extragalactic flux fraction between 0.15 and 0.28 keV. An upper limit of 30% of the observed flux rate of 400 ± 120 photons $(cm^2\ s\ keV\ sr)^{-1}$ was found to be of extragalactic origin. A minimum of 35% of the flux was found to be of Galactic origin, e.g., unaffected by the hydrogen absorbing layers of either the Galaxy or the LMC. Inspection of the measured hydrogen column densities reveals an average transmission of 7 ± 5% which implies an upper limit to the unattenuated extragalactic flux similar to that reported by Margon *et al*.

## II. Flux Fractions

High Galactic latitude ($b_{II} \lesssim -30°$) and a large angular extent make the LMC-SMC complex a promising region for observation of a diffuse X-ray shadow. For this reason, data in the 5° x 10° propane detector was analyzed to determine flux fractions exhibiting absorption due to the Galaxy and the LMC, the Galaxy alone, and no absorption.

A sample of 85 seconds of data was utilized, taken from the first four LMC 0.5° $s^{-1}$ scans when atmospheric absorption was not severe (< 10%). To produce as uniform a coverage as possible, data obtained during the fast pitches at the corners of the "star" (see Figure 2.1) were excluded. An explicit assumption was made that the flux could be separated into three separate components and that variations in the observed flux were due only to absorbing material. In that case the observed counting rate $S_{obs}$ is given by

$$S_{obs} = \eta_L S_L + \eta_H S_H \exp(-\tau_G) + \eta_{EX} S_{EX} \exp(-\tau_{G + LMC}) \qquad (3.1)$$

where $S_i$ are the intrinsic fluxes between 0.15 and 0.28 keV of local (L), halo (H) and extragalactic (EX) origin, where the $\tau_i$ are the effective optical depths of Galactic gas (G) and the Galactic plus LMC gas (G + LMC), and where the $\eta_i$ incorporate all detector efficiencies. This functional form also applies in models in which X-ray volume emissivities are proportional to local hydrogen densities (section IV) as well as in the case where physically identifiable components exist. The spectral dependence of $\eta$ and $\tau$ is examined in section VII. To minimize the number of parameters, Chi-square tests were first performed for a simplified equation, ignoring differences in the detector efficiency for the three X-ray components

$$S_{obs} = S'_L + S'_H \exp(-\tau_G) + S'_{EX} \exp(-\tau_{G + LMC}) \qquad (3.2)$$

The cross section was initially taken to be $0.4 \times 10^{-20}$ cm$^2$ and represents approximately the effective cross section for a flat $E^{-1.5}$ power law convolved through an equivalent of $N_H$ equal to $7 \times 10^{20}$ atoms cm$^{-2}$ with detector response, including both window transmission and Gaussian spreading.

Values of the hydrogen column density were derived from the 21-cm surveys of the LMC and the Galaxy as observed by Hindman _et al_. (1963) and McGee _et al_. (1966) respectively. Both measurements were obtained with a halfpower beam width of 2.2°. Values for the neutral hydrogen column density in the LMC were obtained by constructing a grid of maximum spacing 2.5° by estimating the measured integrated brightness temperatures from the contour map (Figure 1) of Hindman et al. (see Figure 3.1). The Galactic map of McGee et al. was presented in tabular form with a maximum spacing of 5°. Conversion from brightness temperatures to neutral hydrogen column densities was made under the assumption that the gas was optically thin. (This is a good assumption unless the gas is strongly clumped as long as $\bar{T}_b = \int T_b^2\, dv / \int T_b\, dv \ll T_s$ where $T_s$ is the temperature of the neutral hydrogen, typically 120 °K. The measured brightness temperatures of McGee et al. are less than 12 °K in the regions of interest in the Galaxy.) The effective transmission for each second of data utilized was calculated by interpolating between points of the hydrogen maps to a grid with 1° spacings. The average transmission of neutral hydrogen in the Galaxy and the Galaxy plus the LMC was then calculated allowing for the triangular response function of the egg-crate collimator. The effective transmission calculated in this manner varied between 7 and 28% through Galactic gas alone and between 3 and 21% through the combined Galactic and LMC gas.

Relatively little indication of modulation by cold absorbing matter is evident in the raw counting rates (see Figure 3.2). Chi-squared tests were performed to determine relative observed flux fractions. When no clumping in addition to that of the hydrogen surveys was assumed, 90-94% ($2\sigma$) of the observed flux was found to be local, unaffected by the hydrogen layer of our own galaxy. At

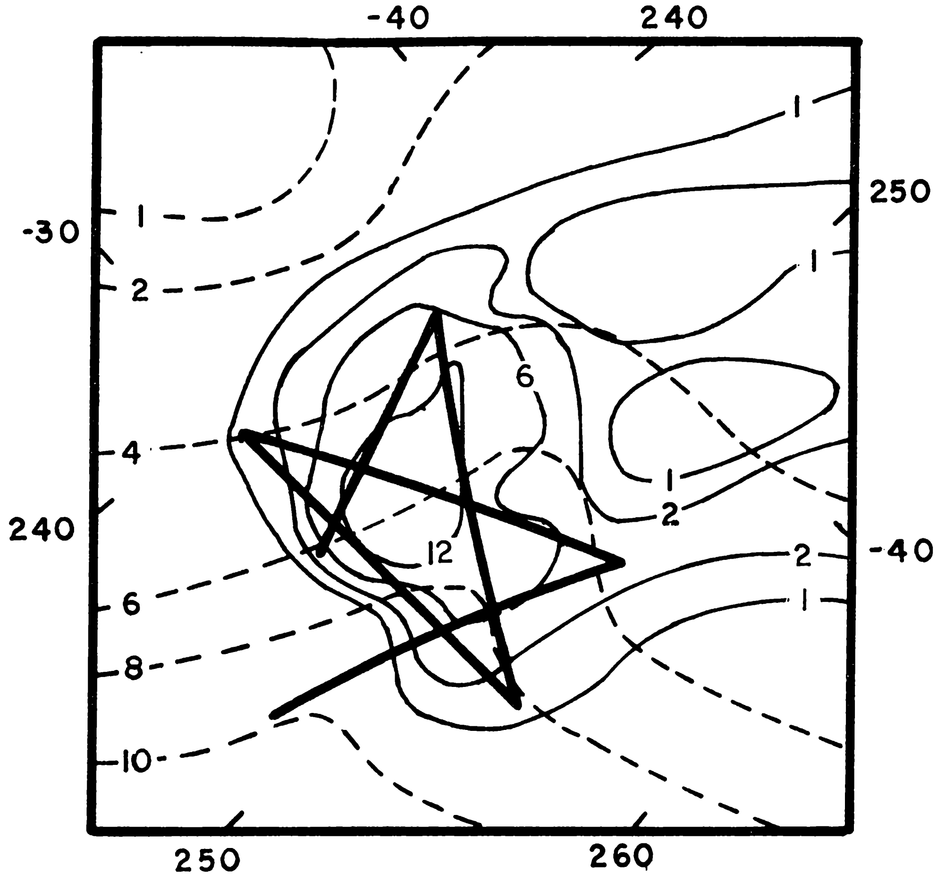


Figure 3.1

The LMC portion of the scan path of flight 1 superimposed on a neutral hydrogen contour map. In units of $10^{20}$ $cm^{-2}$, solid and dashed column density contours are due to the LMC and the Galaxy respectively. Galactic coordinates ($\ell^{II}$, $b^{II}$) are indicated.

most 9% of the observed flux originated beyond the LMC. Limits derived from the current experiment concerning the nature of the diffuse radiation in the direction of the LMC are consistent with, but much stronger than, limits derived by Rappaport et al. (1975) using similar hydrogen data and similar assumptions of no additional clumping. This improvement was due to the 13-fold increase in the number of X-ray counts in the Caltech data sample.

Lack of good correlation of low energy X-rays with hydrogen column density has conventionally been explained by clumpiness of the gas, source contamination and/or lack of knowledge of the absorption properties of the interstellar medium (see Silk 1973). While it is evident that arbitrary variations in the nature of the gas or of the source contribution along different lines of sight can produce apparent isotropy, that these variations do not produce real variations in the observed soft X-ray flux is somewhat surprising and accidental.

## III. Clumpiness

Several observers (Bowyer and Field 1969, Bunner et al. 1969) found that a substantial extragalactic flux excess is consistent with the observed Galactic latitude dependence of the soft X-ray flux if clumping of the interstellar medium into clouds as thick as $10^{21}$ $cm^2$ is allowed. Typically cross sections less than half the theoretical cross section for an unclumped medium were required.

Figure 3.2

Transmission and 0.15 - 0.4 keV counting rate compared. Little or no modulation by neutral hydrogen is evident.

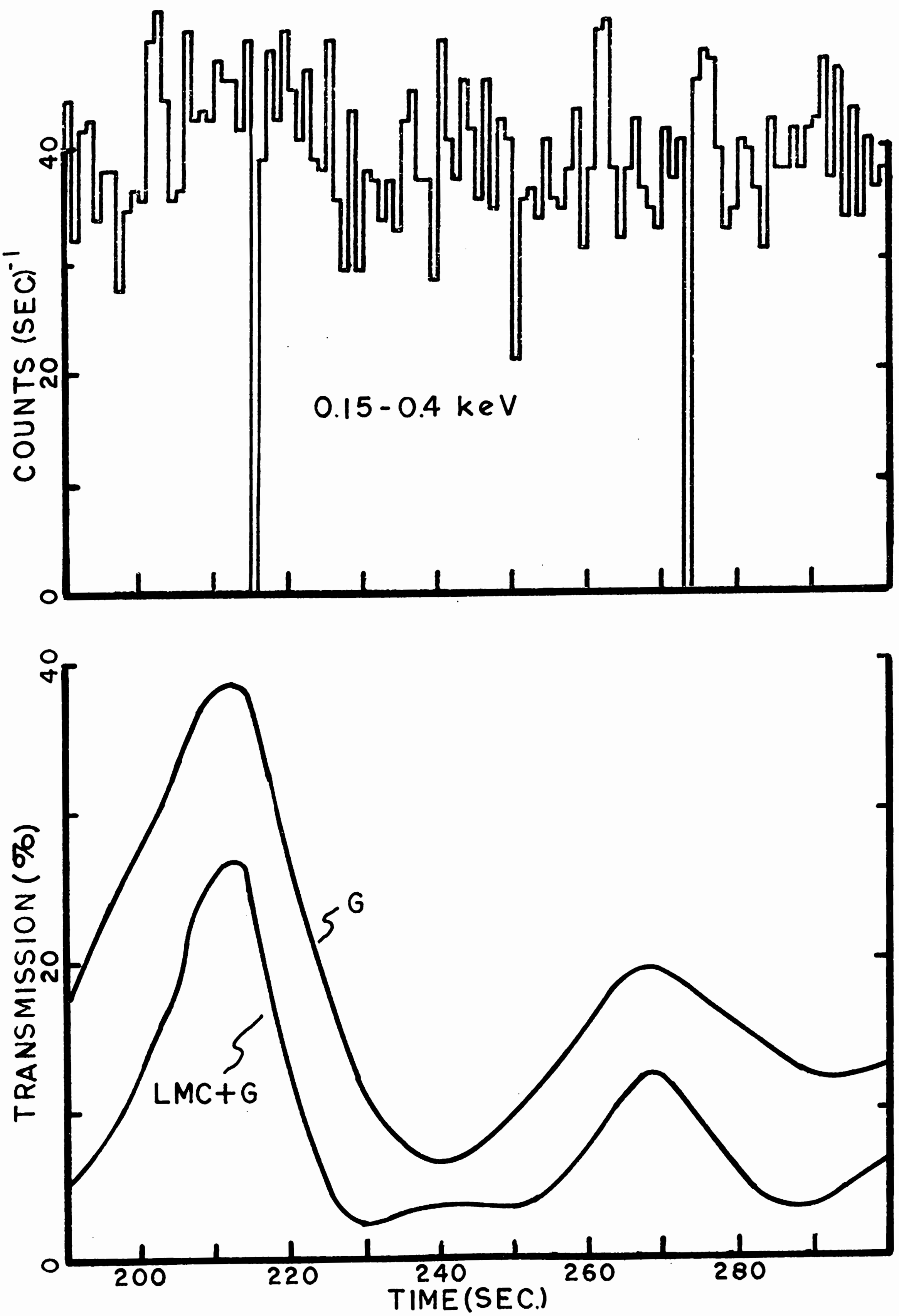
COUNTS (SEC)$^{-1}$
0
20
40
0.15-0.4 keV
TRANSMISSION (%)
0
20
40
G
LMC+G
200
220
240
260
280
TIME (SEC.)

Although these early results were due, at least in part, to the lack of knowledge of the existence of a flux in the Galactic plane, suggestions that clumping affects shadowing measurements persist.

To estimate the effect of possible clumping, we have constructed a simple cloud model which leads to an analytic expression for the effective transmission of 0.25 keV X-rays, depending only on the optical depth through a single cloud and $\langle N_H \rangle$ the average amount of hydrogen along the line of sight.

Consider a slab of cross section A containing spherical clouds of radius $r_c$. Cloud centers are uniformly distributed within the slab. The density within a cloud is assumed fixed but clouds may overlap in which case the density in the overlap region is doubled. The probability that a given line of sight through the slab does not intersect a given cloud i is

$$P_i(0) = 1 - (\pi \, r_c^2/A) \tag{3.3}$$

The probability that the line of sight intersects a chord of length x within the $i^{th}$ cloud is

$$P_i(x) \, dx = (\pi \, r_c^2/A)(x/2r_c^2) \, dx = (\pi x/2A) \, dx \tag{3.4}$$

Thus

$$\langle x_i \rangle = \int_0^{2r_c} x \, P(x) \, dx = 4 \, \pi \, r_c^3/3A \tag{3.5}$$

And if there are n clouds

$$\langle X \rangle = \Sigma \langle x_i \rangle = 4 \pi r_c^3 n/3A \tag{3.6}$$

even if clouds overlap. $\langle X \rangle$ is known. In particular $\langle n_H \rangle$ divided by the cloud density is $\langle X \rangle$. The average transmission through the slab is given by

$$\langle \exp(-\alpha X) \rangle \sim 1 - \alpha \langle X \rangle \quad \text{if } \alpha \langle X \rangle << 1 \tag{3.7}$$

where $\alpha$ = (cloud density) x (cross section). Where the optical depth is not small, evaluation of the average transmission is somewhat more complicated

$$\langle \exp(-\alpha X) \rangle = \prod_i \langle \exp(-\alpha x_i) \rangle = \langle \exp(-\alpha x_i) \rangle^n \tag{3.8}$$

since positions of clouds are independent of one another. Now

$$\langle \exp - \alpha X_i \rangle = 1 \cdot (1 - (\pi r_c^2/A)) + \int dx' \; (\pi x'/2A) \cdot e^{-\alpha x'}$$

$$= 1 - (\pi r_c^2/A) + \{(\pi/2\alpha^2 A) \cdot [1 - (e^{-2\alpha r_c}) \cdot (1 + 2\alpha r_c)]\} \tag{3.9}$$

Thus

$$\langle \exp - \alpha X \rangle = [1 - (\pi r_c^2/A) + \{(\pi/2\alpha^2 A)[1 - e^{-2\alpha r_c}(1 + 2\alpha r_c)]\}]^n \tag{3.10}$$

Eliminating n,

$$\langle \exp - \alpha X \rangle = [1 - (\pi r_c^2/A) + \{(\pi/2\alpha^2 A)[1 - e^{-2\alpha r_c}(1 + 2\alpha r_c)]\}]^{3\langle X \rangle A/4\pi r_c^3} \tag{3.11}$$

We are interested in the limit where $A \to \infty$, i.e.,

$$Q = \lim_{A\to\infty} (1 - B/A)^{CA} \quad (3.12)$$

but

$$\ln Q = CA \ln(1 - B/A) \underset{A\to\infty}{\overset{\lim}{\to}} - CB \quad (3.13)$$

Thus

$$\langle \exp(-\alpha X) \rangle = \exp\{-(3\langle X\rangle/4r_c) \cdot \{1 - [(1/2\alpha^2 r_c^{\,2}) \cdot (1 - e^{-2\alpha r_c}(1+2\alpha r_c))]\}\} \quad (3.14)$$

or rewritten in terms of $\tau_c$, the optical depth through a single cloud, and the cross section at 0.25 keV

$$\langle \exp(-\alpha X) \rangle = \exp\{-(3\tau_{diff}/2\tau_c) \cdot [1 - (2/\tau_c^{\,2})(1 - e^{-\tau_c} \cdot (1+\tau_c))] \quad (3.15)$$

where $\tau_{diff}$ is the optical depth given by $\langle n_H \rangle \sigma$. Alternatively the actual optical depth can be represented in terms of the diffuse optical depth by

$$\tau_{act} = \delta \; \tau_{diff} \quad (3.16)$$

where $\delta$ is an effective clumping factor.

$$\delta = (3/(2\;\tau_c))[1 - (2/\tau_c^{\,2})(1 - e^{-\tau_c}(1 + \tau_c))] \quad (3.17)$$

More complicated models could be constructed without great difficulty. In particular, cloud models with Gaussianly distributed matter or models with a spectrum of cloud radii are easy to build. As long as clumping is not a function of the total amount of hydrogen, actual optical depths will be given by equation 3.16 where $\eta$ depends on the particular cloud model utilized.

Effective transmissions were recalculated for clouds with optical depths ranging from 1.2 to 90. The results of Chi-square fits using various cloud parameters are shown in Table 3.2. Note that a major effect of additional clumping is to render the interstellar medium more transparent, raising the fraction of the observed flux which would be accounted for by an extension of the diffuse power law flux. In general, this effect dominates changes in the increased extra-galactic flux fraction permitted by the model.

21-cm maps of Galactic hydrogen with sufficient angular resolution in the direction of the LMC to exclude the very high optical depth models (of Table 3.1) have not yet been published. However, there is little reason to believe that such dense clouds exist in the direction of the LMC. The Galactic velocity profiles observed by McGee _et al_. do not possess strong features but rather tend to be smoothly varying with maximum brightness temperatures no greater than 25° and velocity FWHM of 35 km $s^{-1}$.

More generally, the case for strong clumping is weak at high Galactic latitudes. Dieter (1965) concluded that clouds (e.g., velocity features) in the direction of the North Galactic Pole had a median column density of $4.2 \times 10^{19}$ $cm^{-2}$. Lower resolution maps made of the South Galactic pole confirmed that there too, few clouds in excess of $2 \times 10^{20}$ $cm^{-2}$ ($\tau_{0.25\ keV} < 1$) could be identified.

The Hat Creek 21-cm line survey for $|b^{II}| > 10°$ (Heiles 1975) unfortunately does not include the LMC region. However, perusal of the integrated brightness temperature profiles at similar Galactic latitudes reveals few isolated clouds with column densities greater than $10^{20}$ cm$^{-2}$. If 0.25 keV high optical depth clouds exist, the angular size of such clouds must be much smaller than the half power beam width 0.5° of the Hat Creek survey.

Radhakrishnan et al. (1972) have suggested that a substantial fraction of the interstellar H I is diffuse, not clumped into optically thick clouds. In this case non-clumped cloud models are justifiable as long as this diffuse medium is strongly correlated with the total H I column densities since modulation should be qualitatively the same. In fact, modulation should be more apparent, in this case, since average transmission would be increased.

On the other hand, 52 large neutral hydrogen concentrations of average density 1 cm$^{-3}$ with average diameter 575 pc constitute a substantial fraction of the total neutral hydrogen in the LMC (McGee and Milton 1966). As indicated in Table 3.2, however, clumping in the LMC alone does not dramatically alter upper limits for the low energy extragalactic flux. Note that clouds whose optical depth at 0.25 keV exceeds 4 have substantial optical depths at 21 cm, e.g.,

$$\tau_{21\text{-cm}} \sim 0.22 \cdot \tau_{0.25\text{ keV}} \cdot (125°/T_S) \cdot (5\text{ km s}^{-1}/\Delta V) \quad (3.18)$$

where $\Delta V$ is the velocity spread within the cloud. Hence the large

Table 3.2

SIMPLE MODELS OF THE INTERSTELLAR MEDIUM USED TO DERIVE

LOCAL, HALO AND EXTRAGALACTIC FLUX FRACTIONS

| | $\sigma$ ($\times 10^{20}$ cm$^2$) | $\langle T_{GAL} \rangle$ | $\langle T_{GAL+LMC} \rangle$ | $\chi^2$ min$^+$ | Local Flux (%) | Halo Flux (%) | Extragal Flux (%) | Power Law Extens(%) |
|---|---|---|---|---|---|---|---|---|
| | .2 | .401 | .257 | 92.6 | 82-95 | 0-11 | 2-16 | 15 |
| Smooth | .4 | .171 | .075 | 92.0 | 90-94 | 0-9 | 0-9 | 4.5 |
| | .6 | .076 | .024 | 92.1 | 93-98 | 0-7 | 0-5 | 1.4 |
| | $\tau$ | | | | | | | |
| | 1.2 | .184 | .083 | 92.0 | 90-97 | 0-9 | 0-8 | 5 |
| Spherical | 6 | .237 | .119 | 92.0 | 88-97 | 0-9 | 1-12 | 7 |
| Clouds | 24 | .420 | .274 | 92.6 | 81-95 | 0-10 | 0-15 | 17 |
| | 60 | .642 | .516 | 94.4 | 71-97 | 0-14 | 3-28 | 31 |
| | 90 | .734 | .631 | 95.5 | 67-100 | 0-17 | 0-33 | 38 |
| | 69* | .171 | .148 | 93.8 | 88-98 | 0-11 | 0-12 | 9 |

+82 degrees of freedom.

*Only gas in the LMC clumped.

neutral hydrogen concentrations do not appear with full weight in the map of Hindman et al. (1963). Although such clouds are optically thick, they do not fill the beam. Rather, the Hindman et al. map, constructed with the assumption that the gas was optically thin at 21 cm, tends to reflect column densities of the more diffuse gas.

## IV. Source Contamination

The effects of contamination by unknown sources are difficult to account for quantitatively in low angular resolution shadowing experiments. The expected X-ray flux from sources seen between 0.4 and 1.5 keV would account for less than one-third of the observed flux between 0.15 and 0.4 keV, assuming an $E^{-2.5}$ photon power law spectrum and no hydrogen absorption in excess of that due to the Galaxy. Various cloud models were tested on the assumption that one-third or one-sixth of the observed flux originated in the LMC. The source population was assumed to reflect the excess flux observed from the LMC between 0.4 keV and 1.5 keV. Results of these models (Table 3.3) do not substantially change the indicated extragalactic flux fractions, and indeed fit the data less well than simple non-clumped, no source models.

The most luminous 0.25 keV X-ray sources which have been identified in the Galaxy are supernova remnants. The Cygnus Loop is not an Uhuru (2-10 keV) source so, in principle, such sources in the LMC could make an important but unknown contribution to the observed X-ray flux at 0.25 keV. However, if the Cygnus Loop remnant were placed at a

Table 3.3

EFFECTS OF SOURCE CONTAMINATION IN THE LMC

| Cloud Model | LMC Source Strength | $\langle T_{GAL} \rangle$ | $\langle T_{GAL+LMC} \rangle$ | $\chi^2_{min}$ | Local Flux(%) | Halo Flux(%) | Extragal Flux(%) | Power Law Extension(%) |
|---|---|---|---|---|---|---|---|---|
| Smooth | 1/6 | 0.171 | 0.075 | 103.2 | 97-100 | 0-2 | 0-3 | 4.5 |
| $\tau = 69^*$ | 1/6 | 0.171 | 0.148 | 103.2 | 98-100 | 0-2 | 0-2 | 9 |
| Smooth | 1/3 | 0.171 | 0.075 | 158.7 | 97-100 | 0-1 | 0-3 | 4.5 |
| $\tau = 69^*$ | 1/3 | 0.171 | 0.148 | 158.7 | 99-100 | 0-1 | 0-2 | 9 |

distance of 55 kpc, the flux at the top of the atmosphere would be less than 0.01 photons $cm^{-2}$ $s^{-1}$ even if no attenuation due to neutral gas were allowed for. If each of the eleven sources suggested by McGee and Newton (1972) were supernova remnants as bright as Vela or the Cygnus Loop, the maximum number of photons observed in 83 seconds from these sources is estimated to be 1.

Suppose, however, that an unknown source population exists such that the volume emissivity is proportional to the local hydrogen density. This source distribution is particularly easy to deal with because the flux along a given line of sight only depends on the column density of hydrogen. Allowing different constants of proportionality for the emissivity in the Galaxy and the LMC, the observed flux $S_{obs}$ takes on the functional form

$$S_{obs} = S_G(1 - e^{-\tau_G}) + S_H\, e^{-\tau_G} + S_{LMC}\, e^{-\tau_G}(1-e^{-\tau_{LMC}}) + S_{EX}\, e^{-\tau_{LMC+G}} \quad (3.19)$$

where the subscripts G, H, LMC and EX refer to the Galactic, halo, LMC, and extragalactic contributions respectively. Note that this equation can be rewritten in the form of equation 3.2, e.g.,

$$S_{obs} = S_G + e^{-\tau_G}(S_H + S_{LMC} - S_G) + e^{-\tau_{G+LMC}}\,(S_{EX} - S_{LMC}) \quad (3.20)$$

If we utilize the flux fractions obtained using non-clumped models and normalize all fluxes S by the total observed flux of approximately 150 photons $(cm^2\ s\ keV\ sr)^{-1}$, then

$$0.90 \leq S_G \leq 0.94 \tag{3.21}$$

$$0.0 \leq 0.17\ (S_H + S_{LMC} - N_G) \leq 0.09 \tag{3.22}$$

$$0.0 \leq 0.075\ (S_{EX} - S_{LMC}) \leq 0.09 \tag{3.23}$$

3.21 and 3.22 imply

$$0.90 \leq S_H + S_{LMC} \leq 1.44 \tag{3.24}$$

and thus

$$0.0 < S_{LMC} < 1.44 \tag{3.25}$$

Rewriting equation 3.23

$$0.0 < S_{EX} - S_{LMC} < 1.20 \tag{3.26}$$

and using equation 3.25

$$0.0 < S_{EX} < 2.64 \tag{3.27}$$

In principle then, the incident extragalactic flux can be as large as 400 photons $(cm^2\ s\ keV\ sr)^{-1}$, still considerably smaller than the extragalactic flux predicted from most measurements of the North Galactic Pole. However, in this limit, the incident flux on the Galaxy from the LMC is

$$S_{LMC}\ (1 - e^{-\tau_{LMC}}) \simeq 0.82 \tag{3.28}$$

or approximately 123 photons $(cm^2\ s\ keV\ sr)^{-1}$. Assuming a distance of 55 kpc to the LMC, this flux corresponds to a luminosity of $3 \times 10^{40}$ erg $s^{-1}$ between 0.15 and 0.28 keV, whereas typical estimates of Galactic emission usually lie around $10^{39}$ ergs $s^{-1}$ in this energy range (see Chapter I, Section IV). Since the hydrogen gas mass as well as the total mass of the LMC is approximately one-tenth that of the Galaxy, the luminosity per unit mass in the LMC must exceed that of the Galaxy by at least two orders of magnitude. We regard this luminosity as unreasonable. This flux is a factor of more than 7 times that of the photon flux observed between 0.4 and 1.5 keV. If, on the other hand, the LMC luminosity is constrained not to exceed that of the Galaxy

$$S_{EX} < 1.3 \ . \tag{3.29}$$

The derived extragalactic flux is less than 200 ± 35 photons $(cm^2$ s keV sr$)^{-1}$. (The error is due only to inaccurate knowledge of the incident flux on the detector.) Thus, although arbitrary source populations can produce the observed isotropy, this model, which was used by Davidsen et al. (1972) to determine an extragalactic flux (described in Chapter I, Section II) of 500 photons $(cm^2$ s keV sr$)^{-1}$, does not seem to allow both apparent isotropy in the direction of the LMC and a large extragalactic flux based on the Caltech observations.

## V. Absorption Properties of the Interstellar Medium

Observed flux fractions are not very sensitive to changes in effective cross section (Table 3.2). The major effect of raising the cross section is to reduce the average transmission of the interstellar medium, increasing the excess observed flux over a power law extension allowed by the data.

Below 0.28 keV, the effective cross section is due mainly to hydrogen and helium. Uncertainties arise chiefly from the unknown amount of molecular hydrogen, which does not radiate at 21 cm and which has a large cross section at low energies.

Reddening may be used as an alternative indicator of the amount of interstellar matter along lines of sight to the LMC. Variations in the reddening of stars in the LMC are predominantly due to dust within the LMC itself and Galactic absorption is small. Using the reddening relation of Jenkins and Savage (1974, $N_H/E_{B-V} = 7.5 \times 10^{21}$ atoms $cm^{-2}$ $mag^{-1}$) and the observed foreground reddening of $E_{B-V} = 0.07 \pm 0.04$ mag (Feast *et al*. 1960) leads to a predicted $\langle N_H \rangle = 5.3 \pm 2.0 \times 10^{20}$ atom $cm^{-2}$, close to typical values of $N_H$ derived from 21-cm data for the Galaxy alone. Such low total extinction renders unlikely the possibility that significant fractional abundances of molecular hydrogen exist, since $H_2$ is destroyed unless shielded from interstellar UV in clouds with $E_{B-V} \gtrsim 0.3$ (Hollenbach *et al*. 1971). (Note that clumping which renders the interstellar medium more transparent tends to nullify the effects of molecular hydrogen formation.)

## VI. An Alternative Approach to Determining Flux Fractions

An alternative, simpler, and possibly more intuitive approach to determine the magnitude of the extragalactic excess is to assume that very little halo flux exists. Then if modulation of the diffuse X-ray background is due to hydrogen along the line of sight (or if the emissivity of space is proportional to the hydrogen density), the observed flux $S_{obs}$ has the functional form

$$S_{obs} = \eta_{eff} \left(S_L + S_{EX}\, e^{-\tau_{LMC+G}}\right) \tag{3.30}$$

By selecting two blocks of data, one in which the absorption is relatively small and one in which the absorption is relatively large, the ratio $R = S_{EX}/S_L$ can be determined. For any block of data, the average observed flux

$$\langle S_{obs} \rangle = \eta_{eff} \left(S_L + S_{EX} \langle e^{-\tau} \rangle\right) \tag{3.31}$$

where the effective efficiency of the detector is assumed to be constant for both portions of the flux. The ratio of the two blocks of data is given by

$$\frac{\langle S_{obs} \rangle_1}{\langle S_{obs} \rangle_2} = \frac{1 + R \langle e^{-\tau} \rangle_1}{1 + R \langle e^{-\tau} \rangle_2} \tag{3.32}$$

As long as $R \langle e^{-\tau} \rangle \ll 1$, equation 3.32 can be rewritten

$$R = \frac{S_{EX}}{S_L} = \left\{ \frac{\langle S_{obs} \rangle_1}{\langle S_{obs} \rangle_2} - 1 \right\} \left\{ \frac{1}{\langle e^{-\tau} \rangle_1 - \langle e^{-\tau} \rangle_2} \right\} \qquad (3.33)$$

As indicated in Table 3.4, two blocks of data have been selected, one in which the total transmission was always greater than 12% and one in which the transmission was always less than 4%. The average transmissions of the two blocks of data differ by a factor of six. The ratio of the unabsorbed fluxes as calculated by equation 3.33 is

$$R = \frac{S_{EX}}{S_L} = 1.1 \pm 0.3 \qquad (3.34)$$

The extragalactic flux fraction observed on the entire flight is given by

$$F_{EX} = \frac{S_{EX} \langle e^{-\tau_{LMC}} + G \rangle}{S_L + S_{EX} \langle e^{-\tau_{LMC}} + G \rangle} = \frac{R(e^{-\tau_{LMC}} + G)}{1 + R\, e^{-\tau_{LMC}} + G} \qquad (3.35)$$

where average transmissions are taken over the whole flight.

$$F_{EX} = 8 \pm 2\% \qquad (3.36)$$

This should be compared to the $2\sigma$ upper limit of 9% when the extragalactic flux fraction is computed by the detailed Chi-squared method.

An identical calculation can be made assuming that the halo flux dominates the extragalactic flux (or that the LMC is not an efficient absorber of X-rays, also shown in Table 3.4.) In this case

$$\frac{S_H}{S_L} = 0.5 \pm 0.2 \qquad (3.37)$$

Table 3.4

DATA USED IN THE HIGH TRANSMISSION - LOW TRANSMISSION MODEL

TO CALCULATE EXTRAGALACTIC FLUX FRACTIONS

| | Trans Criteria | Data Used | Average Trans | Average X-Ray Flux(0.15-0.4 keV) Counts $s^{-1}$ | Non-local Flux |
|---|---|---|---|---|---|
| Extragalactic Model | | | | | |
| High Total Transmission | > 12% | 199-219 | 20% | 44.6 ± 1.5 | 8 ± 2% |
| Low Total Transmission | < 4% | 226-252 | 3.2% | 37.4 ± 1.2 | |
| Halo Model | | | | | |
| High Galactic Transmission | > 23% | 195-222 | 31% | 43.1 ± 1.3 | 7 ± 3% |
| Low Galactic Transmission | < 12% | 229-253 | 8.6% | 39.1 ± 1.3 | |

The average whole flight Galactic transmission of 17% leads to an observed halo flux fraction of 7% ± 3%, consistent with the results obtained using the Chi-squared method.

Unfortunately, the LMC is not an effective enough absorber to allow separation of the halo, extragalactic and local fluxes, a fact also indicated by the Chi-squared fits. Nevertheless, results of flux fractions as determined in this manner are qualitatively similar to results obtained using the Chi-squared method and indicate that the flux fractions obtained are not dominated by the noisy nature of the 1-second summaries.

## VII. A Final Approach--$N_H$ Dependent Cross Sections

An improvement over the fixed effective cross section model of absorption for the interstellar medium can be made by allowing for the effects of spectral slope and of the amount of hydrogen along the line of sight in calculation of $\sigma_{eff}$, the effective cross section. $\sigma_{eff}$ is given by

$$e^{-\sigma_{eff} N_H} = \frac{\int_{E_{min}}^{E_{max}} \eta(E)\, e^{-\sigma(E) N_H}\, S(E)\, dE}{\int_{E_{min}}^{E_{max}} \eta(E)\, S(E)\, dE} \qquad (3.38)$$

where S(E) is the unabsorbed differential photon spectrum. The detector efficiency $\eta(E)$ includes not only the transmission properties of the window and the absorption properties of the counter gas, but also the effects of resolution spreading. The third effect primarily reduces the efficiency for counting X-rays below 0.2 keV.

Since the cross section, approximately given by

$$\sigma = 0.39 \times 10^{-20} \left( \frac{0.25 \text{ keV}}{E} \right)^3 \text{ cm}^2 \qquad (3.39)$$

(Brown and Gould 1970), is sharply increasing at low energies, a steep unabsorbed spectrum results in a higher effective cross section.

The amount of interstellar hydrogen also effectively changes the mean energy of X-rays incident on the counter. When $N_H$ is large, nearly all X-rays which have penetrated the medium must have had an energy near 0.28 keV, while for small $N_H$, the effects of differing absorption on longer and longer wavelength photons are evident in the counting rate, thus increasing the effective cross section.

The value of $\sigma_{eff}$ as a function of $N_H$ and of the spectral slope $\alpha$ is shown in Figure 3.3. As can be seen, the value of the effective cross section used in the fixed value model is applicable only when $\alpha \gtrsim -2$ and for $N_H$ larger than $6 \times 10^{20}$. Typical X-ray spectra of the diffuse X-ray background are dominated by a bremsstrahlung term with $kT \sim 0.3$ keV. For $E < kT$ a bremsstrahlung photon spectrum has a slope which varies between -1 and -2. The value of $0.4 \times 10^{-20}$ cm$^2$ used in the fixed-value model was somewhat lower than optimum in the case where $N_H < 6 \times 10^{20}$ cm$^2$. The average value of $N_H$ for the LMC plus the Galaxy was approximately $7 \times 10^{20}$ cm$^{-2}$.

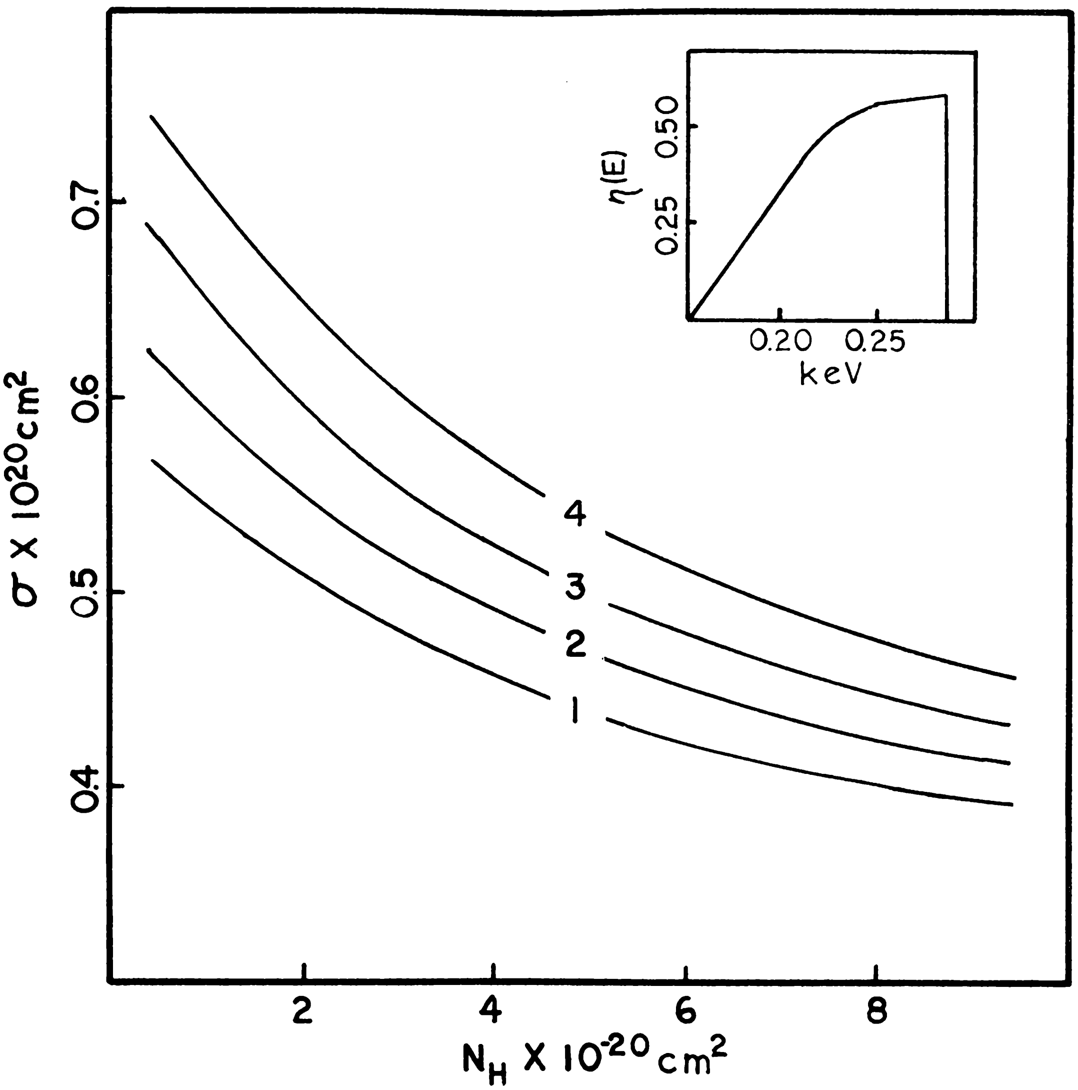


Figure 3.3

The effective cross section of the ISM depends on the hydrogen column density as well as the spectral slope. Effective cross sections for photon power law spectra ($E^{-\alpha}$, $1 \leq \alpha \leq 4$) are shown. The insert indicates the probability that an incident X-ray of energy E will be counted as an X-ray between 0.15 and 0.4 keV.

Since the average transmission by the low $N_H$ regions is less than that predicted by the fixed cross section model, models in which the variation of $\sigma_{eff}$ was explicitly allowed for have been calculated (Table 3.5). Observed flux fractions are nearly identical to the models where $\sigma_{eff}$ was fixed. However, a decrease in the average transmission results in somewhat increased incident extragalactic fluxes between 0.15 and 0.28 keV. The decrease in the average transmission is due to the fact that low $N_H$ regions which have a high effective cross section have relatively more importance in determining the average transmission than high $N_H$, low effective cross section regions. (The error in the maximum allowed flux fractions is due to the lack of knowledge of the spectral shape of photons actually incident on the counter. This error could in principle be eliminated by assuming the local spectrum has an identical shape to the unattenuated extragalactic and halo fluxes.)

We conclude that the extragalactic flux incident on the Galaxy at 0.215 keV is unlikely to exceed 250 photons $(cm^2\ s\ keV\ sr)^{-1}$, or 54 keV $(cm^2\ s\ keV\ sr)^{-1}$ in energy units. This upper limit is a factor of from 2 to 4 lower than fluxes obtained by assuming the North Polar flux is purely of extragalactic origin, and a factor of 2 below the extragalactic flux obtained by Davidsen _et al_. (1972). The results confirm, and are in fact stronger than results of the SMC shadowing experiment reported by McCammon _et al_. The extragalactic enhancement at 0.25 keV seems to be not much more

Table 3.5

FLUX FRACTIONS DETERMINED USING $N_H$ DEPENDENT CROSS SECTIONS

| $\alpha$ | $\langle Trans \rangle_G$ | $\langle Trans \rangle_{G+LMC}$ | $\chi^2_{min}$ | Observed Fraction(%) Local | Halo | Extra | Power Law Ext(%) | Maximum Extragalactic Flux at 0.215 keV (photons $keV^{-1} cm^{-2} s^{-1}$) |
|---|---|---|---|---|---|---|---|---|
| -1.5 | 0.130 | 0.060 | 92.01 | 89-98 | 0-9 | 0-10 | 4.4 | 227 ± 23 |
| -2 | 0.122 | 0.056 | 92.00 | 89-97 | 0-9 | 0-9 | 4.1 | 235 ± 23 |
| -3 | 0.106 | 0.047 | 92.01 | 90-97 | 0-9 | 0-9 | 3.4 | 232 ± 23 |

than a factor of two greater than an 11 $E^{-1.5}$ photon power law would predict and indeed is consistent with no extragalactic enhancement at all.

## VIII. The Intergalactic Medium

The possible existence of a substantial intergalactic medium (IGM) is an important but controversial question--important because the IGM may contain most of the mass energy of the Universe, controversial because unambiguous verification of its existence has not been demonstrated. The basic thrust of investigations has been to attempt to determine whether the density of the IGM can provide sufficient mass energy to close the Universe. The critical density $\rho_c$ is

$$\rho_c = \frac{3H_o^2}{8\pi G} = 4.7 \times 10^{-30} \left( \frac{H_o}{50 \text{ km s}^{-1} \text{ Mpc}^{-1}} \right)^2 \text{ g cm}^{-3} \qquad (3.40)$$

where $H_o^{-1}$ is the Hubble time and G is the gravitational constant.

The smoothed mass energy of known matter in galaxies and of photons is much less than the critical density. According to Noonan (1971)

$$\rho_{Galaxies} \sim 7.5 \times 10^{-32} \text{ g cm}^{-3} \qquad (3.41)$$

which leads to a value of $\Omega(\text{Galaxies}) = \frac{\rho_{Gal}}{\rho_c} \sim 0.016$ (a result which is independent of the Hubble constant). $\Omega$(photons) is even smaller. Suggestions of appreciable mass energy from forms of energy which are difficult to detect include a sea of neutrinos, gravitational radiation, and the IGM. The basic problem and current observational limits have been reviewed by Field (1972). The relevance of the recent discovery of intracluster gas in rich clusters of galaxies has been discussed by Field (1973).

If the intergalactic medium does provide the closure density, the matter must be almost completely ionized. Limits on the neutral hydrogen are derived from Lyman-$\alpha$ absorption of quasars at $z = 2$ (assumed cosmological in origin) and from 21-cm absorption in the spectra of radio galaxies. Limits on a partially ionized gas were derived based on the expected recombination emission. Results are summarized in Figure 3.4.

As pointed out by Hoyle (1963), if the IGM were hot, greater than $10^5$°K,the best hope of detection would be in the X-ray band. Models for expected emission, assuming adiabatic expansion, were initially carried out by Field and Henry (1964). Before considering this model, we discuss a simple non-relativistic, non-expanding model, which although ignoring cosmology, describes simply what is being measured and as it turns out, provides reasonable order of magnitude estimates of the allowed density.

## IX. Qualitative Non-cosmological Model

The emissivity of a pure hydrogen plasma at temperature T is given approximately by

$$\varepsilon = 9.2 \times 10^{-11} \exp(-E/kT)\ T^{-1/2}\ n_e^{\,2}\ \mathrm{keV(cm^3\ s\ keV\ sr)^{-1}} \qquad (3.42)$$

where $n_e$ is the electron density and E is the energy at which the X-ray flux is being measured. (This formula, taken from Allen 1973, p. 102, was converted to X-ray units. The Gaunt factor g, which is of order 1, has been set equal to 1.) The X-ray flux due to bremsstrahlung can be rewritten in terms of an emission measure defined by

$$EM = \int_o^L n_e^{\,2}\ d\ell \qquad (3.43)$$

Thus the observed flux

$$S = 9.4 \times 10^{-11} \exp(-E/kT)\ T^{-1/2}\ EM \qquad (3.44)$$

For cosmological purposes the emission measure is usually rewritten in terms of a clumping factor

$$C = \frac{\langle n_e^{\,2}\rangle}{\langle n_e\rangle^2} \qquad (3.45)$$

A uniform density plasma has the smallest possible clumping factor of 1. Thus for a hydrogen plasma with given $n_e$

$$EM = C\ \langle n_e\rangle^2\ L = C\Omega^2\ EM(\Omega = 1,\ C = 1) \qquad (3.46)$$

The experimentally measured quantity S, the X-ray flux, is used to determine $C\Omega^2$, the ratio of the observed emission measure to the emission measure of a uniform plasma at the critical density. In the non-relativistic, non-expanding model the Hubble distance $1.6 \times 10^{28}$ cm is the relevant length. (Unless otherwise stated the Hubble parameter is assumed to be 50 km $s^{-1}$ $Mpc^{-1}$.) The critical emission measure, assuming a pure hydrogen plasma is

$$EM_{crit} = 1.3 \times 10^{17} \text{ cm}^{-6} = 0.043 \text{ cm}^{-5} \text{ pc} \tag{3.47}$$

Note that this emission measure, like the emission measure of the diffuse flux in the plane of the Galaxy, is not amenable to most standard astrophysical observations of ionized gas. Assuming an upper limit to the extragalactic flux of 54 keV $(cm^2 \text{ s keV sr})^{-1}$ as measured at approximately 0.215 keV, the observed emission measure is given by

$$EM_{obs} \leq 5.8 \times 10^{16} \exp(2.5/T_6)\ T_6^{1/2} \tag{3.48}$$

Thus

$$C\Omega^2 \leq 0.45 \exp(0.25/T_6)\ T_6^{1/2} \tag{3.49}$$

where $T_6$ is the plasma temperature in millions of degrees. Upper limits for $C\Omega^2$ using this qualitative model are shown in Figure 3.4 and indicate that if the IGM contains enough matter to close the Universe, that either clumping is small or the temperature is not in the neighborhood of 1 to 50 x $10^6$°K.

## X. Instantaneous Heating and Adiabatic Expansion

Field and Henry (1964) attempted to calculate the expected X-ray intensity for the IGM with $\Omega = C = 1$. Both steady state and Big Bang cosmologies ($q_o = 1/2, 1$) were considered. Temperatures in the evolving models were assumed to vary adiabatically

$$T = T_o \ (V/V_o)^{\gamma-1} \tag{3.50}$$

where T and V are the temperature and proper volume respectively, and o refers to the present day value. The value $\gamma = 5/3$ corresponds to adiabatic expansion by an ideal gas. At 0.25 keV, electrons are not relativistic so that if the IGM were not gaining or losing energy, $\gamma$ should be approximately 5/3. Photon pressure is negligible. If the medium is gaining (losing) energy, $\gamma$ would be less (greater) than 5/3. If $\gamma$ is less than 2 and greater than 4/3 a cutoff at $z = z_o$ must be introduced to prevent the flux from diverging. This is due to the fact that in this range of $\gamma$ the density increase dominates all other effects, e.g., temperature increases and the reduced flux of objects at cosmological distances. The introduction of a cutoff corresponds to the assumption of instantaneous heating or creation of the IGM at some redshift $z = z_o$.

For similicity, only the model with $q_o = 1/2$ and $\gamma = 5/3$ is considered here. Limits derived using other values of $q_o$ and $\gamma$ are qualitatively similar. With $q_o = 1/2$ and $\gamma = 5/3$, Field and Henry show that

$$S = S_o \int_{w_o}^{1} \exp(-Ew/kT_o) \ w^{-3/2} \ dw \tag{3.51}$$

where $w_o = 1/(1+z_o)$ and where $S_o$ (converted to X-ray units) is given by

$$S_o = 9.4 \times 10^{-11} \, n_o^{\,2} T_o^{\,-1/2} \, C \, H_o^{\,-1} \ \mathrm{keV(cm^2 \ s \ keV \ sr)^{-1}}$$
$$= 2.1 \times 10^2 \, T_6^{\,-1/2} \qquad (3.52)$$

for a pure hydrogen plasma at the critical density with $T_6$, the present-day temperature. Since the IGM may contain primordial helium and possibly even heavy elements, the emissivity calculated in this manner is a lower limit to the expected X-ray flux. As in the "non-cosmological" model, the ratio of the observed emission to the predicted emission with $\Omega = C = 1$ determines the quantity $\Omega^2 C$. Results are plotted in Figure 3.4 with $z_o = 1$ and $z_o = 9$ and an assumed upper limit of 54 keV $(\mathrm{cm^2 \ s \ keV \ sr})^{-1}$. This upper limit is inconsistent with an IGM of sufficient density to close the Universe over a wide range of temperatures unless heating was relatively recent, more recent than quasar or galaxy formation.

The above model of Field and Henry, with $z_o = 1$, has become the standard model with which to compare extragalactic fluxes with possible intergalactic gas at the closure density, despite the fact that severe criticisms can be made. In particular, the nature of the gas prior to $z_o = 1$ is unexplained since the introduction of a cutoff corresponds to instantaneous heating of the IGM. Neutral matter would presumably be evident in the Lyman $\alpha$ absorption measurements of quasars. Accepting the model, however, the lowered upper

Figure 3.4

Upper limits to $\Omega^2C$ are shown, based on the observed X-ray spectrum above 2 keV, the upper limit to the extragalactic flux at 0.215 keV derived in this experiment, and the upper limit to the extragalactic Lyman-α flux obtained by Kurt and Sunyaev (1967). We have interpreted the X-ray data using the model of Field and Henry (1964) with $q_o = 1/2$ and $\gamma = 5.3$. If the IGM were photoionized, limits on $\Omega^2C$ are much weaker than if the IGM were collisionally ionized. Hence, we have included a photoionization model due to Arons and McCray (1969). The curves based on the Lyman-α data should be regarded with some caution in any event. The Kurt and Sunyaev upper limit on the extragalactic flux of 1 x $10^{21}$ ergs (cm$^2$ s Hz sr)$^{-1}$ between 1225 and 1340 Å is based on their determination of the latitude dependence of diffuse UV radiation. In a similar experiment, Hayakawa et al. (1969) reported an upper limit of 1.1 x $10^{20}$ ergs (cm$^2$ s Hz sr)$^{-1}$ between 1350 and 1480 Å, an order of magnitude larger than the Kurt and Sunyaev result. A similar figure, based on the McCammon et al. (1971) soft X-ray upper limit, has been discussed by Bunner (1974).

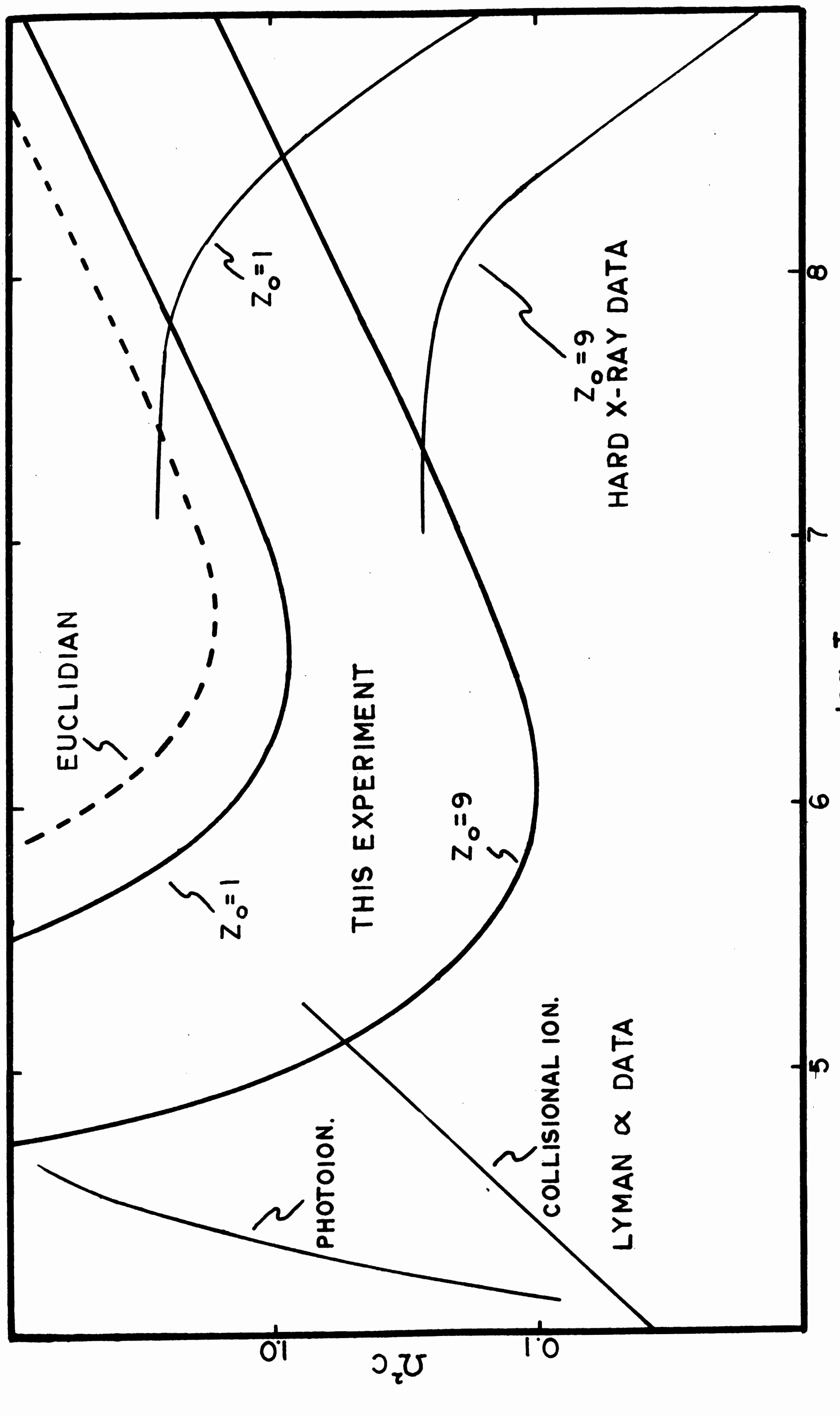
EUCLIDIAN
$Z_o$=1
THIS EXPERIMENT
$Z_o$=9
$Z_o$=1
$Z_o$=9
HARD X-RAY DATA
PHOTOION.
COLLISIONAL ION.
LYMAN α DATA
5
6
7
8
log $T_o$
1.0
0.1
$\Omega_c$

limits on the extragalactic flux imply that essentially no clumping is allowed if the IGM has a present day temperature between $10^6$°K and 2.5 x $10^7$°K, whereas non-shadowing measurements had indicated that $\Omega^2 C$ might be 3 or more in this range.

# CHAPTER IV

# THE SOFT X-RAY BACKGROUND NEAR ERIDANUS

## I. Introduction

In this chapter, we discuss observations and possible interpretations of three enhanced background regions near the constellation of Eridanus. Two of these regions were observed on experiment 2 of the Caltech Australian flights which took place on 9 November 1973 at 17:15 UT, while the third region in Monoceros-Gemini had been observed on a previous flight with the same payload which took place on 24 March 1973 at 3:30 UT. The three regions are all spatially extended and exhibit similar X-ray spectra. Optical and radio observations exhibit no strong correlations from region to region. There are no obvious signatures of what constitutes an X-ray enhancement.

At the time of the Australian flights the strongest soft X-ray feature in the Southern Galactic Hemisphere which had been observed was a 15° x 30° "hot spot" in the constellation of Eridanus (Davidsen *et al*. 1972). Radio maps reveal no outstanding features, although a small radio spur can be seen on the 150 MHz map of Landecker and Wielebinski (1970) between the center of the emission region and the Galactic Plane. Reynolds *et al*. (1974) have reported relatively intense diffuse $H_\alpha$ emission from the general region, which includes not only the spectacular $H_\alpha$ filament known as Barnard's Loop, but also

Figure 4.1

The scan path on flight 2 in the Eridanus region. The first slow scan begins at an R.A. of approximately 81.7 and dec of -17.7. Positions determined from star field photographs are indicated by "crosses" (see the Appendix, Section III). Other marked positions are Uhuru sources, some of which are labeled.

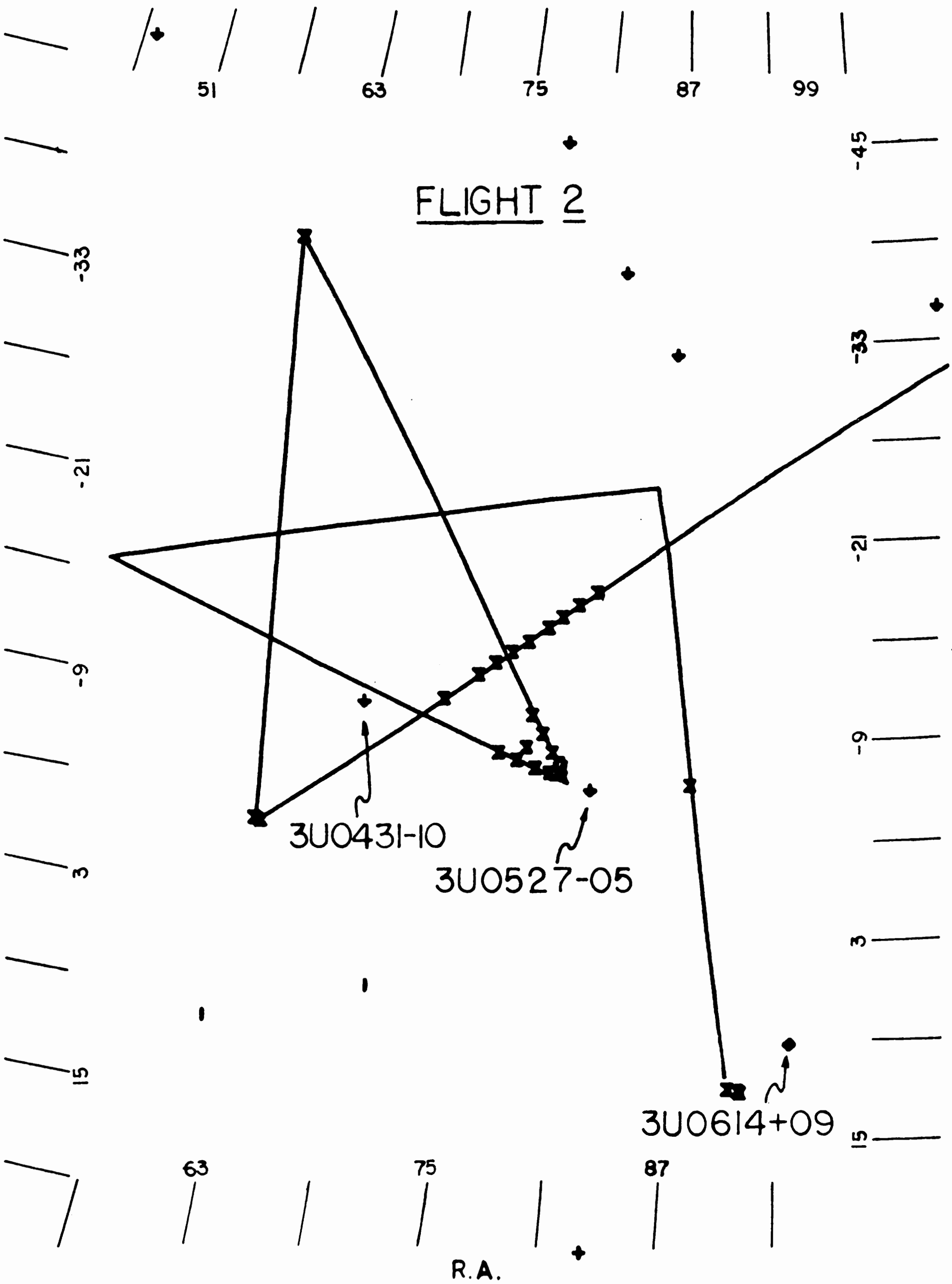
FLIGHT 2
51
63
75
87
99
-33
-21
-9
3
15
-45
-33
-21
-9
3
15
dec
3U0431-10
3U0527-05
3U0614+09
63
75
87
R.A.

several much fainter loop structures centered near the X-ray emission region seen more clearly in the $H_\alpha$ survey of Sivan (1974). As seen in Figure 1, 160 seconds of flight 2 were dedicated to the Eridanus "hot spot" region, in a series of five 1.25° $s^{-1}$ scans, each approximately 30° long. (The aspect solution is described in the Appendix.) The scan path included one of the deep minima in continuum radio emission ($l^{II}$ = 240°, $b^{II}$ = -30°) as well as the weak Uhuru source 3U0527-05 in the Orion Nebula. Hydrogen column densities varied between 1 x $10^{20}$ atoms $cm^{-2}$ at high Galactic latitudes to in excess of 10 x $10^{20}$ atoms $cm^{-2}$ near the Galactic plane.

The anisotropic nature of the emission region is clearly visible in the 0.15 to 0.4 keV channel of the raw data of the 5° x 10° counter between 165 and 325 seconds (Figure 4.2). High count rates between 140 and 160 seconds were due to the Vela supernova remnant, studied on a previous flight (Moore 1975). A telemetry dropout from which data recovery was marginal occurred between 194 and 216 seconds. (The attempt to meld together tapes from various ground stations is also discussed briefly in the Appendix.)

A crude map of emission observed in the 5° x 10° propane counter is shown in Figure 4.3. Two distinct emission regions emerge. The enhancement near $l^{II}$ = 205°, $b^{II}$ = -45°, hereafter designated the "Eridanus" enhancement, is undoubtedly a Galactic feature, since the measured hydrogen column density in this direction is approximately 5 x $10^{20}$ atoms $cm^{-2}$, representing an opacity of 2 optical depths at

Figure 4.2

Raw counting rates obtained from the 5° x 10° propane counter on flight 2 in three energy intervals. The enhancements designated as the low $N_H$ and Eridanus regions appear between scans 2 and 3 and during scan 4 respectively. A telemetry dropout (TM) occurred near 200 seconds after liftoff, which could not be recovered (see the Appendix, Section V). Counting rates during voltage calibrations of the telemetry system have been set to zero. Note that counting rates during the Cen X-3 portion of the flight indicate enhanced emission between 0.4 and 1.5 keV, as discussed in Chapter V.

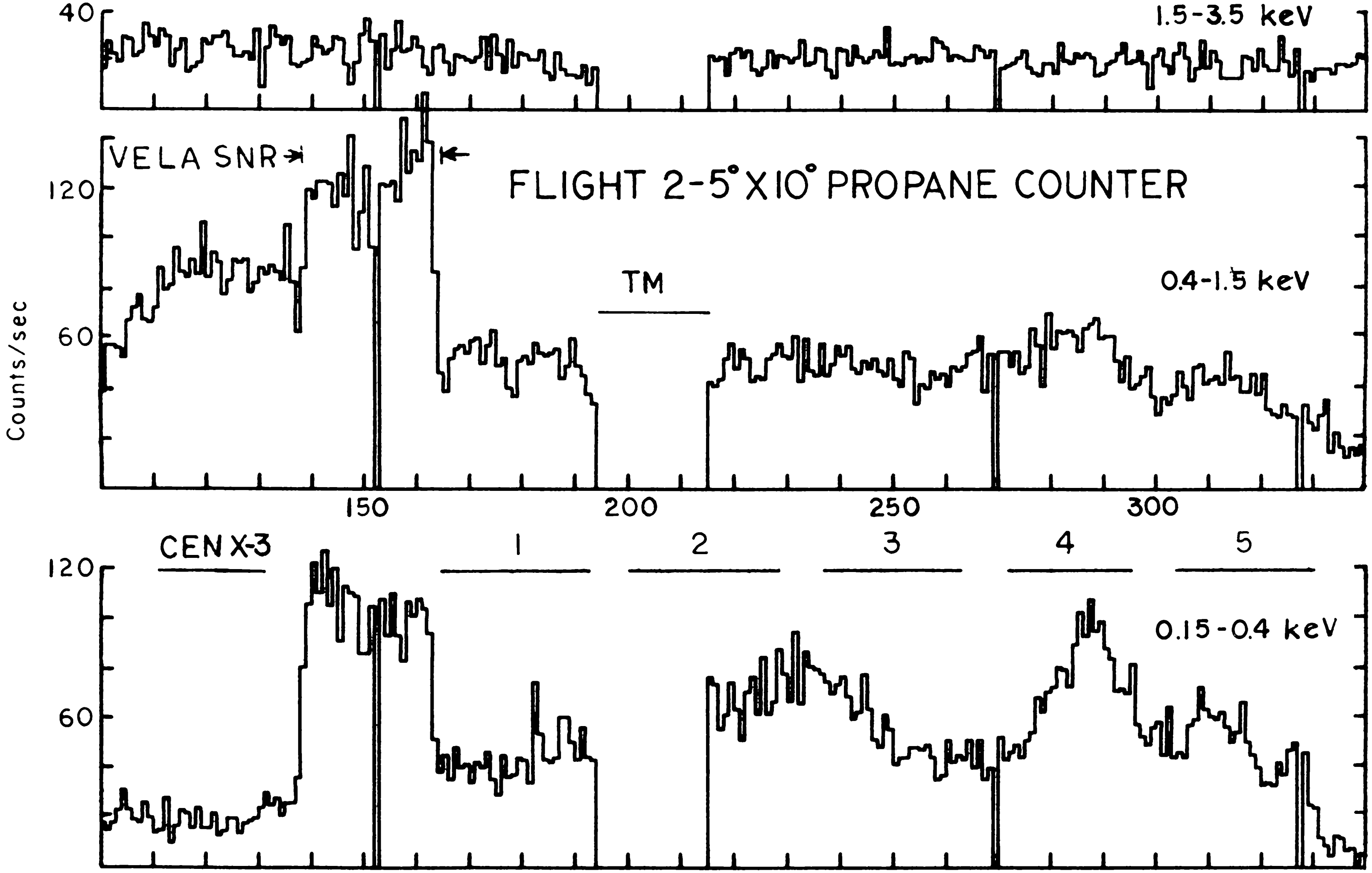
40
1.5-3.5 keV
VELA SNR
FLIGHT 2-5° X10° PROPANE COUNTER
120
TM
0.4-1.5 keV
60
Counts/sec
150
200
250
300
CEN X-3
1
2
3
4
5
120
0.15-0.4 keV
60

Figure 4.3

In this figure we superimpose the scan path on a contour map of Galactic transmission at 0.25 keV as determined from the neutral hydrogen maps. Three-second sums corrected for deadtime and atmospheric absorption of the X-ray counting rate between 0.15 and 0.4 keV in the 5° x 10° propane counter are shown.

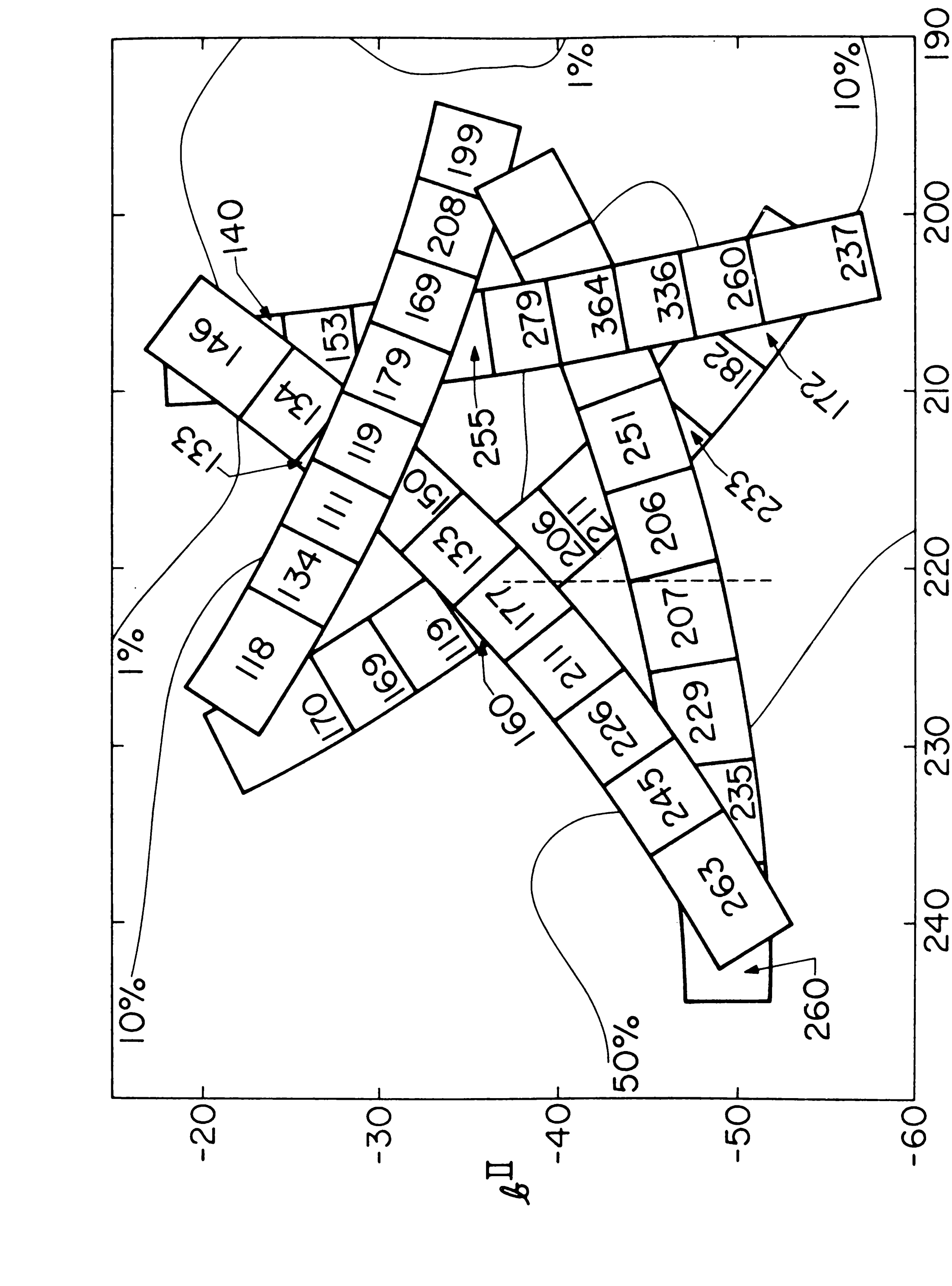

190
200
210
220
230
240
-20
-30
-40
-50
-60
ℓII
bII
10%
1%
50%
10%
1%
199
208
169
179
119
111
134
118
146
134
153
140
133
279
364
336
260
237
182
172
255
150
133
177
211
226
245
263
206
211
251
206
207
229
235
233
170
169
119
160
260

0.25 keV. On the other hand, the "low $N_H$" enhancement, appearing at the corner of the "star", more clearly seen in the 1 second summaries (Figure 4.2) between t = 220 and 235 s, lies in a direction in which the hydrogen column density is no greater than at the Galactic poles.

The gross characteristics of the nature of the soft emission are verified by counter 2, one of the 2° x 20° propane detectors as shown in Figure 4.4. Unfortunately, the gain of the other 2° x 20° counter, #1, increased rapidly after 200 seconds of flight so that a similar map from that counter could not be produced. However, counter 2 furnishes the first scans available of this region on a scale of 2°. The raw data (Figure 4.5) seem to indicate that the region is truly diffuse. However, in some cases a point source with incident X-ray flux between 0.15 and 0.28 keV of 0.3 counts $(cm^2\ s)^{-1}$ would not be ruled out, whereas the maximum incident excess flux observed in the 5° x 20° propane counter was 0.5 counts $(cm^2\ s)^{-1}$ in this energy range. Any point source would have been in the FOV for approximately 4 seconds. Although the Eridanus region is clearly anisotropic, the possibility of making maps using reconstruction techniques applicable to long, narrow collimators is clearly not possible due to the low signal to noise. The total flux observed in counters 2 and 3 during the flight was comparable.

Figure 4.4

A very crude map of 0.25 keV emission in the Eridanus region as determined with the 2.0° x 20° propane counter (#2). Shaded areas are those in which the 1-second counting rate between 0.15 and 0.4 keV was 1σ or greater above the average counting rate for the Eridanus scans. Times in which the counting rate exceeded the average by between 2 and 3 and between 3 and 4σ are indicated.

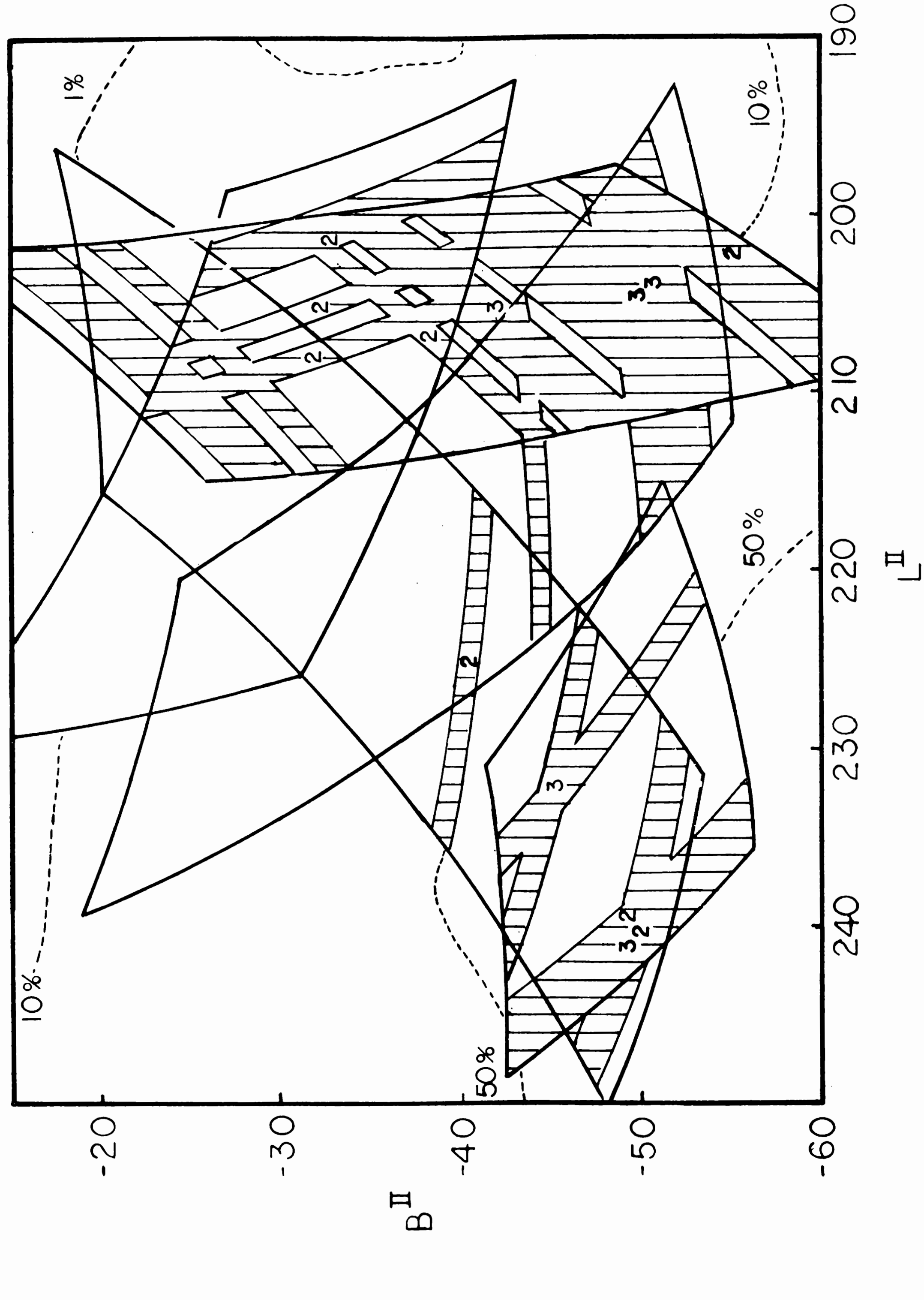

190
200
210
220
230
240
$L^{II}$
-20
-30
-40
-50
-60
$B^{II}$
1%
10%
10%
50%
50%

Figure 4.5

Same as Figure 4.2 for the 2° for the 2° x 20° propane counter (#2).

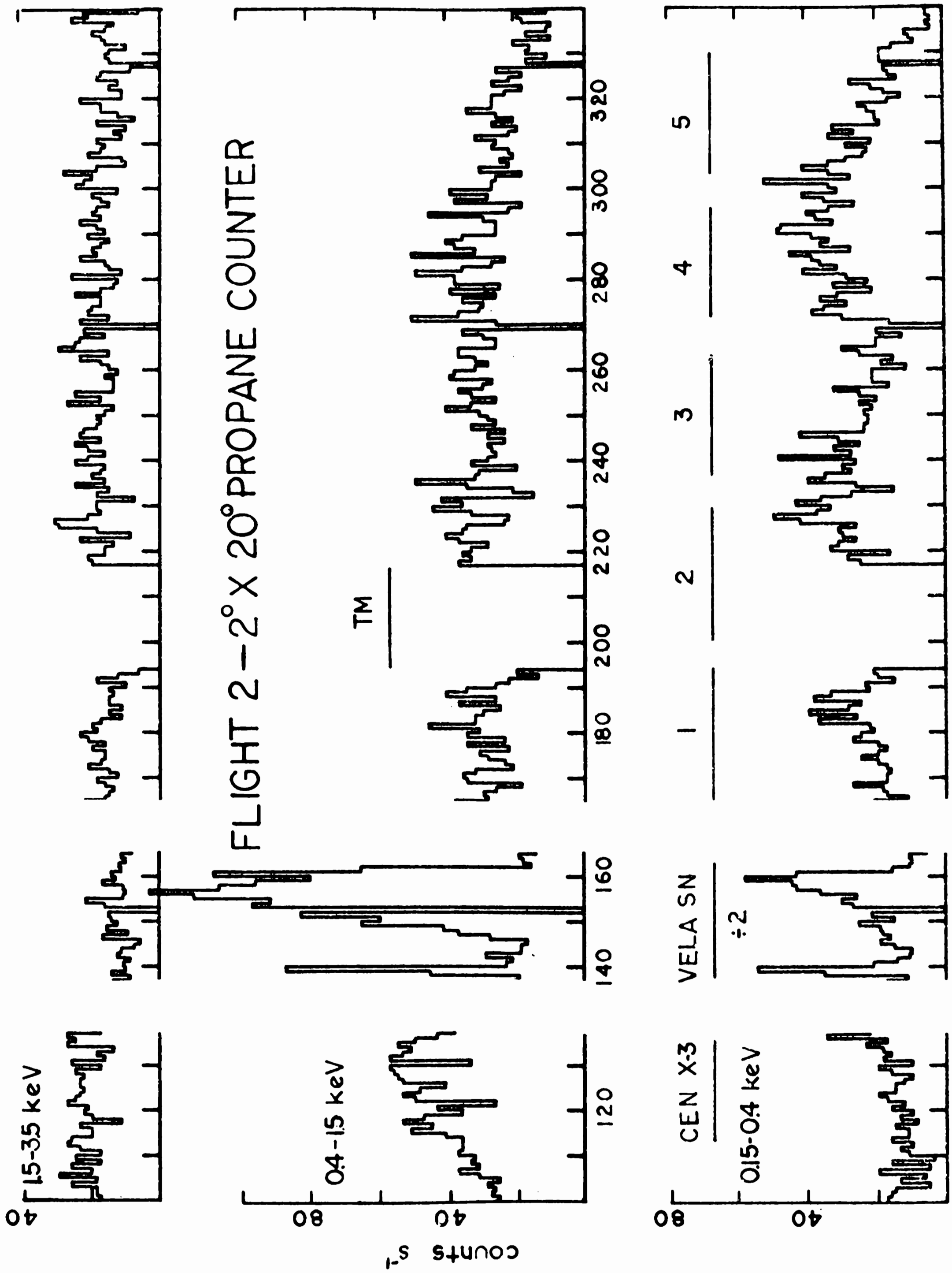
FLIGHT 2 — 2° X 20° PROPANE COUNTER
1.5-3.5 keV
0.4-1.5 keV
0.15-0.4 keV
CEN X-3
VELA SN
÷2
TM
1
2
3
4
5
counts s⁻¹
40
80
40
80
40
120
140
160
180
200
220
240
260
280
300
320

## II. Other X-ray Observations

Since November 1973, a reasonably good soft X-ray map of much of the Southern Galactic Hemisphere near Eridanus has become available as part of the Wisconsin whole sky survey (Williamson et al. 1974). The Wisconsin map, made with a resolution of $\sim 6.5°$, confirms the existence of two apparently separate regions of X-ray enhancement, but in addition provides more uniform coverage. The Eridanus enhancement centered at $l^{II} = 205°$, $b^{II} = -40°$ with typical dimension of 20°, appears separated by a ridge of decreased emission from the "low $N_H$" enhancement which extends along $l^{II} = 235°$ from $b^{II} = -25°$ to $-75°$.

The Eridanus region was also included in the survey of Naranan et al. (1974). Observations above 1 keV on this flight were strongly contaminated by spurious counts due to electrons, the launch having taken place during a period of intense geomagnetic activity. The observers concluded that the 0.25 keV data are reliable, however. In terms of the Eridanus enhancement, the map is similar to the Wisconsin survey. However, the low $N_H$ enhancement does not appear, which is surprising although the region would have been near the local horizon during the flight. Rather a large moderately high intensity swath extends from the SGP to the equator through the Eridanus region toward the Gemini-Monoceros enhancement (see Section VII). The Caltech scans are more consistent with the picture presented by the Wisconsin scans, which suggest absorption by local hydrogen in Gould's Belt.

## III. Correlation of Emission with Neutral Hydrogen Column Densities

Although the Eridanus enhancement is a galactic feature, the Eridanus scans cover a region of the sky approximately four times that of the LMC scans. This region possesses a higher average transmission, and a greater variation in hydrogen column density than the LMC region. As a check on results derived from the LMC data, we have performed Chi-squared fits for the local and extragalactic (or halo) flux fractions using 82 seconds of the Eridanus data. Only simple non-clumped models were considered. Hydrogen data at 5° intervals were taken from the survey summary of Deltabuit and Meyer (1972). The minimum Chi-squared for the entire data stream was 4.7 per degree of freedom as compared to 1.1 per degree of freedom for similar models of the LMC indicating considerable contamination from anisotropic Galactic sources. Of the 4420 X-ray counts observed, 10% would result from an extrapolation of an extragalactic power law compared to the model results that 14 to 19% of the flux was extragalactic. Thus the total extragalactic flux indicated was less than twice the extrapolated power law, similar to the LMC results.

If the data due to the Eridanus enhancement are excluded leaving 58 seconds of data, the minimum Chi-squared value drops to less than 1.7 per degree of freedom as seen in Table 4.1. The model requires an extragalactic flux from 2 to 2.5 ($2\sigma$) times a power law extrapolation, or between 220 and 275 photons $(\mathrm{cm}^2\ \mathrm{s\ keV\ sr})^{-1}$. The extragalactic (or halo) flux thus determined is compatible with, but near the upper

Table 4.1

EXTRAGALACTIC AND LOCAL FLUX FRACTIONS AS DETERMINED FROM ERIDANUS SCANS

| | $\sigma$ (x $10^{20}$ $cm^2$) | $\langle T_{GAL} \rangle$ | $\chi^2_{min}$ | Degrees of Freedom | Local Flux(%) | Extragal Flux(%) | Power Law Extension(%) |
|---|---|---|---|---|---|---|---|
| Smooth | 0.4 | 0.206 | 373.2 | $80^{+}$ | 81-86 | 14-19 | 10 |
| | 0.4 | 0.268 | 92.4 | $56^{++}$ | 67-74 | 26-33 | 13 |

$^{+}$ Data from Eridanus enhancement included.

$^{++}$ Data from Eridanus enhancement not included.

limit allowed by the LMC observations of 250 photons $(cm^2\ s\ keV\ sr)^{-1}$. The model results reflect the fact that the lowest hydrogen column densities in the position of the scan path used in the data sample occurred while crossing the low $N_H$ enhancement.

## IV. The Low $N_H$ Enhancement

Hydrogen column densities in the direction of the low $N_H$ enhancement are approximately $10^{20}$ $cm^{-2}$, based on both the 21-cm maps and the Lyman α absorption measurement to the star μ Col (HD38666, Savage and Jenkins 1972). After convolution through interstellar gas, an $11\ E^{-1.5}$ photon power law produces approximately 25% of the observed 0.25 keV flux in the direction of the enhancement. A manifestly important question associated with this enhancement is what fraction of the observed flux is of extragalactic or halo origin. An immediate upper limit of 440 photons $(cm^2\ s\ keV\ sr)^{-1}$ on the extragalactic flux at 0.215 keV can be derived if the source spectral slope is $\gtrsim -1.5$.

Bremsstrahlung spectra obtained from the low $N_H$ enhancement, where only the standard power law, convolved through the observed hydrogen column density, has been subtracted are shown in Figure 4.6. Although best fit values of $N_H$ tend to exceed that used in the power law convolution, temperatures of approximately $1.7 \times 10^6$ °K and $N_H = 1 \times 10^{20}$ $cm^{-2}$ are consistent with the data ($\chi^2 = 1.1$ per degree of freedom). The spectral results do not change substantially if values as large as $2 \times 10^{20}$ $cm^{-2}$ are used in the power law convolution.

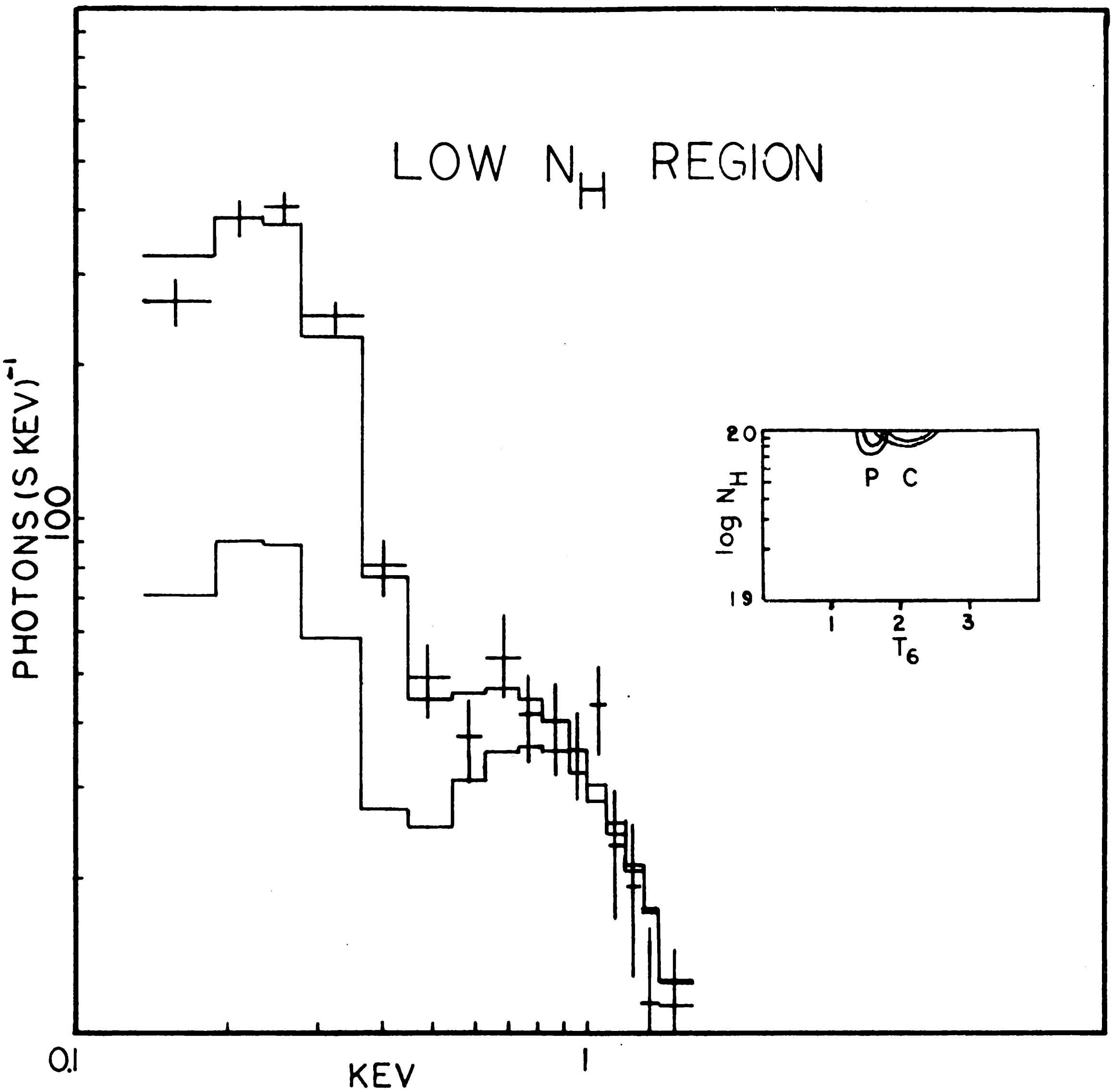


Figure 4.6

Spectrum of the Low $N_H$ region as observed in the 5° x 10° propane counter. Approximately 25% of the flux at 0.25 keV and nearly all of the flux at 1 keV is accounted for by an extragalactic 11 $E^{-1.5}$ photon power law, as indicated by the lower histogram. The best fit continuum spectrum, where $N_H$ is constrained to be less than or equal to $10^{20}$ $cm^{-2}$ and a 11 $E^{-1.5}$ power law has been subtracted, is shown. $\chi^2 + 1$ and $\chi^2 + 3$ contours are indicated in the inset.

Table 4.2

SPECTRAL RESULTS - LOW $N_H$ ENHANCEMENT

| Model† | Deg of Freedom | $\chi^2_{min}$ | $N_H \times 10^{-20}$ cm$^2$** min | best | max | $\alpha$ or $T_6$** min | best | max |
|---|---|---|---|---|---|---|---|---|
| Power law | 16 | 29.2 | 0.8 | < 1.0 | < --- | 3.1 < | 3.3 | < 3.5 |
| Brems | 16 | 17.7 | 0.9 | < 1.0 | < --- | 1.7 < | 2.0 | < 2.6 |
| Plasma | 16 | 19.0 | 0.8 | < 1.0 | < --- | 1.6 < | 1.8 | < 2.2 |

† Background subtracted was 11 $E^{-1.5}$ power law convolved through $10^{20}$ equivalent H atoms cm$^{-2}$.

** Minimum and Maximum values were based on $\chi^2_{min} + 3$. Models constrained so that $N_H \leq 10^{20}$ equivalent H atoms cm$^{-2}$.

The incident flux is approximately 400 photons $(cm^2\ s\ keV\ sr)^{-1}$ if restricted to cases where $N_H$ is less than or approximately equal to $10^{20}\ cm^{-2}$. This result represents a considerable excess over upper limits placed on the halo or extragalactic flux utilizing Chi-squared techniques on either the LMC or the Eridanus data, although it is somewhat less than typical values given for the extragalactic flux summarized by Silk (1973).

The assumption that there is no Galactic contribution to the soft X-ray flux in the direction of the low $N_H$ enhancement is unlikely. As reflected in the Chi-squared results, the flux only decreased by a factor of two as the rocket moved off the low $N_H$ enhancement into regions where the hydrogen column density increases rapidly. In fact, there is no compelling reason to believe that the low $N_H$ enhancement is not completely Galactic, similar to the Eridanus enhancement in origin.

## V. Spectra of the Eridanus Enhancement

The raw spectra of the two enhancements observed in the Eridanus region on the Australian flight are remarkably alike, both in shape and intensity. Two types of thermal spectra were fitted to the Eridanus enhancement data (as well as to the data from the low $N_H$ enhancement). First a simple continuum bremsstrahlung model was used, with the Gaunt factor (for a pure hydrogen plasma) taken from Karzas and Latter (1961). Secondly, a model, essentially that of

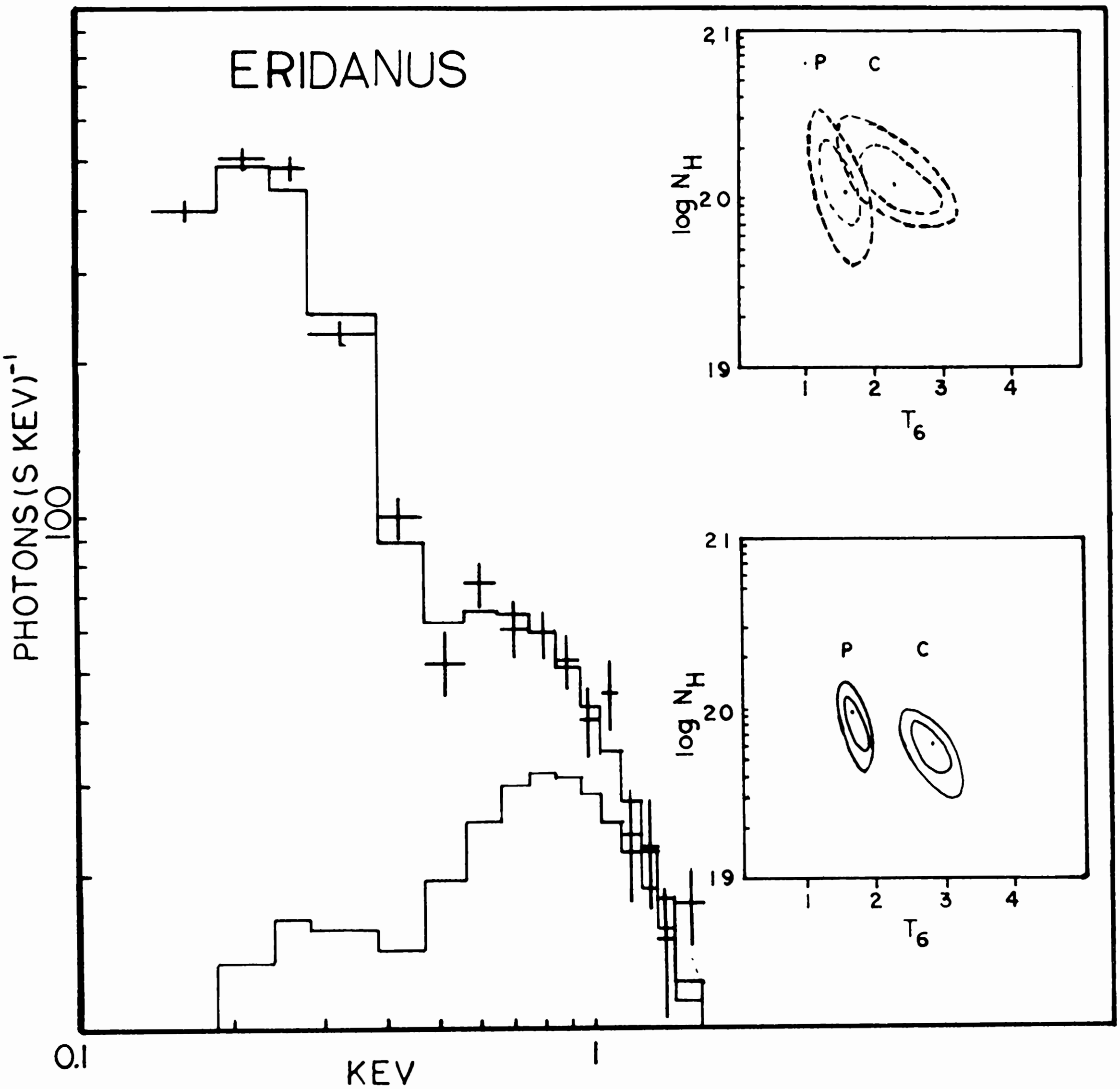


Figure 4.7

Similar to Figure 4.6 for the Eridanus enhancement. Dashed contours on the inset indicate that an adjacent non-enhanced region was subtracted from the raw spectrum, whereas solid contours indicate an 11 $E^{-1.5}$ power law was subtracted. The best fit bremsstrahlung spectrum is shown.

Table 4.3

SPECTRAL RESULTS - ERIDANUS ENHANCEMENT

| Model | Deg of Freedom | $\chi^2_{min}$ | $N_H \times 10^{-20} cm^{-2}$** min < | best < | max | $\alpha$ or $T_6$** min | < max < | best |
|---|---|---|---|---|---|---|---|---|
| Brems† | 19 | 25.3 | 0.4 < | 0.6 | < 0.9 | 2.4 | < 2.8 < | 3.1 |
| Brems†† | 5 | 4.4 | 0.8 < | 1.3 | < 3.0 | 1.5 | < 2.3 < | 3.2 |
| Plasma† | 14 | 33.8 | 0.4 < | 0.9 | < 1.3 | 1.5 | < 1.6 < | 1.9 |
| Plasma†† | 5 | 3.6 | 0.4 < | 1.1 | < 3.0 | 1.0 | < 1.6 < | 2.0 |

† Background subtraction was 11 $E^{-1.5}$ photon power law convolved through 5 x $10^{20}$ equivalent H atoms $cm^{-2}$.

†† An adjacent background region was subtracted using data obtained between t = 272-276, 297-301 seconds.

** Minimum and maximum values based on $\chi^2_{min}$ + 3.

Tucker and Koren (1972), was utilized which included line emission from an astrophysical plasma with cosmic abundances. Line strengths between 88 and 125 Å were supplied by Raymond and Cox (private communication 1975). In both cases the free parameters were the hydrogen column density $N_H$ and the temperature of the plasma T, as well as an overall normalization factor. Results of the two models for the Eridanus enhancement (Figure 4.7) are similar. The line calculation tends to produce lower temperatures, primarily due to the influence of the strong oxygen lines which appear at temperatures of 1 to $2 \times 10^6$ °K. (Power law spectra will fit the Eridanus enhancement equally well, but, in view of the lack of intense radio emission from the region, do not seem physically justified.)

The spectrum of the Eridanus enhancement as observed in the 5° x 10° propane counter demonstrates that the enhancement must be a Galactic feature. OAO-2 Lyman-α absorption measurements to HD28497 ($l^{II} = 209°$, $b^{II} = -37°$) imply that $5 \times 10^{20}$ hydrogen atoms $cm^{-2}$ lie within 465 pc along a line of sight to a star which is approximately 8° from the center of the emission region (Savage and Jenkins 1972). The average hydrogen density in the direction to HD28497 of 0.3 $cm^{-3}$ is typical of other stars surveyed near the Eridanus enhancement, e.g., stars with $190° \lesssim l^{II} \lesssim 220°$, $-40° \lesssim b^{II} \lesssim -10°$. If the hydrogen to HD28497 is distributed uniformly along the line of sight, the distance to the edge of the Eridanus enhancement must be less than or approximately equal to 300 pc.

The excess incident X-ray flux from the entire Eridanus enhancement was $0.4 \times 10^{-9}$ ergs $(cm^2\ s)^{-1}$ between 0.15 and 0.28 keV, which corresponds to a surface brightness of $7.3 \times 10^{-9}$ ergs $(cm^2\ s\ sr)^{-1}$. The total intrinsic luminosity is dependent upon the true spectrum and the true value of the neutral hydrogen, as well as the assumed distance. The best fit values imply a total luminosity for the enhanced portion of the flux of $2.3 \pm 1.0 \times 10^{33}$ ergs $s^{-1}$, if the source is 150 pc distant. Note that in the fitted spectra, large values of $N_H$ imply smaller values of kT. Thus the practical reason for the variation in values of the intrinsic luminosity is evident. Lowering kT and increasing $N_H$ results in a much larger fraction of the total flux between 0.15 and 0.28 keV being absorbed in the ISM and the detector window.

## VI. The Eridanus Enhancement--A Possible Supernova Remnant?

A number of features of the Eridanus region suggest the possibility that the Eridanus enhancement may be the site of an old supernova remnant, as recently noted by Shulman et al. (1975). Unlike X-ray emission previously reported from "old" supernova remnants ($10^4$ - $5 \times 10^4$ yrs), where most of the radiation is thought to originate in a hot thin shell generated as the supernova shock passes through the ISM, X-rays from a truly "old" supernova remnant ($10^6$ yrs) would originate in a core occupying most of the remnant volume. Unless density inhomogeneities dominate, relatively diffuse radiation is expected, consistent with the 2° x 20° propane counter observations. From a theoretical viewpoint, numerical calculations indicate that the necessary low density plasma ($10^{-1}$ - $10^{-2}$ $cm^{-3}$), high temperature ($10^6$ - $10^7$ °K) core is present at the end of the shell cooling stage (see Chevalier 1974, 1975 and references therein), although detailed calculations for a $10^6$ year-old supernova remnant have yet to be reported.

The original suggestion that a supernova remnant might exist in the Eridanus region was made by Öpik (1952) in an attempt to explain $H_\alpha$ emission from Barnard's Loop. This suggestion was later revived by Menon (1957) to explain double-peaked 21-cm line profiles observed between $l^{II}$ = 203° and 210°, $b^{II}$ = -19° to -26°. The radial expansion was estimated to have a velocity of 8-12 km $s^{-1}$. The supernova age, assuming a distance of 150 pc and a diameter of 15-20°, would be several million years. This estimated distance would place the supernova remnant diameter at 40-50 pc. Ilovaisky and Lequeux (1972b) have argued that many such old, low surface brightness, large diameter (> 25 pc) supernova remnants have gone undetected in radio continuum surveys.

The X-ray emitting region appears to be surrounded in the north by two low velocity hydrogen features on the map by Fejes and Wesselius (1973): the so-called Orion ridge extending south from the Galactic plane at $l^{II}$ = 215°, south to approximately -40° and the Taurus ridge, emerging from the plane at $l^{II}$ = 190° and extending to $l^{II}$ = 180°, $b^{II}$ = -40°.

In $H_\alpha$ emission, several loop-like structures can also be seen in the contour map of diffuse Galactic $H_\alpha$ of Reynolds *et al*. (1975, see Figure 4.8). However, the filamentary nature of the $H_\alpha$ emission is more evident in the survey of Sivan (1974), as well as the fact that filaments appear to extend as far south as $b^{II} = -50°$. The center of the structure ($l^{II} = 200°$, $b^{II} = -25°$) observed by Reynolds *et al*. is somewhat dislocated ($\sim$ 15°) from the center of the X-ray emitting region. Reynolds *et al*. note that although the I Ori O association may be the source of most of the ionization in the northern portions of the region, whether these stars could ionize the $l^{II} = 180$–$200°$, $b^{II} = -30$ – $-40°$ region is debatable. Perhaps the energy source for both the enhanced diffuse Hα and X-ray emission in the south is the SN remnant core, highly evacuated by the explosion and thus extremely slow to cool.

The suggestion that the PSR 0450-18 was associated with the Eridanus remnant was first made by Shulman *et al*.(1975). The spin-down rate of PSR 0450-18 is consistent with a very old supernova remnant. The age of a pulsar is roughly given by

$$T = \frac{1}{2}\,(P/\dot{P}) \tag{4.1}$$

as long as the radiated power is proportional to $P^{-4}$, e.g., dipole radiation with the moment of inertia regarded as constant. The measured spindown rate of $4.2 \pm 0.1 \times 10^{-15}$ and period of 0.548935 s (McCulloch *et al*. 1973) yield a lifetime of $10^6$ years, as compared to $4 \times 10^4$ years for the Vela pulsar.

The dispersion measure of 25.6 $cm^{-3}$ pc (Maran and Modali 1970) tends to indicate that the distance to PSR 0450-18 is greater than that to the enhancement itself. Typical values of the mean interstellar electron density of 0.03 $cm^{-3}$ lead to a distance of 850 pc. However, the Vela PSR 0833-45 has a dispersion measure of $69.2 \pm 0.1$ (Manchester and Taylor 1972) which implies a distance of 2.3 kpc whereas the actual distance is estimated to be 600 pc. In the case of the Vela PSR the discrepancy in distance may be attributed to the existence of the Gum Nebula or possibly to electrons in the vicinity of the pulsar. For the Eridanus remnant, a fossil sphere would have cooled too much in $10^6$ years to account for the required electrons (see Schwarz 1973) and the environment of PSR 0450-18 would seem to be more likely to resemble pulsars not in relatively young supernova remnants. Nevertheless we feel that the discrepancy in the distance to 0450-18 is not so large as to exclude the possibility that the pulsar is associated with Eridanus, particularly in view of the extended $H_\alpha$ emission, uncommon at such high Galactic latitudes.

Unlike Shulman _et al_. we feel that the 3U source 0431-10 is difficult to explain as the high energy flux of an old supernova remnant, or more explicitly any thermal bremsstrahlung solution to the observed spectrum. Fits with the maximum kT of $3 \times 10^6$ °K produce less than 0.5 Uhuru counts as compared to the 3 Uhuru count strength of the source. The spectrum implies that $2 \times 10^{-11}$ ergs $cm^{-2}$ sec between 2 and 6 keV would have been incident on the detector of which

90% of the radiation would have been between 2 and 2.5 keV. Although Giacconi *et al*. (1973) state that one Uhuru count is approximately $1.7 \times 10^{-11}$ ergs $(cm^2\ s)^{-1}$, the efficiency between 2 and 2.5 keV is less than half the average efficiency of the Uhuru detector over the 2-6 keV range. Lower temperatures imply an even smaller Uhuru flux.

While the *possibility* that the Eridanus enhancement is an old supernova remnant exists, the *probability* is by no means apparent. Supernova remnant interpretations of the diffuse X-ray background are motivated, as noted in Chapter I, because of the ease in satisfying the necessary energy requirements. However, the existence of million year-old supernova remnants or supernova-generated tunnel structures remains difficult to prove in view of our limited understanding of what sort of observational features we should expect to find.

A particular problem which must be solved is the radio emission characteristics of such old supernova remnants, or indeed any large ionized structure expanding with a velocity greater than the ambient medium. One's naive expectation is that the magnetic field should be concentrated in such structures and that as a result they should be the site of enhanced synchrotron emission.

## VII. The Gemini-Monoceros Enhancement

Directly across Gould's Belt from the Eridanus enhancement is a region of X-ray enhancement coincident with a small continuum radio feature evident on the 150-MHz whole sky map of Landecker and

Figure 4.8

Similar to Figure 4.3 for scans of the Gemini-Monoceros region. The approximate boundaries of the region (light dashed contour) represent the combined results on this experiment and that of Bunner *et al*. (The heavy dashed line represents the scan path of the Wisconsin experiment.) The position of the Monoceros supernova remnant (dotted circle) is shown.

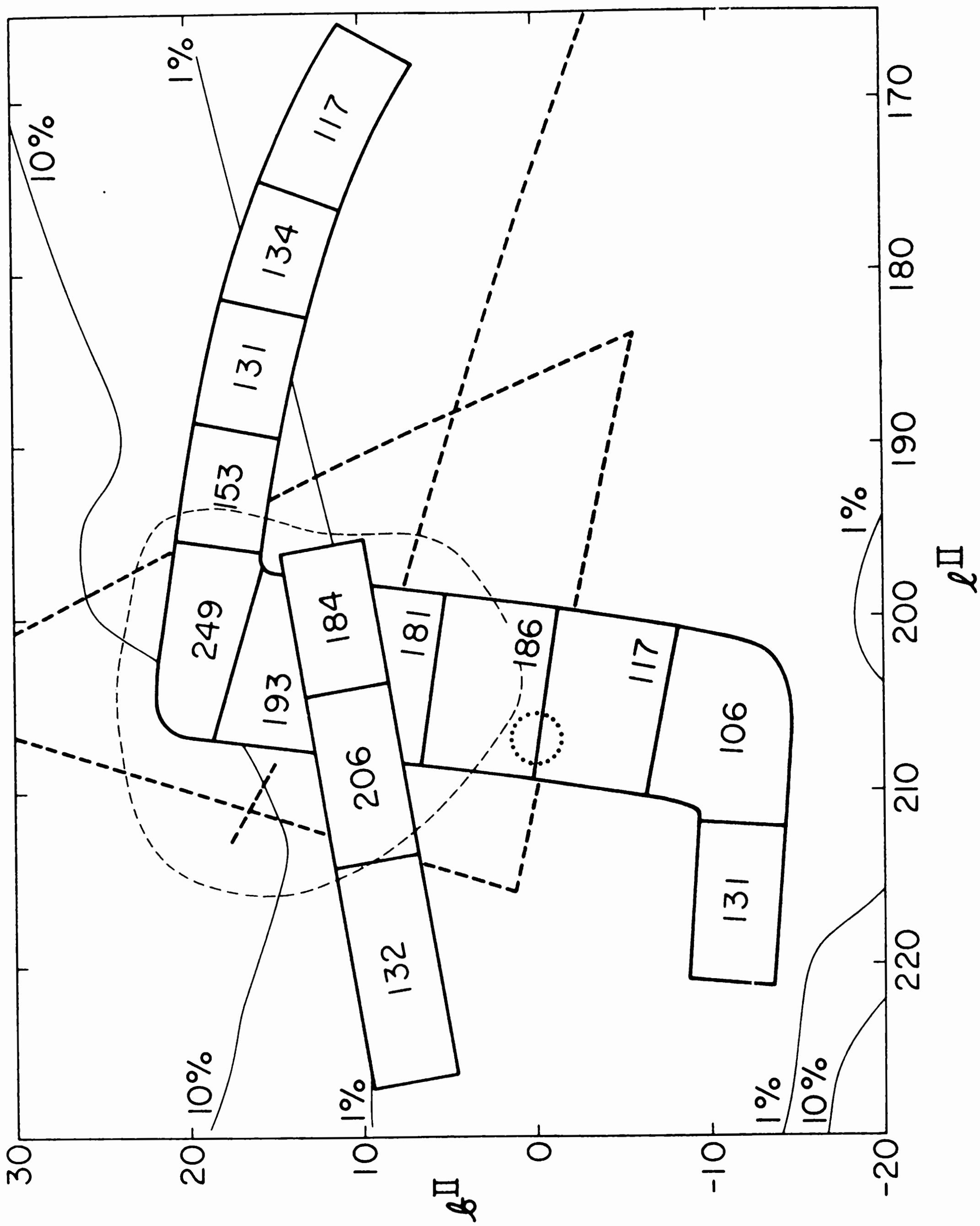
117
134
131
153
249
193
184
181
186
117
106
206
131
132
1%
10%
1%
10%
1%
1%
10%
170
180
190
200
210
220
30
20
10
0
-10
-20
ℓII
bII

Wielebinski (1970). Unlike the Eridanus region, the Gemini-Monoceros enhancement does not show up as a diffuse $H_\alpha$ "hot spot", either in the map of Reynolds et al. or of Sivan. In terms of its X-ray properties, however, the Gemini-Monoceros or Mono-Gem, enhancement is quite similar to the other two enhancements which have been discussed.

A previous flight of the Caltech X-ray payload (Moore 1975) included several scans over and a long hold (approximately 35 sec) on this enhancement. A crude spatial map of the region as determined from that flight, shown in Figure 4.9, indicates that the region is somewhat larger than the Eridanus enhancement. Note that the scan path had been chosen to complement the data of Bunner et al. (1973) and allowed definition of the southern boundary of the region at $b^{II} \simeq 0°$. The measured surface brightness of the enhancement at 0.25 keV of 140 photons $(cm^2\ s\ keV\ sr)^{-1}$ is a factor of 2 brighter than measured by Bunner et al. (1973). Assuming a solid angle for the source of 400 square degrees, the incident flux from the Mono-Gem enhancement totals $1.1 \times 10^{-9}$ ergs $(cm^2\ s)^{-1}$.

During the Mono-Gem hold near $l^{II} = 203°$, $b^{II} = 13°$, a raw spectrum of high statistical accuracy, containing more than 4500 X-ray events between 0.1 and 1.2 keV, was acquired. In view of the existence of the radio spur, power law spectra as well as both types of thermal spectra were fitted to the X-ray data, with results shown in Table 4.4. For convolution of the extragalactic power law spectrum, a hydrogen column density of $1 \times 10^{21}$ atoms $cm^{-2}$ was utilized. The most outstanding feature of all the model fits is the inconsistency of the data with all models which have more than 5 x $10^{19}$ atoms $cm^{-2}$ of absorbing material, implying that the source is extremely local. Column densities to the star 15 Mon ($l^{II}$ = 203°, $b^{II}$ = 2°) indicate very low hydrogen densities, approximately 0.05 $cm^{-3}$, in the star's direction. Despite the low density, the suggested distance to the Mono-Gem enhancement is less than 300 pc. The luminosity of the enhanced region between 0.15 and 0.28 keV is

$$2.8 \times 10^{33} (D/150 \text{ pc})^2 \text{ ergs s}^{-1},$$

approximately that of the Eridanus enhancement.

The Mono-Gem enhancement does not appear to be associated with any nearby supernova remnants, e.g., Monoceros N, IC 443, or the Origem Loop (Spoelstra 1973). The possible association with the radio spur was originally pointed out by Berkhuijsen (1973). The spur extends from $l^{II}$ = 193°, $b^{II}$ = 5° to $l^{II}$ = 205°, $b^{II}$ = 25°. A probable continuation of this spur appears below the Galactic plane between $l^{II}$ = 197°, $b^{II}$ = -10° and $l^{II}$ = 207°, $b^{II}$ = -20°. Part of this continuation was crossed by the scan path of the Mono-Gem flight, but as indicated in Figure 4.9, no excess flux was seen. This may not be surprising since emission occurring at a distance of several hundred parsecs would probably be absorbed in Gould's Belt, which coincides with the local plane of Galactic hydrogen.

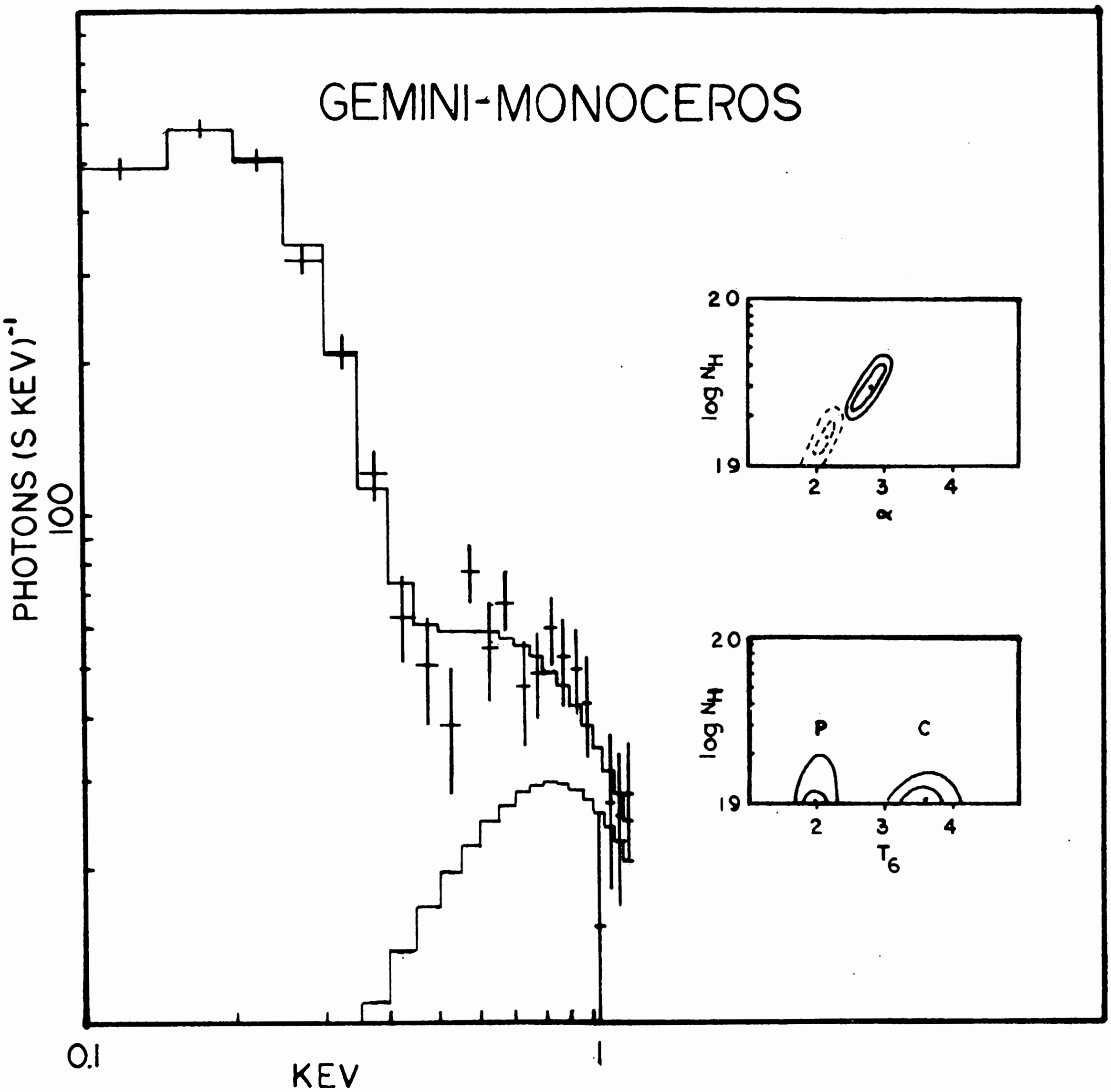


Figure 4.9

Similar to earlier spectrum figures. Contours for power law fits with spectral index α are also shown.

Table 4.4

SPECTRAL RESULTS - GEMINI-MONOCEROS ENHANCEMENT

| Model | Deg of Freedom | $\chi^2_{min}$ | $N_H \times 10^{-20} cm^{2}$** min < best < max | $\alpha$ or $T_6$** min < best < max |
|---|---|---|---|---|
| Power law† | 20 | 21.6 | 0.15 < 0.25 < 0.40 | 2.55 < 2.65 < 3.0 |
| Power law†† | 18 | 19.7 | 0.1 < 0.16 < 0.25 | 1.9 < 2.1 < 2.2 |
| Brems† | 19 | 19.4 | 0.0 < 0.1 < 0.17 | 3.1 < 3.6 < 4.1 |
| Brems†† | 18 | 30.8 | 0.0 < .1 < 0.2 | 5.3 < 5.8 < 6.3 |
| Plasma† | 19 | 43.2 | 0.0 < 0.025< 0.17 | 1.8 < 2.0 < 2.2 |
| Plasma†,††† | 18 | 34.3 | 0.0 < 0.03 < 0.2 | 1.6 < 1.9 < 2.2 |
| Plasma†† | 17 | 92 | 0.0 < 0.03 < 0.1 | 2.2 < 2.4 < 2.6 |

†Background subtraction was 11 $E^{-1.5}$ photon power law convolved through $10^{21}$ equivalent H atoms $cm^{-2}$.

††An adjacent background region was subtracted using data obtained between t = 113-117, 304-307 seconds.

†††The 100-150 eV data point was excluded.

**Minimum and Maximum values were based on $\chi^2_{min} + 3$.

Several other diffuse non-thermal loops, or radio spurs, seem to be associated with enhanced soft X-ray radiation, notably the North Polar Spur and Loop IV (Rapley et al. 1975). Such a coincidence seems to suggest synchrotron emission as a mechanism to explain X-ray, as well as radio, enhancements in these regions.

On the other hand, the existence of a plasma, possibly hot enough and diffuse enough to account for the soft X-ray background has recently been discovered in the form of OVI absorption lines in the spectra of nearby young stars using the Copernicus UV spectrometer (Jenkins and Meloy 1974).

## VIII. OVI and the Diffuse X-ray Background

The discovery of interstellar OVI furnishes strong support for explanations of soft X-rays involving the existence of diffuse hot matter in space. Deduced from absorption line (1031.945 and 1037.627 Å) spectra in bright hot stars, line of sight OVI abundances are currently available for 32 positions (Jenkins and Meloy 1974). The distribution of $\langle n_{OVI} \rangle$, similar to the soft X-ray background, is quite patchy, although any correlation with soft X-ray features is somewhat unclear as yet (see Figure 4.10). Detailed correlation may be improbable for three reasons: (1) Most observed soft X-ray regions seem to have temperatures in excess of $10^6$ °K, where the fractional abundance of OVI is greatly decreased as compared to the maximum value of 13% at $3 \times 10^5$ °K. (2) The interstellar medium is rather opaque to soft X-rays while it is relatively transparent at 1030 Å. (3) Most soft

X-ray detectors are insensitive to thermal bremsstrahlung spectra with values of kT much below $10^6$°K. Regions in which OVI is observed may very well be regions which were once hotter and have cooled somewhat or represent boundary layers between $10^6$°K gas and cooler H II or H I regions. Perhaps coincidentally the low $N_H$, Eridanus and Mono-Gem enhancements lie near to stars, μ Col, HD28497, and 15 Mon respectively, along which rather high total column densities of OVI have been measured.

In the case of the low $N_H$ enhancement, OVI measurements can be interpreted as strong evidence that the enhancement is local. Perhaps more important than the total OVI column density to μ Col ($l^{II}$ = 237°, $b^{II}$ = -27°), which lies in the northern tip of the low $N_H$ enhancement is that the temperature indicated by assuming line widths are generated by Doppler broadening is greater than 2 x $10^6$°K. The temperature is very close to best-fit temperatures using the X-ray data. Other interstellar absorption lines (SIII, H2, SiII) in the direction of μ Col are much narrower than the OVI line widths (see Figure 1 of York 1974) ruling out the possibility that OVI line widths are simply due to motions in the ambient ISM.

Temperatures based on the Doppler broadening assumption using 15 Mon and HD28497 data also indicate plasma temperatures in excess of $10^6$°K. (Two distinct OVI absorption lines were measured by Jenkins and Meloy in the direction of 15 Mon, only one of which leads to such a large temperature.) In other stars observed the derived temperatures were in general lower, as low as 2 x $10^5$°K for 59 Cygnus.

Arguments based on line widths are clearly only suggestive. Under equilibrium conditions along the line of sight $\ell$ (465 pc) to HD28497, the bulk of the OVI ($10^{13.86}$ $cm^{-2}$) must be contained in cooler regions than the line profile would indicate or the expected radiation would exceed the observed flux S (ergs $(cm^2\ s\ sr)^{-1}$) by several orders of magnitude.

$$S \gtrsim \varepsilon\ A^2\ N_{OVI}^2\ \ell^{-1} \sim 10^{-6}\ \text{ergs}\ (cm^2\ sr)^{-1} \qquad (4.1)$$

where $\varepsilon$ is the emissivity between 0.18 and 0.28 keV ($1.2 \times 10^{-24}$ ergs $(cm^3\ s\ sr)^{-1}$ at $10^6$°K, Tucker and Koren 1972).

$$A = n_e/n_{OVI} \sim (n_H/n_o)(n_o/n_{OVI}) \sim 10^{3.18} \cdot 10^{2.42} = 10^{5.6} \qquad (4.2)$$

where values of the abundance and ionization fraction have been taken from Allen (1973) and Jordan (1969, $T_6 = 1$) respectively. This should be compared with the total observed flux in the direction of the Eridanus enhancement which was less than $10^{-8}$ ergs $(cm^2\ s\ sr)^{-1}$.

The case of HD28497 is somewhat exceptional since the average density of OVI along the line of sight $\langle n_{OVI} \rangle$ was $5.2 \times 10^{-8}$ $cm^{-3}$ as compared to the overall average of $1.7 \times 10^{-8}$ $cm^{-3}$. Jenkins and Meloy (1974) show that even with a filling factor of one, only about 10% of the OVI need be in regions as hot as $10^6$°K to produce the observed diffuse X-ray background, based on the general criterion (discussed in Chapter 1) that $\langle n_e^2 \rangle$ approximately equal $10^{-5}$ $cm^{-6}$. This picture then fits at least qualitatively the general model of a diffuse hot plasma, more or less at pressure equilibrium with the ISM, whose energy source is ultimately due to supernova explosions.

Castor, McCray and Weaver (1975) have, however, proposed an alternative explanation for the OVI absorption lines, e.g., as a circumstellar rather than interstellar feature. They propose that stars with spectral types earlier than B2 possess strong stellar winds with velocities of 1500-3000 km $s^{-1}$ and mass loss rates of $10^{-6}$ $M_{\odot}$ $year^{-1}$, and evaluate the time evolution of the bubble which the star will create in the ISM. The time development of the bubble region whose typical radius approaches 30 pc over the lifetime of the star, is analogous to supernova remnant evolution. The majority of the lifetime of the star is spent in the snow-plow phase, where swept up interstellar gas has collapsed into a cold shell. OVI originates in a transition region, created by thermal conduction, between the hot $10^{6}$°K core, which has a density of $10^{-2}$ $cm^{-3}$, and the cold shell. The X-ray luminosity of the core of a fairly evolved source would approach 4 x $10^{33}$ erg $s^{-1}$.

Naive arguments indicate that it is unlikely that this mechanism alone can account for the diffuse X-ray background. The space density of stars with spectral types earlier than B2 near the Galactic plane is approximately $10^{-7}$ stars $pc^{-3}$ (Ostriker _et al_. 1974) which leads to a volume emissivity between 0.18 and 0.28 keV of $10^{-29}$ ergs $(cm^3\ s)^{-1}$ as compared to 1.5 x $10^{-28}$ ergs $(cm^3\ s)^{-1}$ required for the diffuse X-ray background. The birthrate of such stars of less than 3 x $10^{-14}$ stars $pc^{-3}$ $yr^{-1}$, assuming an average main sequence lifetime of greater than $3 \times 10^6$ years, implies that fossil bubbles do not contain the necessary thermal energy to raise the predicted volume emissivity significantly. The reason why very young stars fail to account for the diffuse X-ray background despite the similarities of the fossil spheres with old supernova remnants is due to their low birthrate, which is orders of magnitude less than the supernova rate.

Resolution of the question of the origin of the OVI currently hinges upon interpretation of the observed velocities of the absorbing material versus the velocity of the star and should be resolved with future observations, both of the OVI line and by attempts to observe X-ray emission from young hot stars. The X-ray luminosity of a $10^6$-year-old core is similar to the observed luminosity of the Eridanus enhancement. At 500 pc the angular extent of such a stellar source should be approximately 7°. However, HD28497, the OVI star in Eridanus is really not at the center of X-ray emission in the enhancement. A similar situation prevails with respect to 15 Monoceros in the Mono-Gem enhancement.

## IX. Synchrotron or Thermal Emission?

The existence of large OVI column densities along lines of sight to certain enhanced background regions suggests thermal emission, although in view of the objections of Castor et al.(1975) this interpretation must be questioned. The correlation of some radio spurs with enhancements suggests synchrotron emission, although soft thermal X-ray sources, such as the Cygnus Loop, are often synchrotron radio sources.

Broad band X-ray measurements are probably inadequate to distinguish between the two mechanisms. Physical conditions undoubtedly vary along the line of sight, the relative positions of absorbing and emitting regions being unknown. Spectra obtained with proportional counters are therefore mainly parameterizations and usually just reflect the ratio of the 0.25 keV to 0.6 keV flux, particularly for spectra with a bremsstrahlung temperature less than 0.25 keV.

Even for diffuse enhancements, presumably due to a single source, the problem of background subtraction is severe since there exists no obvious method to remove the X-ray background from spectra of the discrete region which causes the enhancement. Typical enhanced regions are only twice as bright as unenhanced regions. The spectrum of the so-called enhanced regions is not necessarily spatially constant, although on flight 2 non-enhanced regions exhibited a generally flatter spectrum than enhanced regions.

Narrow band measurements, capable of resolving strong X-ray lines which should be present in a hot diffuse plasma, will undoubtedly resolve the X-ray emission mechanism question. Even the factor of two gain in resolution which should be achieved using scintillation proportional counters (see Policarpo _et al_. 1972) would probably suffice, particularly if counters could be made which were sensitive down to 75 eV.

Detailed spatial maps of the X-ray emitting regions may also shed considerable light on whether synchrotron mechanisms are viable.

If supernovae are the ultimate cause of the radio loops, the age of the loops must be approximately $10^6$ years to account for the large number of such loops observed. Electron radiative lifetimes of $10^5$ years are short compared to this probable age implying a continual source of electrons is necessary. Kafatos and Morrison (1973), who have developed a fossil Stromgrën sphere model for the loops, feel that ambient cosmic ray electrons which diffuse into the high magnetic field intensity regions of the expanding shell are sufficient to account for the X-ray emission. This argument does not depend on the fossil Stromgrën sphere origin of the magnetic shell and also would apply to supernova remnant interpretations. In both cases, X-ray and radio emission should be highly correlated. (Bunner _et al_. (1972) have suggested that in the case of the strongest radio loop, the North Polar Spur, the X-ray emitting region lies somewhat inside the radio shell.) On the other hand, thermal bremsstrahlung emission would not necessarily be coupled with radio synchrotron emission. In passing we note that if very low frequency radio maps ($\sim$ 1 MHz) were available with angular resolutions of 10° or better, the correlation of X-ray and radio features might be easier to determine since at low radio frequencies the opacity of the ISM increases due either to synchrotron self absorption and/or free-free absorption (Alexander _et al_. 1970).

## X. Diffuse Enhancements and the Soft X-ray Background

Although observational problems hinder the elimination of synchrotron emission mechanisms from specific X-ray enhancements, the case against a synchrotron origin for the Galactic background at 0.25 keV is much stronger. At 1 GHz, the pole flux is approximately $10^{-21.3}$ Watts $(m^2 \text{ Hz sr})^{-1}$ (Allen 1973, p. 272). When this flux is extrapolated to 0.25 keV, using the observed radio spectral index of 0.8, we find an expected X-ray flux of $7 \times 10^{-9}$ ergs $(cm^2 \text{ s keV sr})^{-1}$ as compared to observed values of $\sim 10^{-7}$ ergs $(cm^2 \text{ s keV sr})^{-1}$. At 1 GHz, the optical depth of the ISM is small, which explains why the high latitude rather than the plane flux should be used.

The extrapolation discussed above should be regarded as an upper limit since the theoretical arguments exist, indicating a steepening in the cosmic ray electron spectrum at an energy of several hundred GeV. These arguments are based on the relatively short lifetime of $10^{13}$ eV electrons against radiative losses, a few thousand years, as compared to the primary cosmic ray lifetime of a few million years, derived from observed light element ratios (see Daniel and Stephens 1970). In calculation of the electron lifetime, synchrotron and Compton losses contribute almost equally. The fact that both are proportional to $E_e^2$ implies a break in the electron spectral index of $\sim 1$ if the source spectrum was initially a pure power law. Verification of the break is an extremely difficult and currently controversial experimental problem; see Weinberg and Silk (1973) for references and discussion.

On the other hand, a common emission mechanism for enhanced and non-enhanced regions seems likely, in view of the small variation in emissivity required. For example, if the Mono-Gem enhancement is a roughly spherical emission region

$$\varepsilon_x = S_x \, (\theta^3 D)^{-1} \tag{4.3}$$

where $S_x$ is the unattenuated X-ray flux $\sim 0.9 \times 10^{-9}$ ergs $(cm^2\ s)^{-1}$ between 0.18 and 0.28 keV, $\theta$ is the angular radius $\sim 10°$, and D is the distance to the source $\sim 150$ pc. Thus the excess emissivity is approximately $3.6 \times 10^{-28}$ ergs $(cm^3\ s)^{-1}$ as compared to $3 \times 10^{-28}$ ergs $(cm^3\ s)^{-1}$ for the ISM in general. Only small perturbations in the required density of hot gas or fraction of the medium occupied by $10^6$°K gas would produce the necessary enhancement. We conclude that a thermal origin for both the diffuse X-ray background and for the enhancements is a natural explanation.

# CHAPTER V

# CENTAURUS X-3

## I. Introduction

Centaurus X-3 was the first compelling example of a pulsating, eclipsing binary X-ray source (Giacconi *et al*. 1971, Schreier *et al*. 1972). The first variations in the 4.84 second period were found to be Doppler shifts as the X-ray source moved around its companion in a 2.09 day period. The companion eclipsed the primary for approximately a tenth of the period. In addition to the periodic eclipses, the source was found to undergo times of extended low in which the intensity was less than one-tenth the maximum.

An intensive optical search resulted in the identification of the optical counterpart, a 13.35 magnitude star, by Krzeminski (1973). The identification was based on observations of a 0.12 magnitude variation in the light curve, reflecting the known orbital period of the X-ray system. The light curve of Petro (1975) reveals that the effective solid angle of the Roche lobe of the primary dominates the light curve and that gravity darkening is more important than X-ray heating. Osmer, Hiltner and Whelan (1975) have classified Krzeminski's star as 06.5, while slightly later spectral types have been found by Rickard (1974). Based on the orbital parameters derived from analyses of the light curve, Petro has concluded that Krzeminski's star must be on the main sequence. Today Cen X-3 is one of the best studied of all compact X-ray sources.

The conventional model of the Cen X-3 system involves a neutron star with accretion powered by the stellar wind of the primary. Broad P-Cygni profiles, indicating supersonic expansion velocities of approximately 800 km $s^{-1}$ were observed by Vidal *et al.* (1974) in He II 4686 and Hβ. The fact that the X-ray intensity does not go to zero during X-ray eclipse is also consistent with the idea of Compton scattering in an ionized stellar wind.

The X-ray spectrum observed by Uhuru is flat and has exhibited a variable X-ray cutoff between 1.5 and 4 keV. However, the surprising result, in view of the observed Uhuru cutoff, of the existence of a strong soft X-ray flux from Cen X-3 was reported by Bleeker *et al.* (1973). In a spinning rocket experiment, the Dutch-Nagoya collaborators reported an observed counting rate of 0.5 counts $(cm^2\ s)^{-1}$ between 0.39 and 2 keV, which corresponds to a soft X-ray energy flux equal to that observed between 2 and 6 keV. A thermal bremsstrahlung temperature of $0.3 \lesssim kT \lesssim 0.5$ keV with $0.5 \lesssim N_H \lesssim 1.0 \times 10^{21}$ $cm^{-2}$ was found to fit the low energy data. In a companion paper, Hayakawa and Tanaka (1973) interpreted the Dutch-Nagoya results in terms of the absorption of X-rays in a partially ionized circumstellar envelope which was nearly transparent to X-rays below OVII $K_\alpha$ edge.

Primarily to obtain an accurate low energy spectrum of Cen X-3, the early portions of flights 1 and 2 were dedicated to a continuous observation of Cen X-3. The results, however, indicate that the apparent soft X-ray emission from the Cen X-3 region is due to a separate source, perhaps a diffuse feature in the X-ray background.

## II. Experimental Results--Flight 1

The first launch at 17:30 UT 1973 November 1 was at phase 0.21, based on the orbital ephemeris of Schreier et al. (1972), approximately 4 hours after emergence from eclipse. Cen X-3 was observed continuously from 100-135 seconds at which point a series of 3 slow scans across the nearby η Carina region was initiated (Figure 5.1).

During the 7850 $cm^2$ s observation with the P-10 counter, approximately 1385 excess counts ($1 \lesssim E_X \lesssim 14$ keV) were observed. A satisfactory thermal bremsstrahlung fit to the spectrum was obtained with kT = 15 keV, $N_H = 10^{22}$ $cm^{-2}$ although because of the decreasing efficiency of P-10 above 10 keV, higher temperatures with $N_H = 4 \times 10^{22}$ fitted equally well (Figure 5.2). Either value for the estimated hydrogen column density corresponds to a cutoff of approximately 2 keV. The observed 2-6 keV intensity was 0.13 counts $(cm^2\ s)^{-1}$ compared with the maximum Uhuru intensity of 0.19 counts $(cm^2\ s)^{-1}$ (Giacconi et al. 1974).

On flight 1, the 2° x 20° field of view soft X-ray detector viewed Cen X-3 with an average geometric area of 57 $cm^2$ during the Cen X-3 hold. Atmospheric absorption of low energy X-rays is quite severe at low altitudes as discussed in the Appendix. Consequently, only the last 15 s, those above 120 km, were used to derive low energy fluxes from Cen X-3. These observed counting rates were 0.00 ± 0.02 counts $(cm^2\ s)^{-1}$ between 0.4 and 1.0 keV and 0.08 ± 0.02 counts $(cm^2\ s)^{-1}$ between 1 and 2 keV. The observed counting rates represent the actual

Figure 5.1

On flight 1, the first portion of the flight was dedicated to a hold on Cen X-3 of approximately 35 seconds duration. Then, as indicated on the figure, a series of three rolls was carried out over the Cen X-3, $\eta$ Car region. In the figure, the dots indicate positions obtained at one second intervals from the star field photographs. Data from the $5^{o}$ x $10^{o}$ counter is also shown and indicates some anisotropy in the region. A similar flux between 0.4 and 1.5 keV was observed on flight 2.

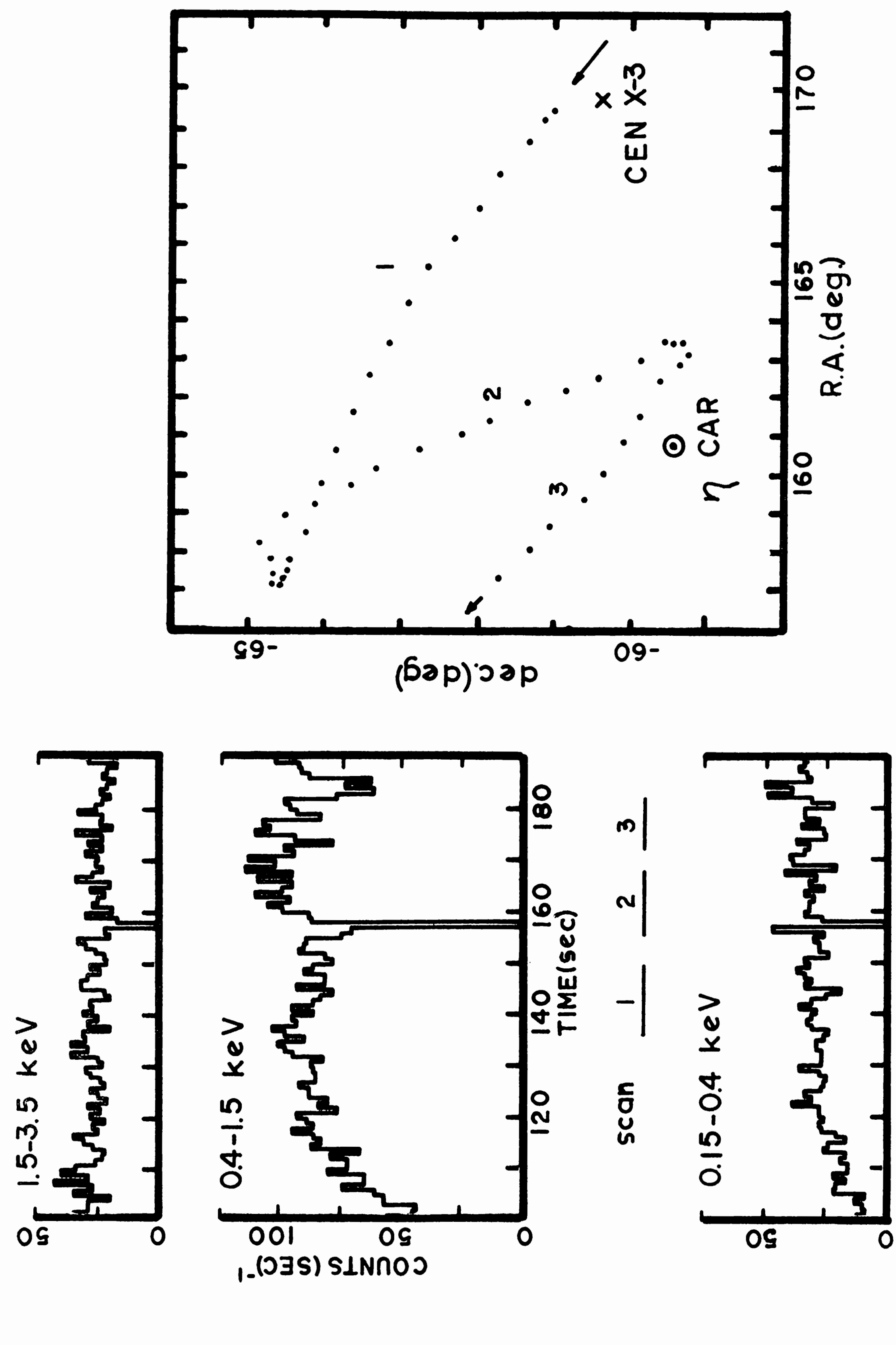
dec.(deg)
R.A.(deg)
CEN X-3
η CAR
1.5-3.5 keV
0.4-1.5 keV
0.15-0.4 keV
COUNTS (SEC)$^{-1}$
TIME(sec)
scan

Figure 5.2

The spectrum of Cen X-3 obtained with the P-10 counter on flight 1. $\chi^2 + 1$ and $\chi^2 + 3$ contours are shown.

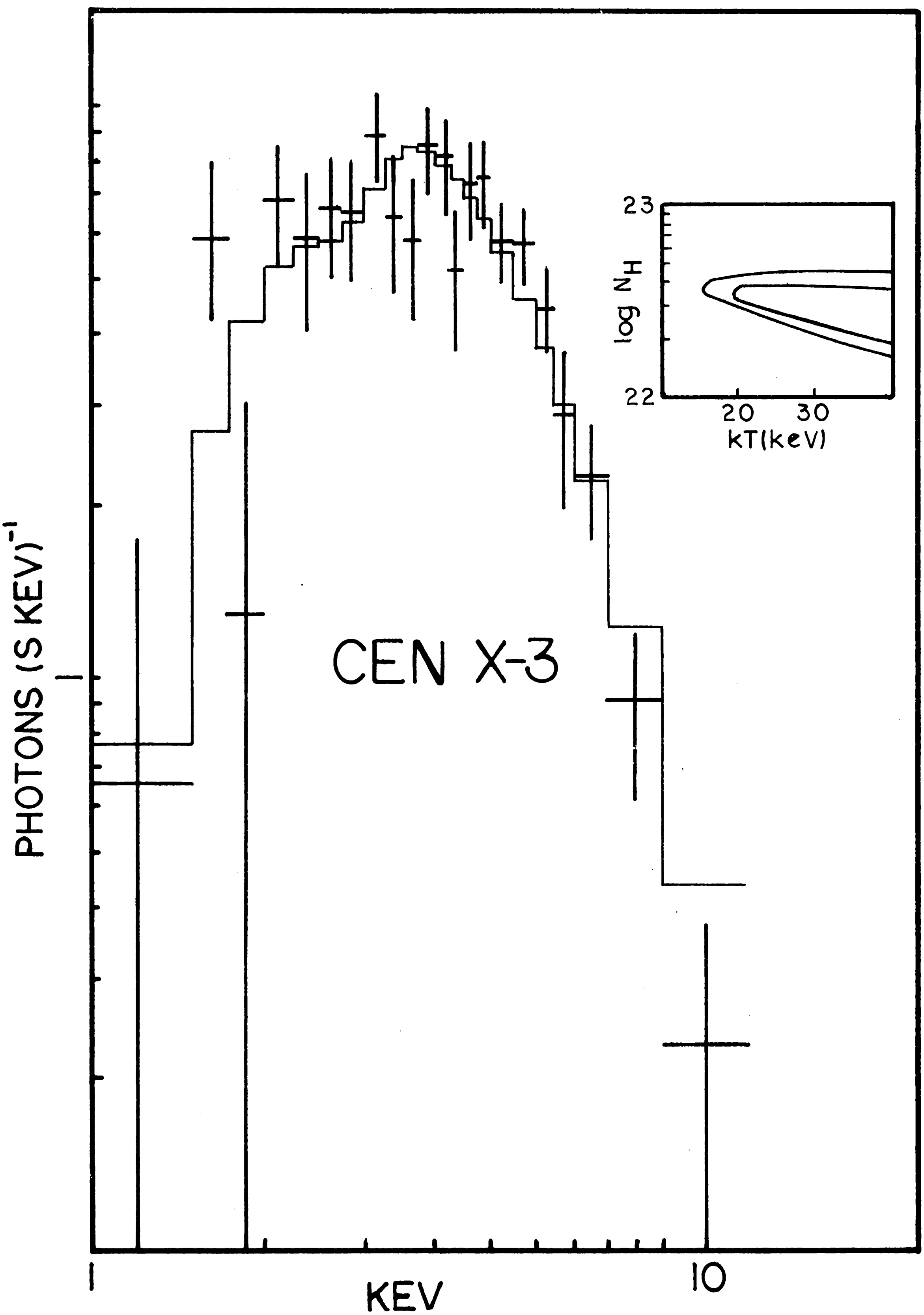
PHOTONS (S KEV)$^{-1}$
1
CEN X-3
1
10
KEV
23
22
log $N_H$
20
30
kT(keV)

rate corrected for atmospheric absorption after subtraction of instrument background and diffuse background, obtained between 143 and 157 seconds when the $\eta$ Car region was in the field of view. The atmospheric correction which was used was 20% between 0.4 and 1.0 keV and 10% between 1 and 2 keV. The $4\sigma$ positive signal observed between 1 and 2 keV was consistent with the spectrum derived from the P-10 data, convolved through the detector response of the propane counter.

The data comprising approximately seven pulse periods from both the P-10 counter and the 2° x 20° propane counter as well as the 5° x 10° propane counter were divided into 0.484 second time bins and folded modulo 10. As expected, the propane counter data is consistent with a steady X-ray flux. However, the resulting profiles (Figure 5.3) in the P-10 counter between 3.5 and 8 keV are not consistent with a steady source. The pulse shape observed is statistically different, primarily due to its double pulsed nature, from the average pulse shapes given by AS&E (1973) or by Schreier et al. (1975). However, perusal of the early Uhuru raw data rates of Cen X-3 (see Schreier et al. 1972) reveals that the pulse profile is quite noisy, thus a short stream of data would not necessarily be expected to be consistent with much longer time averaged pulsations.

As evidenced by Figure 5.4, the pulsed fraction appears to decrease at low energies. Following Ulmer et al. (1974), the pulsed fraction of Cen X-3 observed in the P-10 counter on flight 1 was

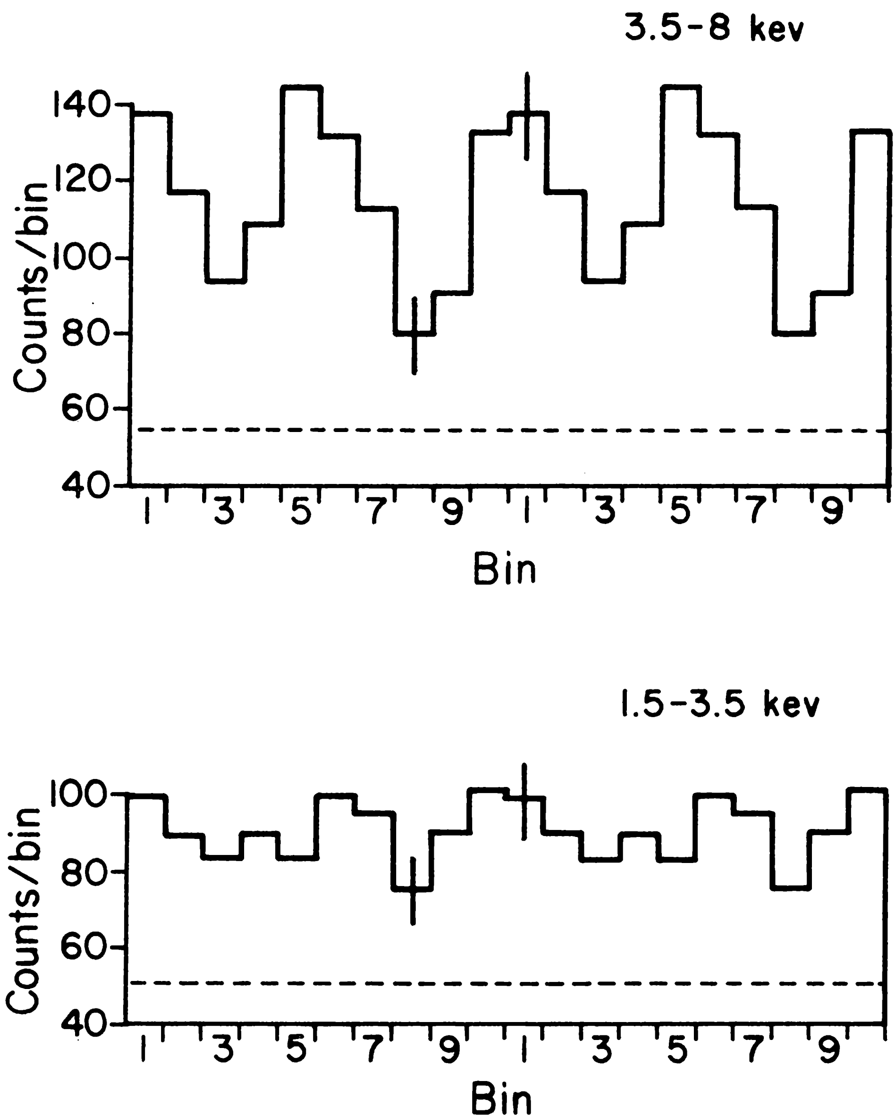


Figure 5.3

Pulse profiles of Cen X-3 observed on flight 1 in the P-10 counter. The dotted lines indicate the sum of instrument and diffuse background. Typical 1σ error bars are shown.

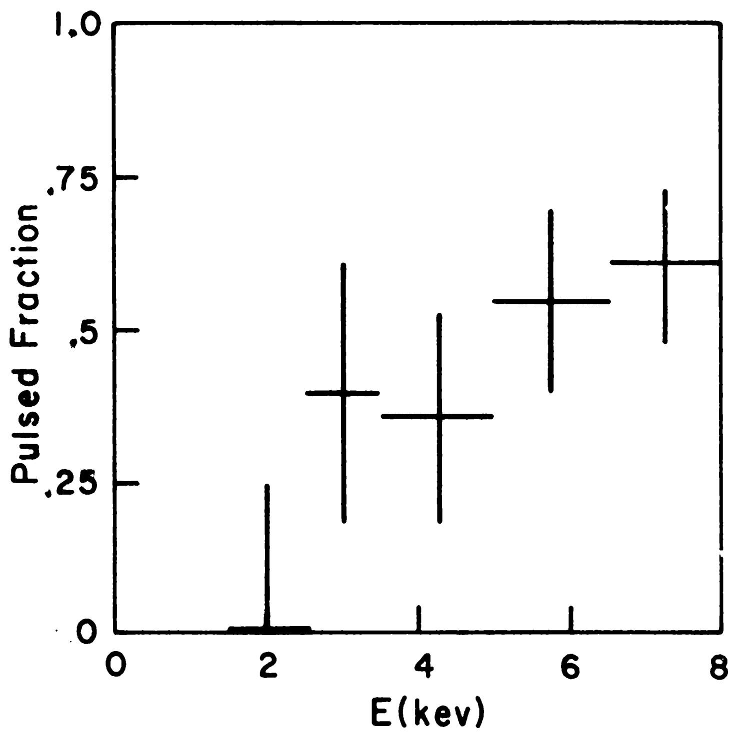


Figure 5.4

The pulsed fraction of Cen X-3 on flight 1 in the P-10 counter based on an on-duty cycle of 80%.

calculated as a function of energy based on a conservative ON duty-cycle of 80%. The results are suggestive but by no means conclusive.

## III. Experimental Results--Flight 2

The second launch at 17:15 UT November 9 was at a phase of 0.046, close to the center of the predicted eclipse. The observation of Cen X-3 consisted of a slow scan toward Cen X-3 at a very low altitude (< 115 km), a hold of 21 seconds duration, and a fast scan away from the source toward 3U0900-40.

The observed flux in the P-10 counter was $0.02 \pm 0.02$ counts $(cm^2\ s)^{-1}$ between 1 and 3 keV, $0.04 \pm 0.06$ counts $(cm^2\ s)^{-1}$ between 3 and 7 keV and $0.01 \pm 0.02$ counts $(cm^2\ s)^{-1}$ between 7 and 14 keV. This should be compared to a typical Uhuru eclipse 2 to 6 keV intensity of 0.02 counts $(cm^2\ s)^{-1}$ (Schreier *et al*. 1975).

Similarly the observed flux (calculated as in flight 1) from the 2° x 20° propane counter was $0.00 \pm 0.02$ counts $(cm^2\ s)^{-1}$ between 1 and 2 keV. The diffuse background subtracted was the observed flux on the scan along the Galactic plane toward 3U0900-40. No pulsations were seen when the data was folded modulo 4.84 s.

## IV. Other X-ray Observations

Soft X-ray coverage of Cen X-3 as a function of phase is not complete. The observation of Bleeker *et al*.(1973) occurred at phase 0.63

while the Caltech ON-observation occurred at phase 0.21. A rocket observation consisting of a scan of the Galactic plane including Cen X-3 at phase 0.52 was reported by Hill *et al*. (1972). An examination of the published counting rate of that flight revealed an upper limit of approximately 0.05 counts $(cm^2\ s)^{-1}$ between 0.2 and 2.67 keV, while 0.25 counts $(cm^2\ s)^{-1}$ were observed between 2 and 20 keV.

Observations with the Copernicus focusing parabola as Cen X-3 emerged from eclipse indicated no need for an additional soft component to the spectrum (Margon *et al*. 1975). The observed flux between 0.6 and 1.9 keV of $1.0 \times 10^{-10}$ ergs $(cm^2\ s)^{-1}$ was comparable to the flux of the Caltech ON-observation between 1 and 2 keV.

Schreier *et al*. (1975) have analyzed Uhuru data of Cen X-3 during which the source emerged from a state of extended low. The source emerged gradually. Initially the cutoff was lowest and the intensity highest near phase 0.5. The intensity spike gradually widened and increased in strength over approximately 5 orbital periods. This behavior is highly suggestive that Cen X-3 was "burning" its way out of a dense, probably time variable, stellar wind. The minimum observed cutoff was $2.0 \pm 0.2$ keV. However, Uhuru would have been insensitive to the type of excess seen by Bleeker *et al*.

## V. Stellar Wind Models

Expressing concern about the diameters derived from eclipse durations, Pringle (1973) suggested the possibility of phase-dependent stellar wind models. Mass loss rates of approximately $10^{-6}$ $M_{\odot}$ $yr^{-1}$ are required to power compact X-ray sources in stellar wind models, resulting in large line of sight absorption even for keV X-rays. Although hydrogen and perhaps helium are ionized by the primary star, the complete stripping of heavy element electrons must be accomplished by the interaction of the X-ray source with the stellar wind. Variable, phase-dependent X-ray cutoffs may result. Interaction in the form of photoionization has been considered by Buff and McCray (1974), whereas the importance of a bowshock has been emphasized by Jackson (1975).

The Buff and McCray models, which are based on local photoionization and recombination balance, produced cutoffs as low as 0.25 keV. However, improved model calculations by McCray and Hatchett (private communication 1974), which treat the radiative transfer problem in the accelerating wind more exactly, indicate that unless the distance to Krzeminski's star is less than 5 kpc, steady-state winds lead to cutoffs of at least 1.5 keV.

Unfortunately, very little is known about the time variability of dense stellar winds from OB stars (see Rosendhal 1973). Thus one can imagine that a dense stellar wind fills up the accretion disc-reservoir of the X-ray source and then recedes allowing very low energy X-rays to escape. This scenario was used by Schreier *et al.* (1975) to explain observations at higher energies. As the reservoir may contain enough matter to power Cen X-3 for several months, the

X-ray luminosity cannot be used to determine short term properties of the stellar wind, the particles of which reach the X-ray star in several hours. Thus stellar wind models can be constructed which do not require that Cen X-3 be nearby in order to produce very low X-ray cutoffs.

## VI. Grain Scattering and the Distance to Cen X-3

Trümper and Schönfelder (1973) have suggested the possibility of source distance determination due to the scattering properties of low energy X-rays off interstellar grains. Scattered flux, which increases as exp (constant $\lambda^2$) would appear unpulsed due to the differing path lengths of individual photons even if the source were originally completely pulsed.

The theory of grain scattering of X-rays has recently been reviewed by Hayakawa (1970). The differential scattering is essentially constant for $\theta_{sc} << \lambda/2\pi a$ where a is the grain radius and $\lambda$ is the photon wavelength. The total scattering cross section is

$$\sigma_{sc} = 2\pi a^2 \{(r_e \lambda a n_e)^2 + (\frac{\mu a}{2})^2\} \qquad (5.1)$$

where $r_e$ is the classical electron radius, $n_e$ is the electron density and $\mu$ is the absorptive opacity. The extinction cross section is

$$\sigma_{ext} = \frac{4}{3} \pi a^3 \mu. \qquad (5.2)$$

Grain scattering of X-rays may prove an interesting probe of interstellar dust. The scattered flux would create a halo around an X-ray point source, typically 1-3' wide. If the grains were aligned there is a distinct possibility that the halos would not appear symmetrical. However, the apparent decrease in pulsation at lower energy cannot be consistently explained as a grain effect, whether the X-ray source is relatively nearby as indicated by the Bleeker et al. measurement or relatively distant as is commonly assumed.

If the source is at a distance of 5 kpc or greater, typical delay times of photons scattered by an angle $\theta_{sc} = 1'$ would be of the order of the eclipse duration of Cen X-3, e.g.,

$$t_{delay} \sim \frac{\ell \, \theta_{sc}^2}{8 \, c} \sim 2.8 \left(\frac{\ell}{5 \text{ kpc}}\right)\left(\frac{\theta_{sc}}{1'}\right)^2 \text{ hrs} \qquad (5.3)$$

as compared to the Cen X-3 eclipse time of approximately six hours. Thus, if grain scattering were important and if the intrinsic pulsed fraction of Cen X-3 were energy independent, a number of qualitative features of the eclipse could be predicted: (1) a large 2-3 keV flux during eclipse on the order of 50% of the non-eclipsed intensity, (2) a general softening of the spectrum during eclipse, and (3) an asymmetric gradually decreasing X-ray light curve during eclipse. None of these effects have been reported. The eclipsed intensity is typically 10% of the uneclipsed intensity. The light curve appears symmetrical, although the eclipse edges are not sharp and may be energy dependent. Only lower limits to kT for bremsstrahlung fits to the eclipsed spectra have been published.

Production of a decreased pulsed fraction is somewhat more difficult to rule out if the source is nearby as the data of Bleeker et al. suggest, although the grain parameters used by Hayakawa (1970) fail to give enough scattering. Grain scattering is a sensitive function of grain radius a since

$$\frac{I_{halo}}{I_{total}} = 1 - \exp\left(-2\pi r_e^{2} a^{4} \lambda^{4} n_e^{2} n_g L\right) \tag{5.4}$$

where $n_g$ is the grain number density and L is the distance to Cen X-3. In terms of the observed ratio, the grain radius is

$$a \sim 0.3 \left\{ \left(\frac{E}{2\ \text{keV}}\right)^2 \left(\frac{3.3 \times 10^{23}\ \text{cm}^{-3}}{n_e}\right)^2 \left(\frac{10^{-12}\text{cm}^{-3}}{n_g}\right) \left(\frac{1\ \text{kpc}}{L}\right) C \right\}^{1/4} \mu \tag{5.5}$$

where

$$C = - \ln\left(1 - I_{halo}/I_{total}\right) \tag{5.6}$$

This value (0.3μ) for the grain radius is a factor of two larger than grain radii suggested by Hayakawa and a factor of two larger than grain sizes efficient in absorbing visible light. Grain sizes are, however, difficult to determine to this accuracy.

An alternative argument, however, allows us to rule out pulse decreases due to grain scattering within 5 kpc unless the hydrogen density along the line of sight averages more than 3 $\text{cm}^{-3}$.

$$\tau_{sc} = 2\pi r_c^{2} \lambda^{2} n_e^{2} a^{4} n_g L \tag{5.7}$$

where the absorptive part of the scattering cross section has been assumed small. Now

$$n_g \sim 3\ \rho_{dust}/4\pi\ a^3 \qquad (5.8)$$

where $\rho_{dust}$ is the density of dust by mass in the ISM. As reviewed by Aanestad and Purcell (1973), models of dust grains generally lead to a total dust density

$$\rho_{dust} \sim 10^{-26}\ \rho_{grain}\ A_v/L \qquad (5.9)$$

where $A_v$ is the visual extinction to some star in magnitudes and L is the distance to the star in kpc. Assuming a normal reddening ratio of $A_v/E_{B-V} = 3$ and the reddening relation of Jenkins and Savage (1974), $n_H L/E_{B-V} = 7.5 \times 10^{21}$ cm$^{-2}$ mag$^{-1}$,

$$n_g = 0.3 \times 10^{-26}\ a^{-3}\ n_H \qquad (5.10)$$

Thus

$$\tau_{sc} \sim 2.1 \times 10^{-18}\ E^{-2}\ a\ n_H\ L \qquad (5.11)$$

Unless $\tau_{sc} \gtrsim 1$, the halo flux will be small. Hence, using the maximum value of $N_H$ determined by Bleeker _et al_. $10^{21}$ cm$^{-2}$ and $E_x = 2$ keV, the condition for large amounts of scattering is

$$a \gtrsim 18.6\ \mu \qquad (5.12)$$

While such grains may exist, that the average grain size is this large seems inconceivable. Even values of the grain radius of 1 μ seem very unlikely, corresponding to $n_H L$ of $2 \times 10^{23}$ $cm^{-2}$, much greater than the value of $N_H$ determined from the spectrum of Cen X-3.

We conclude that grain scattering will not produce the apparent decrease in pulsations in the Cen X-3 data. If real, the decrease must be intrinsic to the source. A possibility is Compton scattering in a partially ionized stellar wind. In this case, at energies above 10 keV, one would expect pulsations to decrease again. Another possibility is the existence of a steady source, perhaps the accretion disc itself. At any rate the suggested decrease in pulsations does not bear directly on the distance to Cen X-3.

## VII. Optical Constraints on the Distance and on $N_H$

Despite the lack of a firm optical underpinning for specific stellar wind models, ground-based observations strongly suggest that the Bleeker *et al*. upper limit on $N_H$ of $1.0 \times 10^{21}$ $cm^{-2}$ is too low, difficult to reconcile with conventional understanding of Krzeminski's star. Making use again of the reddening relation of Jenkins and Savage, the Bleeker data leads to the conclusion that $E_{B-V}$ is approximately 0.1. On the other hand, the study of Fitzgerald (1968) reveals that stars roughly a kpc distant in the direction of Cen X-3 are reddened by $E_{B-V} \gtrsim 0.3$, giving an upper limit to the distance to the X-ray source. At 1 kpc, the absolute visual magnitude of the primary is approximately 3.1, 7 to 9 magnitudes fainter than normal absolute visual magnitudes of the spectral type ascribed to

Krzeminski's star. With an interstellar reddening correction of $E_{B-V} \sim 0.1$ and the observed maximum Uhuru flux of 160 counts $s^{-1}$ ($2 \leq E \leq 6$ keV), the X-ray luminosity of Cen X-3 would exceed the visible luminosity of Krzeminski's star by a factor of 10. The visible light curve would be dominated by X-ray heating, as in the case of Her X-1, in which maximum light occurs at phase 0.5 when the X-ray source is between HZ Her, the low mass primary, and the earth.

Rickard (1974) has approached the problem from a somewhat different viewpoint. Based on his observed spectral type (09.5 - B0.5 Ib), he derives the reddening $A_V = 4.13$ magnitudes which combined with a minimum visual luminosity of $M_V = -5.8$ implies a distance of 10 kpc. If $R = A_V/E_{B-V}$ the Jenkins and Savage relation implies that $N_H$ is approximately $10^{22}$, which Rickard concludes is consistent with 21-cm estimates of the hydrogen column density in that direction. Rickard's method is more sensitive to the reddening ratio R. However, both methods strongly imply that the "Cen X-3" of the Dutch-Nagoya measurement and Krzeminski's star are not the same object.

## VIII. The Soft X-ray Sky Near Cen X-3

Although, within the accuracy of the measurements, all propane counters on flights 1 and 2 appear to observe identical X-ray fluxes while pointed at Cen X-3, the observed spectrum in that direction is unusually hard for the diffuse X-ray background. The observed

Figure 5.5

The spectrum of the Centaurus region is much harder than that of enhancements discussed in Chapter IV. Only the instrument background has been subtracted from the propane counter data shown, obtained on flight 1 with the 5° x 10° counter. The spectrum is very similar to other spectra obtained near the Cen X-3 region, attributed to Cen X-3 by Bleeker et al. and to $\eta$ Car by Hill et al. $\chi^2$ in the best fit spectrum was 14.4 with 13 degrees of freedom. In the inset $\chi^2 + 1$ and $\chi^2 + 3$ contours are shown.

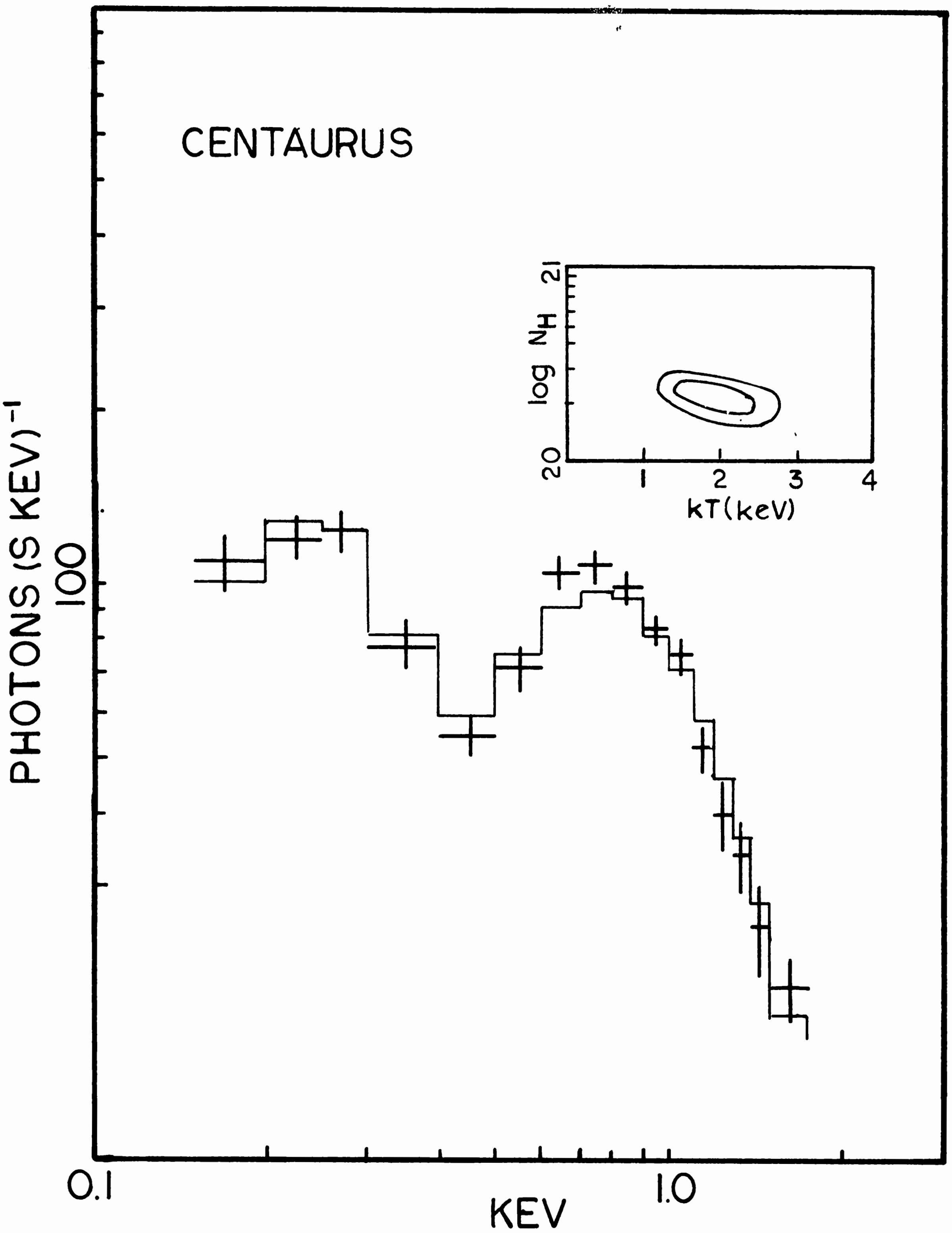
CENTAURUS
PHOTONS (S KEV)$^{-1}$
100
0.1
1.0
KEV
log $N_H$
21
20
1
2
3
4
kT(keV)

flux peaks at about 0.7 keV, with a total incident intensity of 0.6 photons $cm^{-2}$ $s^{-1}$, enhanced by a factor of 2 between 0.5 and 1.5 keV over typical background regions observed in the Eridanus scans. Chi-squared fits of the observed spectrum between 120 and 150 seconds, shown in Figure 5.5, indicate kT = 1.9 $\pm$ 0.4 keV with hydrogen column densities of approximately 0.2 x $10^{21}$ $cm^{-2}$. Only an instrumental background has been subtracted in determining the raw spectrum, however, so interpretation of these spectral results is unclear. Sanders (private communication, 1974) confirms that this region is quite prominent on the Wisconsin rocket survey above 0.5 keV.

The Bleeker et al. spectrum of Cen X-3 also peaks at about 0.7 keV, a further suggestion that although Cen X-3 is not a soft X-ray source, some source must exist in the vicinity of Cen X-3. Bleeker et al. state that the soft source (0.37 - 1.9 keV) which they observe is coincident to within 1° of the hard source (1.9 - 6.9 keV). However, in view of the short observing times involved in spinning rocket observations, the difficult aspect determination procedure required, and the large solid angle (72 square degrees) of the Dutch-Nagoya experiment, the possibility of source confusion is very real.

Some indication that emission in the region is not isotropic is contained in the scans performed on flight 1 in the $\eta$ Car region nearby (Figure 6.1). Interestingly, Hill et al. (1972), on the same flight in which no soft emission was observed from Cen X-3, did report a source in the region which they identified with $\eta$ Car. The spectrum is similar in intensity to that observed by Caltech with the 5° x 10° propane counter. This observation motivated the Caltech scan over the region; however, no source, including $\eta$ Car, was seen. Among the objects excluded as originators of the X-ray flux are the three known supernova remnants in the region, MSH 11-54, MSH 11-62, and MSH 11-61a (Iloviasky and Lequeux 1972). (The 1$\sigma$ upper limit on the incident flux between 0.4 and 1.5 keV in counter 2 for sources scanned was 0.08 counts $(cm^2\ s)^{-1}$.) Copernicus X-ray observations confirm that $\eta$ Car is not a soft X-ray source (Margon, private communication 1974).

Clearly, the soft X-ray sky near Cen X-3 requires more study on a scale of a few degrees to sort out the nature of the region. That the spectral measurements of the Dutch-Nagoya, LRL, Wisconsin and Caltech experiments are in reasonable accord seems to indicate the existence of a source somewhere in the region. Based on the Caltech data, the most likely region for the source is between +1° and +5° in $b^{II}$ and between 285° and 290° in $l^{II}$.

# CHAPTER VI

## SUMMARY

We have discussed X-ray data between 0.15 and 15 keV obtained on two Nike-Aerobee sounding rocket experiments launched on 1 and 8 November 1973 from Woomera, Australia at 17:30 and 17:15 UT respectively. An experiment description is contained in the Appendix. We have obtained the following results:

(1) The X-ray luminosity of the LMC is approximately $10^{38}$ ergs $s^{-1}$ between 0.4 and 1.5 keV, approximately 1/10 that of the Galaxy, consistent with the ratio of the masses. The total spectrum is similar to the spectrum obtained by Price *et al*. (1971) at higher energies. The optical bar of the LMC does not appear in the Caltech data as a strong soft X-ray source as reported by Rappaport *et al*. (1975).

(2) The extragalactic flux of diffuse X-rays is less than 250 photons $(cm^2\ s\ keV\ sr)^{-1}$ at 0.215 keV, based on the lack of modulation of the observed X-ray flux between 0.15 and 0.28 keV by neutral hydrogen in the direction of the LMC. This upper limit is from 2 to 4 times smaller than extragalactic fluxes inferred from observations of the North Galactic Pole and is consistent with no enhancement over an extrapolation of the power law flux observed between 2 and 10 keV.

(3) Spectra obtained of the low $N_H$, Eridanus, and Gemini-Monoceros extended soft X-ray enhancements are similar (Figures 4.6,

4.7, and 4.9 respectively). The Eridanus and Gemini-Monoceros regions are Galactic in origin with distances no greater than a few hundred parsecs. Due to the low total H I column density in the direction of the low $N_H$ enhancement, its spatial location cannot be unambiguously established. Volume emissivities ($\sim 4 \times 10^{-28}$ erg $(cm^3\ s)^{-1}$) and best fit temperatures ($T_6$ from $1 \lesssim T_6 \lesssim 4$) indicate a common origin for both enhanced and unenhanced soft X-ray background regions, which we interpret in terms of a very diffuse hot plasma.

(4) Although wide field of view observations in the direction of Cen X-3 confirm the existence of an intensified 0.4 to 1.5 keV flux in this direction, narrow beam detectors show that this excess flux is not associated with the Cen X-3 system. Optical constraints which can be placed on the binary system confirm this result; nor is the enhancement due to $\eta$ Car as suggested by Hill et al. (1972). The energy dependence of the X-ray pulsed fraction, suggested by the Caltech data, can not be explained by dust grain scattering, and, if real, is intrinsic to the X-ray source.

REFERENCES

Aannestad, P. A., and Purcell, E. M. 1973, Ann. Reviews of Astron. and Astrophys., 11, 309.

Agrawal, P. C., Moore, W. E., and Garmire, G. P. 1973, Proceedings of the 13th International Cosmic Ray Conference (Denver, Colorado), 4, 2697.

Alexander, J. R., Brown, L. W., Clark, T. A., and Stone, R. A. 1970, Astron. and Astrophys., 6, 476.

Allen, C. W. 1973, Astrophysical Quantities, (Athlone Press, University of London).

Arons, J., and McCray, R. 1969, Astrophys. Lett., 5, 123.

AS&E X-ray Astronomy Group, 1973 NATO Advanced Study Institute on Physics of Compact Objects (Cambridge, England: Institute of Astronomy).

Bennett, A. S. 1962, M.N.R.A.S., 68, 163.

Berkhuijsen, E. M. 1971, Astron. and Astrophys., 14, 359.

Bleeker, J. A. M., Deerenberg, A. J. M., Yamashita, K., Hayakawa, S., and Tanaka, Y. 1973, Ap. J. (Letters), 183, L1.

Bok, B. J. 1966, Ann.Reviews of Astron. and Astrophys., 4, 95.

Borken, R., Doxsey, R., and Rappaport, S. 1972, Ap. J. (Letters), 178, L115.

Bowyer, C. S., and Field, G. B. 1969, Nature,223, 573.

Bowyer, C. S., Field, G. B., and Mack, J. E. 1968, Nature, 217, 32.

Bowyer, S., Margon, B., Lampton, M., and Cruddace, R. 1974, Ap. J., 190, 285.

Brown, R. L., and Gould, R. J. 1970, Phys. Rev. D., 1, 2252.

Buff, J., and McCray, R. 1974, Ap. J., 189, 147.

Bunner, A. N., Coleman, P. L., Kraushaar, W. L., and McCammon, D. 1972, Ap. J.(Letters), 172, L67.

Bunner, A. N., Coleman, P. L., Kraushaar, W. L., McCammon, D., and Williamson, F. O. 1973, Ap. J., 179, 781.

Bunner, A. N. 1974, Proceedings of the International Conference on X-Rays in Space (Calgary, Canada), p. 410.

Castor, J. I., McCray, R., and Weaver, T. A. 1975, Ap. J. (Letters), 200, L107.

Catura, R. C., Acton, L. W., and Johnson, H. M. 1975, Ap. J. (Letters), 196, L47.

Chevalier, R. A. 1974, Ap. J., 188, 501.

Chevalier, R. A. 1975, preprint.

Cooke, B. A., and Pounds, K. A. 1971, Nature Phys. Sci., 229, 144.

Cox, D. P., and Smith, B. W. 1974, Ap. J. (Letters), 189, L105.

Daniel, R. R., and Stephens, S. A. 1970, Space Sci. Rev., 10, 599.

Davidsen, A., Schulman, S., Fritz, G., Meekins, J. F., Henry, R. C., and Friedman, H. 1972, Ap. J., 177, 629.

de Korte, P. A. J., Bleeker, J. A. M., Deerenberg, A. J. M., Tanaka, Y., and Yamashita, K. 1974, Ap. J. (Letters), 190, L5.

Deltabuit, E., and Meyer, S. 1972, Astron. and Astrophys., 20, 415.

de Vaucouleurs, G., and Freeman, K. C. 1972, Vistas in Astron., 14, 163.

Dieter, N. H. 1965, Astron. J., 70, 552.

Feast, M. W., Thackeray, A. D., and Wesselink, A. J. 1960, MNRAS, 121, 25.

Fejes, I., and Wesselius, P. R. 1973, Astron. and Astrophys., 24, 1

Field, G. B. 1972, Ann. Reviews of Astron. and Astrophys., 10, 227.

Field, G. B. 1974, in IAU Symposium #63, "Confrontation of Cosmological Theories with Observational Data," ed. Bradt, H. and Giacconi, R., (Boston), p. 13.

Field, G. B., and Henry, R. C. 1964, Ap. J., 140, 1002.

Fitzgerald, M. P. 1968, Astron. J., 73, 983.

Giacconi, R., Gursky, H., Kellogg, E., Schreier, E., and Tananbaum, H. 1971, Ap. J. (Letters), 167, L67.

Giacconi, R., Murray, S., Gursky, H., Kellogg, E., Schreier, E., Matilsky, T., and Koch, D. 1974, Ap. J. Suppl #237, 27, 37.

Gorenstein, P., and Tucker, W. H. 1972, Ap. J., 176, 333.

Gould, R. J., and Sciama, D. W. 1964, Ap. J., 140, 1634.

Hayakawa, S., Yamashita, K., and Yashioka, S. 1969, Astrophys. and Space Science, 5, 497.

Hayakawa, S. 1970, Prog. in Theor. Phys., 43, 1224.

Hayakawa, S., and Tanaka, Y. 1973, Ap. J. (Letters), 183, L5.

Heiles, C. 1975, Astron. and Astrophys. Suppl., 20, 37.

Henke, B.L.,and Elgin,R.L.1970, Advances in X-ray Analysis, 13, 639.

Henry, P., Cruddace, R., Lampton, M., Paresce, F., and Bowyer, S. 1975, preprint accepted by Ap. J. (Letters).

Henry, R. C., Fritz, G., Meekins, J. F., Friedman, H., and Byram, E. T. 1968, Ap. J. (Letters), 153, L11.

Hill, R. W., Burginyon, G., Grader, R. J., Palmieri, T. M., Seward, F. D., and Stoering, J. P. 1972, Ap. J., 171, 519.

Hindman, J. V., Kerr, F. J., and McGee, R. X. 1963, Aust. J. of Phys., 16, 570.

Hollenbach, D. J., Werner, M. W., and Salpeter, E. E. 1971, Ap. J., 163, 165.

Holt, S. S., ed. 1974, Proceedings of the Workshop on Electron Contamination in X-ray Astronomy Experiments, May, 1974, GSFC.

Ilovaisky, S. A., and Lequeux, J. 1972a, Astron. and Astrophys., 15, 169.

Ilovaisky, S. A., and Lequeux, J. 1972b, Astron. and Astrophys., 20, 347.

Jackson, J. C. 1975, submitted to MNRAS.

Jenkins, E. B., and Meloy, D. A. 1974, Ap. J. (Letters), 193, L121.

Jenkins, E. B., and Savage, B. D. 1974, Ap. J., 187, 243.

Jordan, C. 1969, MNRAS, 142, 501.

Kafatos, M. C., and Morrison, P. 1973, Astron. and Astrophys., 26, 71.

Karzas, W., and Latter, R. 1961, Ap. J. Suppl., 6, 167.

Krzeminski, W. 1973, I.A.U. Circular #2612.

Kurt, V. G., and Sunyaev, R. A. 1967, J.E.T.P. Lett., 5, 246.

Landecker, T. L., and Wielebinski, R. 1970, Aust. J. of Phys., Ap. Supp., 16, #1.

Leong, C., Kellogg, E., Gursky, H., Tananbaum, H., and Giacconi, R. 1971, Ap. J. (Letters), 170, L67.

Manchester, R. N., and Taylor, J. A. 1972, Astrophys. Lett., 10, 67.

Maran, S. P., and Modali, S. B. 1970, Earth and Extraterrestrial Sciences, 1, 147.

Margon, B. 1974, private communication.

Margon, B., Bowyer, S., Cruddace, R., Heiles, C., Lampton, M., and Troland, T. 1974, Ap. J. (Letters), 191, L117.

Margon, B., Mason, K. O., Hawkins, F. J., and Sanford, P. W. 1975, Ap. J. (Letters), 196, L51.

Margon, B., and Ostriker, J. P. 1973, Ap. J., 186, 91.

Mark, H., Price, R., Rodrigues, R., Seward, F. D., and Swift, C. D. 1969, Ap. J. (Letters), 155, L143.

Markert, T. H., and Clark, G. W. 1975, Ap. J. (Letters), 196, L55.

Mathewson, D. S., and Healy, J. R. 1963, IAU Symposium #20, Canberra, The Galaxy and the Magellanic Clouds, p. 245.

McCammon, D., Bunner, A. N., Coleman, P. L., and Kraushaar, W. L. 1971, Ap. J. (Letters), 168, L33.

McCray, R., and Hatchett, S. 1974, private communication.

McCulloch, P. M., Komesaroff, M. M., Ables, J. G., Hamilton, P. A., and Rankin, J. M. 1973, Astrophys. Lett., 14, 169.

McGee, R. X., and Milton, J. A. 1966, Aust. J. of Phys.Astro.Supp. #2

McGee, R. X., Milton, J. A., and Wolfe, W. 1966, Aust. J. of Phys. Astro. Supp. #1.

McGee, R. X., and Newton, L. M. 1972, Aust. J. of Phys., 25, 619.

Menon, T. K. 1957, Radio Astronomy IAU Symposium #4, ed. by H. C. van der Hulst (Cambridge: Cambridge U. Press), 56.

Moore, W. E. 1975, Ph.D. Thesis, California Institute of Technology.

Naranan, S., Friedman, H., Fritz, G., Henry, R. C., and Shulman, S. 1974, in Proceedings of the Workshop on Electron Contamination in X-ray Astronomy Experiments, ed. by S. S. Holt, GSFC.

Noonan, T. W. 1972, Ap. J., 171, 209.

Öpik, E. J. 1953, Irish Astronomical Journal, 2, 219.

Osmer, P. S., Hiltner, W. A., and Whelan, J. A. J. 1975, Ap. J., 195, 705.

Ostriker, J. P., Richstone, D. O., and Thuon, T. X. 1974, Ap. J. (Letters), 188, L87.

Petro, L. D. 1975, Ap. J., 195, 709.

Policarpo, A. J. P. L., Conde, E. A. N., and Alves, M. A. F. 1968, Nuclear Inst. and Meth., 58, 151.

Price, R. E., Groves, P. J., Rodrigues, R. M., Seward, F. D., Swift, C. D., and Toor, A. 1971, Ap. J. (Letters), 168, L7.

Pringle, J. E. 1973, Nature Phys. Sci., 243, 90.

Radhakrishnan, V., Murray, J. D., Lockhart, P., and Whittle, R. P. J. 1972, Ap. J. Suppl. #203, 24, 15.

Rapley, C. G., Bell Burnell, S. J., and Culhane, J. L. 1975, preprint.

Rapley, C. G., and Tuohy, I. R. 1974, Ap. J. (Letters), 191, L113.

Rappaport, S., Levine, A., Doxsey, R., and Bradt, H. V. 1975, Ap. J. (Letters), 196, L15.

Raymond, J., and Cox, D. 1975, private communication.

Reynolds, R. J., Roesler, F. L., and Scherb, F. 1974, Ap. J. (Letters), 192, L53.

Rickard, J. J. 1974, Ap. J. (Letters), 189, L113.

Rosendhal, J. D. 1973, Ap. J., 186, 909.

Sanders, W. T. 1974, private communication.

Savage, B. D. and Jenkins, E. B. 1972, Ap. J., 172, 491.

Schreier, E., Levinson, R., Gursky, H., Kellogg, E., Tananbaum, H., and Giacconi, R. 1972, Ap. J. (Letters), 172, L79.

Schreier, E. J., Schwartz, K., Giacconi, R., Fabbiani, G., and Morin, J. 1975, submitted to Ap. J.

Schwartz, J. 1973, Ap. J., 184, 5.

Seward, F., Burginyon, G., Grader, R., Hill, R., Palmieri, T., Stoering, P., and Toor, A. 1975, submitted to Ap. J.

Shrewsberry, D. 1973, private communication.

Shulman, S., Naranan, S., Friedman, H., Fritz, G., and Henry, R. C. 1975, Bulletin of the American Physical Society, 20, 603.

Silk, J. 1973, Ann. Reviews of Astron. and Astrophys., 11, 269.

Sivan, J. P. 1974, Astron. and Astrophys. Supp., 16, 163.

Spoelstra, T. A. Th. 1973, Astron. and Astrophys., 24.

Stevens, J. C. 1973, Ph.D. Thesis, California Institute of Technology.

Trümper, J., and Schönfelder, V. 1973, Astron. and Astrophys., 25, 445.

Tucker, W. H., and Koren, M. 1971, Ap. J., 168, 283.

Tuohy, I. R., and Rapley, C. G. 1975, Ap. J. (Letters), 198, L69.

Ulmer, M. P., Baity, W. A., Wheaton, W. A., and Peterson, L. E. 1974, Ap. J., 191, 593.

Van der Laan, H. 1962, MNRAS, 128, 19.

Vanderhill, M. J., Borken, R. J., Bunner, A. N., Burstein, P. H., and Kraushaar, W. L. 1975, Ap. J. (Letters), 197, L19.

Vidal, N. V., Wickramasinghe, D. T., Peterson, B. A., and Bessell, M. S. 1974, Ap. J. (Letters), 191, L23.

Weinberg, S. L., and Silk, J. 1973, Ap. J., 183, 47.

Williamson, F. O., Sanders, W. T., Kraushaar, W. L., McCammon, D., Borken, R., and Bunner, A. N. 1974, Ap. J. (Letters), 193, L133.

York, D. G. 1974, Ap. J. (Letters), 193, L127.

# APPENDIX

# EXPERIMENT DESCRIPTION AND CALIBRATION PROCEDURES

## I. Introduction

The cosmic X-ray payload used in these experiments consisted basically of four large-area proportional counters whose fields of view were defined by mechanical collimators. Ancillary equipment included electronics for processing X-ray data and transmitting it to the ground, a camera for post-flight aspect determination, and gas control systems to maintain the proper pressure in the propane detectors.

The payload had been flown three times previously from White Sands, New Mexico. However, the data for this thesis were obtained on two launches from Woomera, Australia in the early morning hours of November 1 and 8, 1973. For the Australian flights several modifications were made to the payload, of which the most noteworthy was that one low energy detector was converted to operate as a sealed medium energy detector, thus increasing the dynamic energy range to include X-rays from 0.15 to 15 keV. (Other descriptions of the payload, as configured for previous flights, have been presented by Moore 1975, Agrawal *et al*. 1973 and Stevens 1972.)

Figure A.1

The Caltech X-ray astronomy payload, back, side and front views.

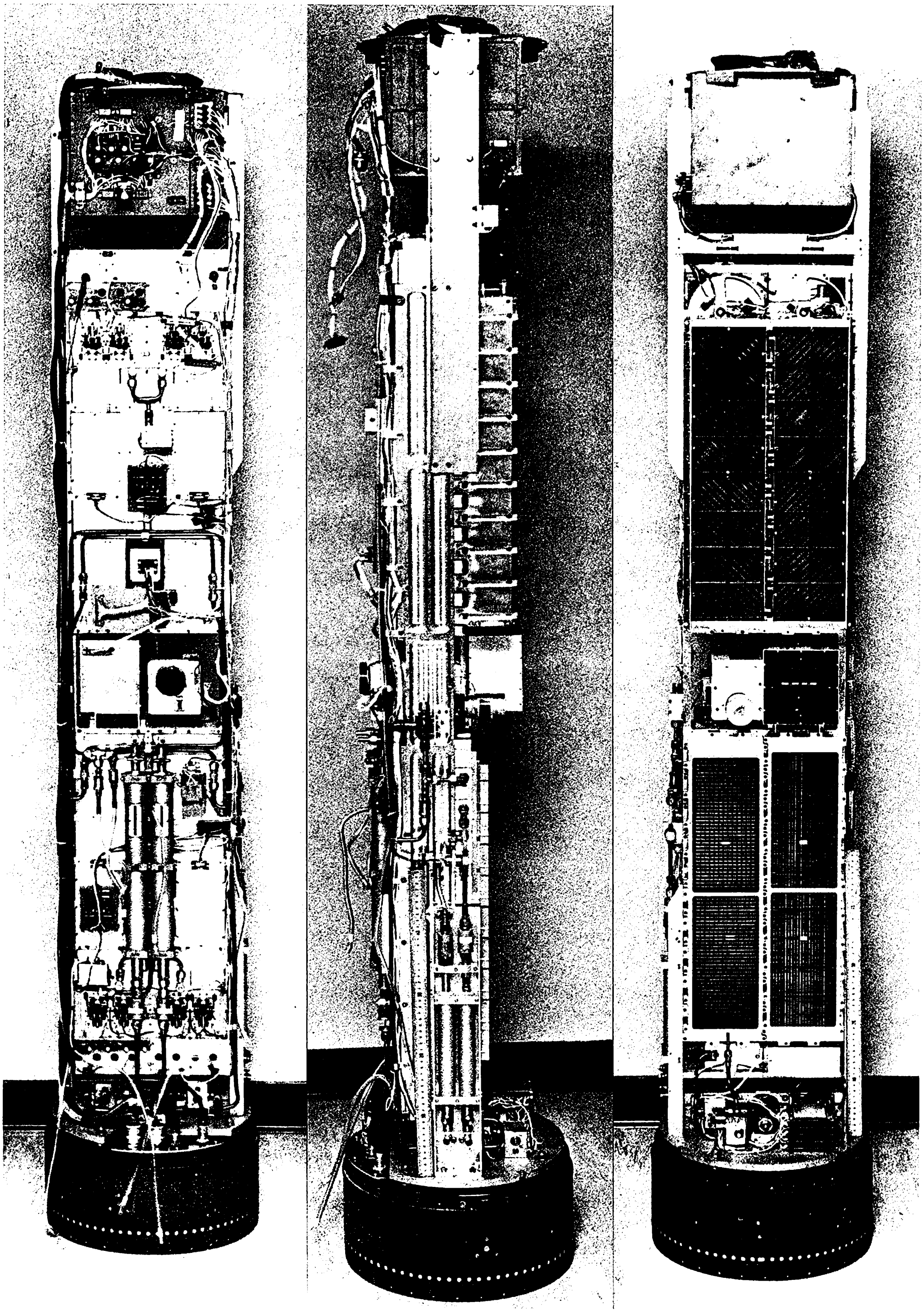

## II. Flight Parameters--Mechanics of the Flight

The Caltech payload, with a total recoverable weight of 350 lbs., was launched atop unguided Nike-Aerobee sounding rockets. A solid-fueled booster originally designed for use in anti-aircraft defense, the first stage Nike burned for 3.5 seconds during which the payload was subjected to noise spikes of up to 30 g. After staging at 10,000 feet, thrust was provided by the liquid-fueled Aerobee sustainer. Approximately 57 seconds after liftoff at an altitude of 52 km, the Aerobee's fuel exhausted, the payload, with the spent Aerobee still attached, began to coast upward reaching a peak altitude exceeding 100 miles.

Immediately after burnout, the payload, which had been spun up to several rps to stabilize the vehicle during fuel burning, was mechanically despun by releasing a lead-weighted rope which had been wrapped around the payload. A gas-jet gyro system then began a series of preplanned maneuvers. Before opening the experiment door at approximately 95 seconds, the soft X-ray counters were flushed with propane for a final time and calibrations of the gain and resolution were made of all counters. After door opening, approximately 255 seconds of data were acquired during each flight. Gain and resolution calibrations were repeated after the door closed in preparation for reentry. After separation from the Aerobee, the experiment payload was parachuted to the ground and recovered intact. Launch was carried out by the personnel of Goddard Space Flight Center, Sounding Rocket Division, under the range control of the Weapons Research Establishment of the Australian government. Caltech responsibility covered the scientific portion of the payload.

Below an altitude of 130 km, significant absorption due to the residual atmosphere affected the observed X-ray flux during the flights (at 130 km, when looking at the zenith, transmission is $\sim$ 95% at both 0.25 and 1 keV) Unfortunately peak altitudes of 167 and 171 km of flights 1 and 2 respectively were considerably lower than peak altitudes of the same experiment at White Sands with a consequential reduction of approximately 50 seconds of useful data acquisition time. These less advantageous profiles were a result of the lower altitude of the Woomera launch site, use of a heavier, but not more powerful Aerobee sustainer, and use of a different, aerodynamically poorer antenna configuration.

## III. Attitude Control and Aspect Determination

The Strap-III attitude control system, provided by NASA, was a 3-axis stabilized system. Maneuvers, initiated by torqueing a master set of gyros to which the payload is slaved, consisted either of rolls, pitches or yaws of specified duration and rate. The collimator beams were aligned to be centered on the negative pitch axis of the 3-axis system. Thus pitches rotated the fields of view about a fixed point in the sky while rolls and yaws moved the centers of the collimator beams in perpendicular directions. Typically the flight plan consisted of holds on or pitches about one or more known

X-ray point sources and a series of slow rolls in various directions across an extended region of the sky. The "star" pattern which was used in both flights 1 and 2 allowed a maximal number of non-parallel scans utilizing a minimum number of maneuvers.

The attitude control system used has an initial pointing error of 3° (3σ), an important consideration when designing the flight plan. On each subsequent maneuver, an additional error of 0.25° or 1% of the total maneuver could be accrued (Shrewsberry 1973, private communication). The actual position would lag or lead the mean position as determined by the gyro-servo system by approximately 1° during slow rolls. Finally, somewhat more complicated variations from the mean position could occur during fast (5° $s^{-1}$) pitches.

In order to provide accurate aspect information, 1-second exposure in-flight photographs were taken with a 16 mm f/1.5 star field camera which had a field of view of approximately 8° x 12°. When two or more known star tracks were visible in the photographs, the attitude of the rocket platform could be determined to better than 0.15° using computer generated clear plastic overlays. A wide field of view and extremely fast film (Kodak 2485) were used because effective exposure times were extremely short when the rocket was scanning. Despite these precautions, due to the scarcity of bright stars at high galactic latitudes and possibly due to less than ideal developing conditions, many photographs contained one or no stars. In practice no stars were seen when scanning at 0.5° $s^{-1}$ of visual magnitude greater than 4.3. Positions determined using the photographs are indicated by the "crosses" in Figure 2.1 of the LMC scans and in Figure 4.1 of the Eridanus scans. The aspect was completely determined using the star field photographs in the Cen X-3 region, which is in the plane of the Galaxy.

When, as was often the case, the aspect could not be determined using the star field photographs, we have assumed that rolls and yaws have continued in great circles from known positions. Based primarily on our experience with the Strap-III system on previous flights, but also on telemetered attitude servo-voltages, we estimate the error in these scan paths to be approximately 0.5° perpendicular to the predicted scan lines, except near points of the "star" where $5° \ s^{-1}$ pitches were being executed. A lag or lead by approximately one second in the roll maneuvers is, of course, not ruled out, making identification of weak sources observed on multiple scans difficult. Since the actual maneuver times were known, modelled scan rates could be calculated. In all cases this rate turned out to be within 5% of the preplanned rate. In principle, this aspect solution could have been improved somewhat using the servo-voltages, which indicate the orientation of the payload with respect to the gyros. However, in view of the weak emission observed on the two flights, relatively little use was made of the narrow field of view detectors so that "fine-tuning" was not deemed necessary.

## IV. Fields of View

Mechanical collimators were used to define the varying fields of view (FOV) of each of the four counters of the Caltech payload (indicated in Figure 1.2). The long narrow collimators of counters 1 and 2 formed an "X" on the sky and were designed to allow mapping of extended bright soft X-ray sources, such as the supernova remnants in Vela and Cygnus (Moore 1975, Stevens 1972). Counter 3's 5° x 10° collimation, with a much larger area, was intended for spectral determinations as well as for observing coarser, but fainter variations in the soft X-ray sky. The 2° x 10° collimation of the P-10 counter represented a compromise, with a FOV small enough to eliminate source confusion near Cen X-3, but large enough so that spectra could be determined from hard X-ray sources.

Each counter had at least one slat, or "Venetian blind", collimator to provide support for the counter window, as well as coarse angular collimation. Slats for these collimators had been constructed from 0.010" aluminum sheet, sanded to provide an unburred surface for windows to rest upon but "roughed" so that low energy X-rays would not be reflected at low angles of incidence. An "egg crate" was constructed by slotting the slats and epoxying (Fuller Resiweld 7004) the structure together, producing a triangular response function in two directions.

Three of the four counters possessed an additional collimator to further limit the field of view. For the P-10 counter, a slat collimator was constructed especially for the Australian flights with an angular response of 2° FWHM. Constructed with slats in one direction only, these slats were positioned with metal spacers. In the other direction the FOV was defined by the window support collimator alone.

Because low energy electrons can be a severe problem in X-ray experiments (see Holt 1974), ceramic magnets (Indox I) were built into the 2° collimator to act as a magnetic broom. The minimum field strength between the slats was measured to be approximately 100 Gauss. Laboratory tests of similar magnets installed in the 5° x 10° window support collimator used on counter 3, indicate that at least 99% of all electrons up to 20 keV are rejected. Most higher energy electrons are rejected by the anti-coincidence scheme or because they deposit so much energy in the first layer of the counter that they are not counted as X-ray events.

Etched-grid or modulation-type collimators possess a number of advantages over conventional slat collimators for producing very narrow fields of view and were used to define fan beams of counters 1 and 2. An etched-grid collimator eliminates the portion of the slats which is redundant for shadowing purposes, replacing slats with etched grids and spacers. Stevens (1972) has discussed in detail the design and construction of these specialized collimators. A geometric progression is the basic spacing required to theoretically ensure complete shadowing. One of the advantages that the etched-grid collimators constructed at Caltech have over most conventional collimators is that they can be easily reconfigured to change the field of view. To widen the field of view all that is required is to remove the most widely spaced grids. On previous flights the minimum FOV of 0.4° FWHM had been utilized, but at launch the soft X-ray flux of the LMC was not known and therefore the FOV of counter 2 was also widened to 2°, because at a scan rate of 1.25° $s^{-1}$, a point source would have been in the beam for less than one second had a 0.4° FWHM collimation been utilized.

Modulation-type collimators built at Caltech rely primarily on their small solid angle to reject electrons. The etched grids do not reflect low energy electrons as slat collimators tend to do because there are few low angle reflections. No evidence of electron contamination was seen in any counter on either flight.

The calibration of all pre-existing and unmodified collimators was checked at several positions over each collimator and found to be consistent with previous calibrations. Systematic calibrations were carried on the reconfigured etched-grid collimators and on the 2° collimator for the P-10 counter. Calibration of the etched-grid collimator of counter 2 was carried out after return to Caltech.

Briefly the standard calibration procedure was to measure the transmission of a pre-collimated beam of 8.05 keV copper $K_\alpha$ X-rays through the test collimator which had been attached to a combination rotary table, X-Y table and angle plate. Copper $K_\alpha$ X-rays were

Figure A.2

Sample calibration curves for the collimators of counters 2 and 4. For counter 4, calibrations over the width of the collimator have been summed which serves to average out the interference between the 2° slat collimator and the 10° x 10° window support collimator. For counter 2, the collimators were tipped by 45° with respect to the axis of rotation during the test. The collimator FWHM given in this measurement is then 2.5° x 0.71 $\sim$ 1.8° in this calibration. Note the side lobes of the etched grid collimator. They are a result of the fact that grids are not rectangular in cross section but have rounded edges as well as possibly a slight misalignment of the grids.

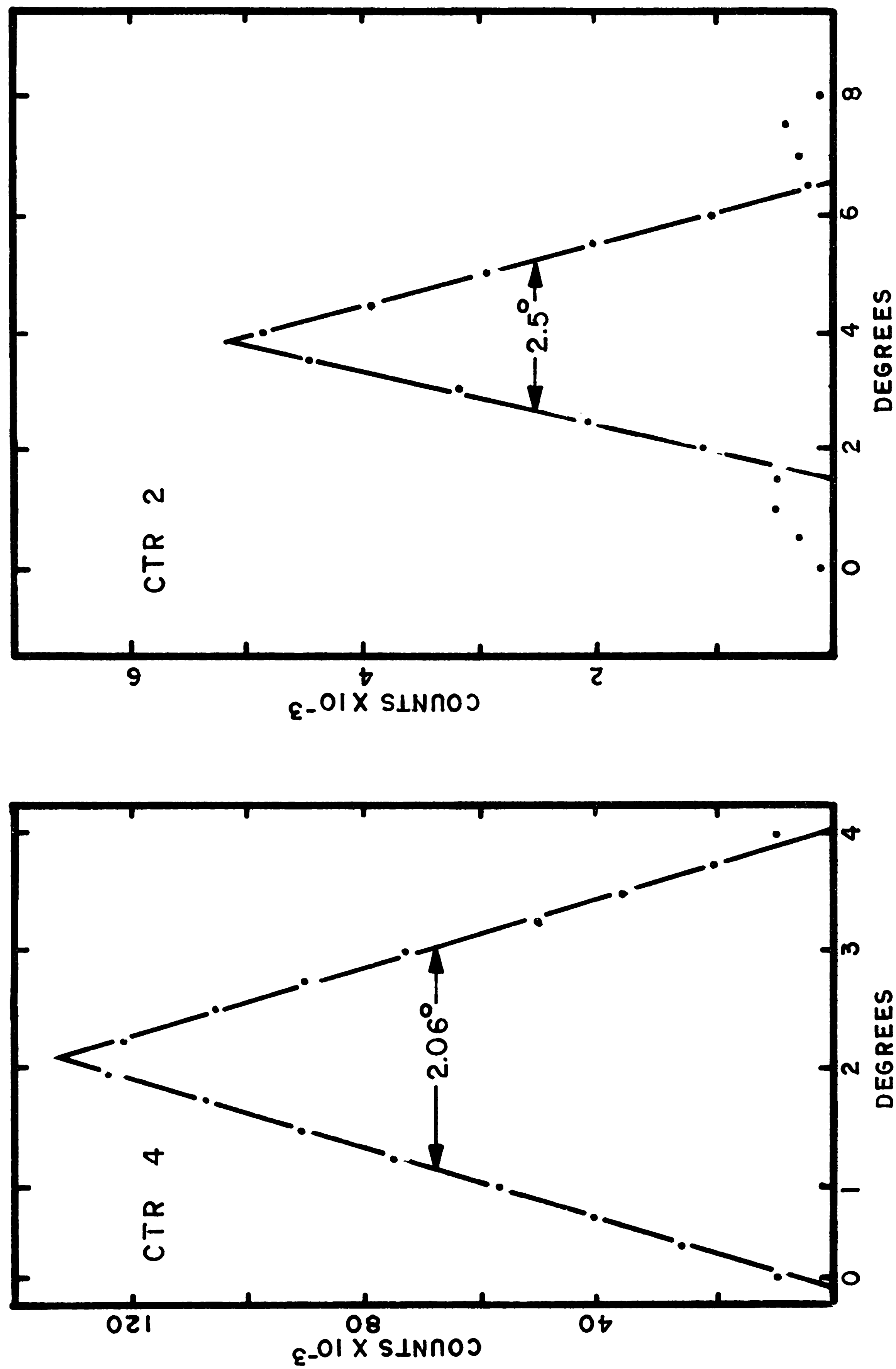
CTR 2
2.5°
DEGREES
COUNTS X 10⁻³
CTR 4
2.06°
DEGREES
COUNTS X 10⁻³

obtained by placing a copper foil (0.007") in the path of a beam of continuum X-rays which had been generated with a conventional X-ray machine (16 keV potential). The beam was pre-collimated to approximately 0.05°. The stability of the beam was monitored by placing a small proportional counter in front and slightly to the side of the last X-ray beam collimator. A P-10 filled proportional counter, placed behind the collimator being tested, was used to measure X-ray transmission at arbitrary angles in both directions with respect to the X-ray beam.

Results of calibration of the 2° collimator for the P-10 counter indicated FWHM of 1.97° ± 0.05°. When used in conjunction with the 10° x 10° window support collimator substantial interference between the two collimators was noted resulting in rather asymmetric transmission profiles at some positions on the collimator. On the average, however, the total transmission of the P-10 counter was well represented in terms of a 2° x 10° triangular response function. Small sidelobes appeared in the transmission of both etched grid collimators when the field of view was widened to 2°; however, in no case was the maximum transmission in the sidelobe greater than 10% of the peak transmission. Calibrations indicated a FWHM of 1.9 ± 0.1° for both the reconfigured collimators.

V. Proportional Counters--Description and Performance

Despite their relatively poor energy resolution by optical astronomy standards ($\lambda/\Delta\lambda \sim 3\sqrt{E_x/1.48\ \text{keV}}$), proportional counters, due to their relatively high effective area and low cost, have been the standard device for detecting medium and low energy X-rays in X-ray astronomy.

The proportional counters used in the Caltech payload consisted of a gas box, divided into eight anode cells, each 1" x 1" x 20" (Figure A.3). One wall of the gas box was formed by a thin plastic window through which X-rays pass. The 0.003" diameter tungsten anode wires, running the length of the cells, were spring mounted at one end inside Kel-F insulators, to maintain tautness during the observations but to prevent breakage in the launch environment. Ground planes of 0.012" copper-beryllium wire separated the cells. Thus all anode wires of a single counter shared the same gas volume.

The choice of counting gas was predicated by the energy range which we hoped to study, as well as ease of handling and to a lesser extend cost of the gas. Pure propane was used in the soft X-ray detectors. This gas has very good energy resolution, theoretically nearly 70% ($\Delta E/E$ FWHM) at 0.28 keV, somewhat better than can be attained with other common counting gases such as methane or P-10. Because propane is relatively dense ($2 \times 10^{-3}$ g cm$^{-3}$ at STP), it can be operated at the low pressure of 150 torr, which protects the thin polypropylene windows but preserves appreciable quantum efficiency up to 3 keV. Finally, because of propane's low liquefaction pressure ($\sim$ 125 psi at room temperature), enough propane can be carried aloft to allow for in-flight purging and maintenance of pressure in the

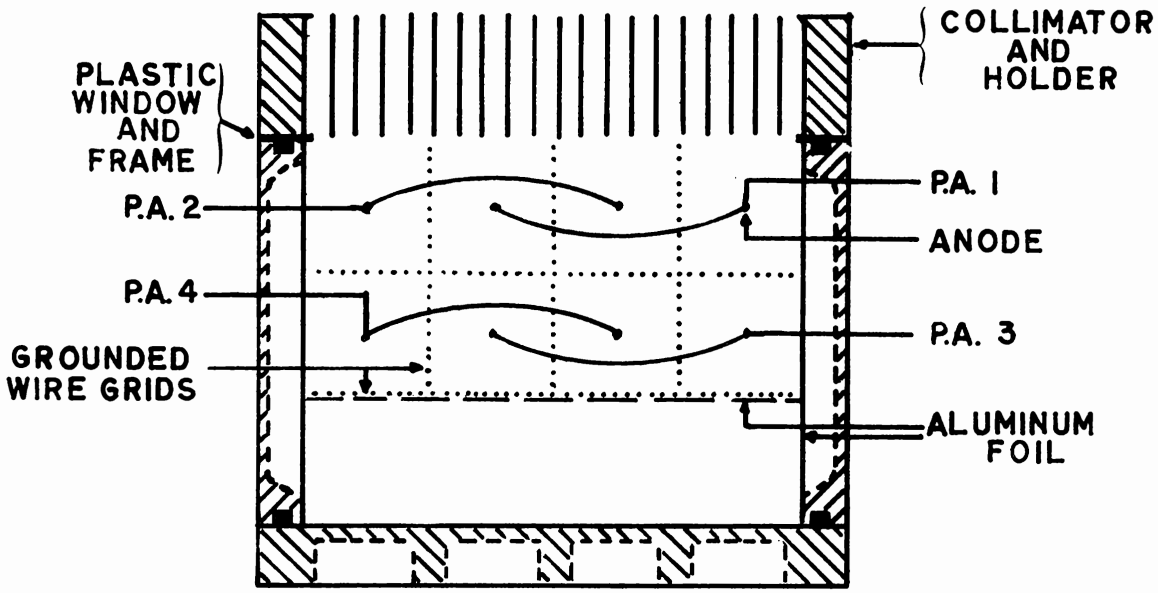


Figure A.3

An end view of the proportional counters used in the Caltech experiment. Although originally designed to have 3 layers, the third layer has not been utilized in recent flights because the alternating anti-coincidence scheme has proven to have a lower instrument background rate.

counters should small leaks develop. For the medium energy counter, a higher Z material was required. P-10, a standard counting gas, was selected and provided substantial absorption to X-rays below 15 keV (see Figure A.4). To check the performance of proportional counter high voltage and gas integrity, in-flight gain and resolution calibrations of the proportional counters were carried out using the characteristic $K_\alpha$ X-rays of aluminum (1.48 keV) and manganese (5.9 keV) for the propane and P-10 counters respectively. A commercial Iron-55 source (200 μC), which decays by electron capture, was used to produce the manganese X-rays. An α-emitter Polonium-210 (5 mC) covered with 0.0015" aluminum foil was used for the propane counter calibration. Counters 3 and 4 were calibrated with sources mounted directly on the experiment door, while on counters 1 and 2, sources were mounted on a source wheel between the etched-grid and window support collimators.

These gain and resolution calibrations indicate that all of the counters performed nominally with a few important exceptions: (1) At the beginning of both flights, the gain of counter 3 was a factor of 2 lower than planned and was observed to have increased during the flight. (2) The calibration spectra of counters 1 and 2 were not symmetrical and exhibited a low energy tail, e.g., were not gaussian. (3) The gain of counter 1 increased rapidly after 200 seconds of flight 2.

The gain change in counter 3 was due to the fact that the solenoid gas control system did not properly regulate the pressure of that

Figure A.4

Gas absorption (g), window transmission (t) and total (t) quantum efficiencies are shown for the detectors used on the Caltech Australian flights. Solid and dashed lines apply for the propane and P-10 counters respectively.

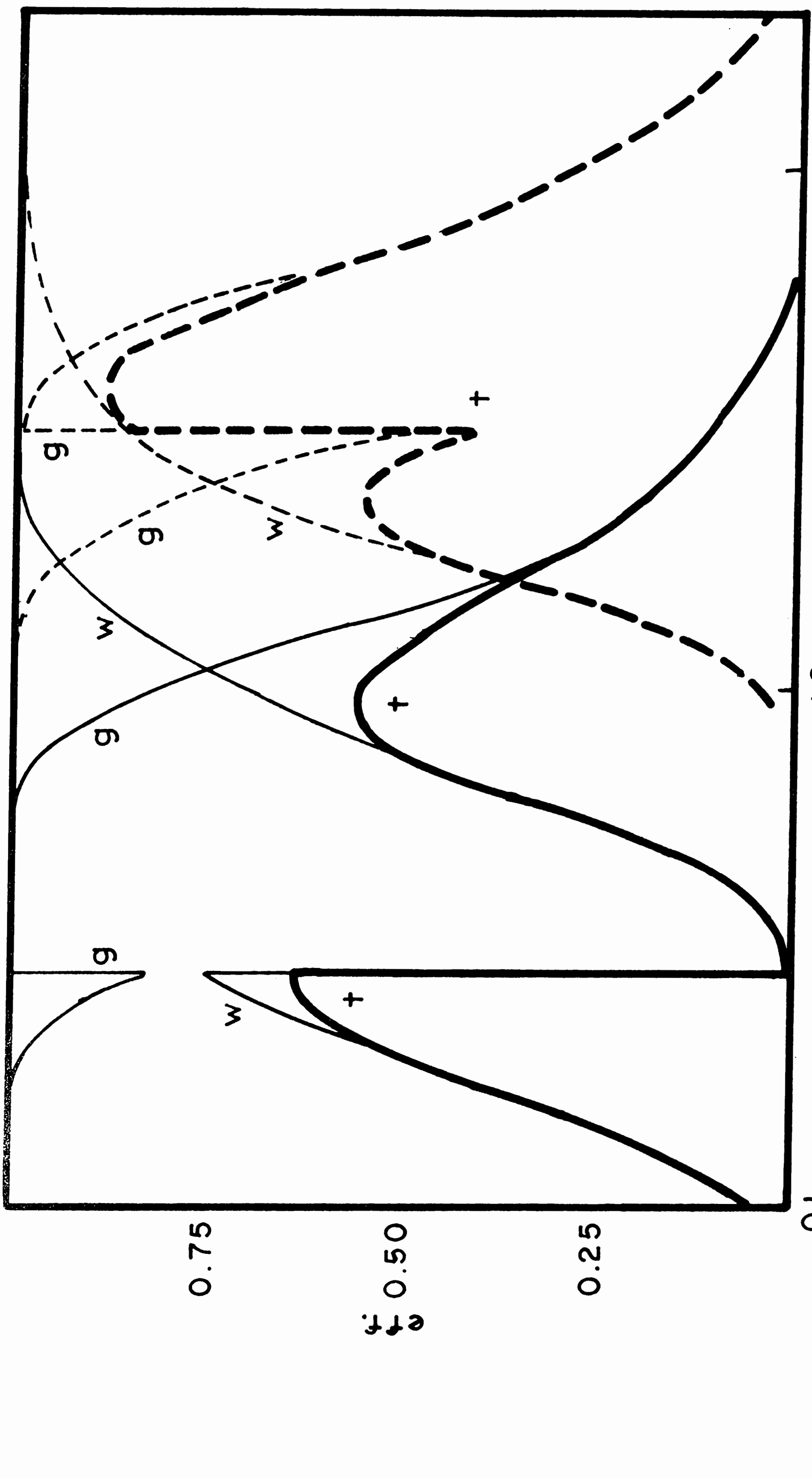
eff.
0.75
0.50
0.25
0.1
1.0
10
keV
g
w
+

counter. Instead the counter operated as a sealed counter during the flights and the gain change was due to a small (5%) change in the pressure as gas leaked out of the counter throughout the flight. To correct for this effect, we have assumed that the pressure linearly decreased as a function of time. In this case the gain would have increased as $e^{\alpha(t-t_o)}$ where $\alpha$ is a constant. Since two calibrations for each flight existed, the gain could thus be completely determined throughout.

The presence of asymmetric calibrations in counters 1 and 2 has been noted on previous flights and seems to be due to the charging up of the counter window in the vicinity of the calibrations source as well as due to end effects due to location of the calibration sources, rather than indicative of a serious failure in the counter. In any event, counters 1 and 2 were not used for detailed spectral determinations.

The dramatic gain increase of counter 1 in the middle of flight 2 indicates exhaustion of the gas supply, possibly due to gross window rupture. As a result counter 1 was utilized only for the Cen X-3 portion of that flight, e.g., before 140 seconds after launch. Except for this failure, we conclude that neither gain nor resolution problems seriously compromised the experiment.

In each gas volume, anode wires were linked as indicated in Figure A.3, reducing the number of parallel data processing units required, but still leaving four semi-independent proportional counters. The four data streams were operated in anticoincidence to reduce the

Table A.1

IN-FLIGHT RESOLUTION CALIBRATIONS

| | Counter | Calibration Energy (keV) | Resolution (%, FWHM) Beg. | End |
|---|---|---|---|---|
| Flight 1 | | | | |
| | 1 | 1.48 | ∿ 34+ | ∿ 35+ |
| | 2 | 1.48 | ∿ 35+ | ∿ 35+ |
| | 3 | 1.48 | 32++ | 30++ |
| | 4 | 5.9 | 19++ | 18++ |
| Flight 2 | | | | |
| | 1 | 1.48 | ∿ 37+ | -- |
| | 2 | 1.48 | ∿ 36+ | ∿ 38+ |
| | 3 | 1.48 | 32++ | 30++ |
| | 4 | 5.9 | 22++ | 20++ |

+ Estimated from portion of calibration curve with energy greater than the peak only. For reasons discussed in the text, we feel that the actual resolution of counters 1 and 2 is somewhat better than indicated by the calibration.

++ Results of Chi-squared fits to the calibrations. In all cases the best-fit value had a Chi-squared minimum value of less than 1 per degree of freedom.

Figure A.5

Sample in flight calibrations of the gain and resolution of the P-10 counter and the 5° x 10° propane counter. The escape peak in the P-10 counter is ∿ 8% of the main calibration peak. Because the probability for angle deexcitation relative to radiative deexcitation is very high in propane, no escape peak is seen in the soft X-ray calibration.

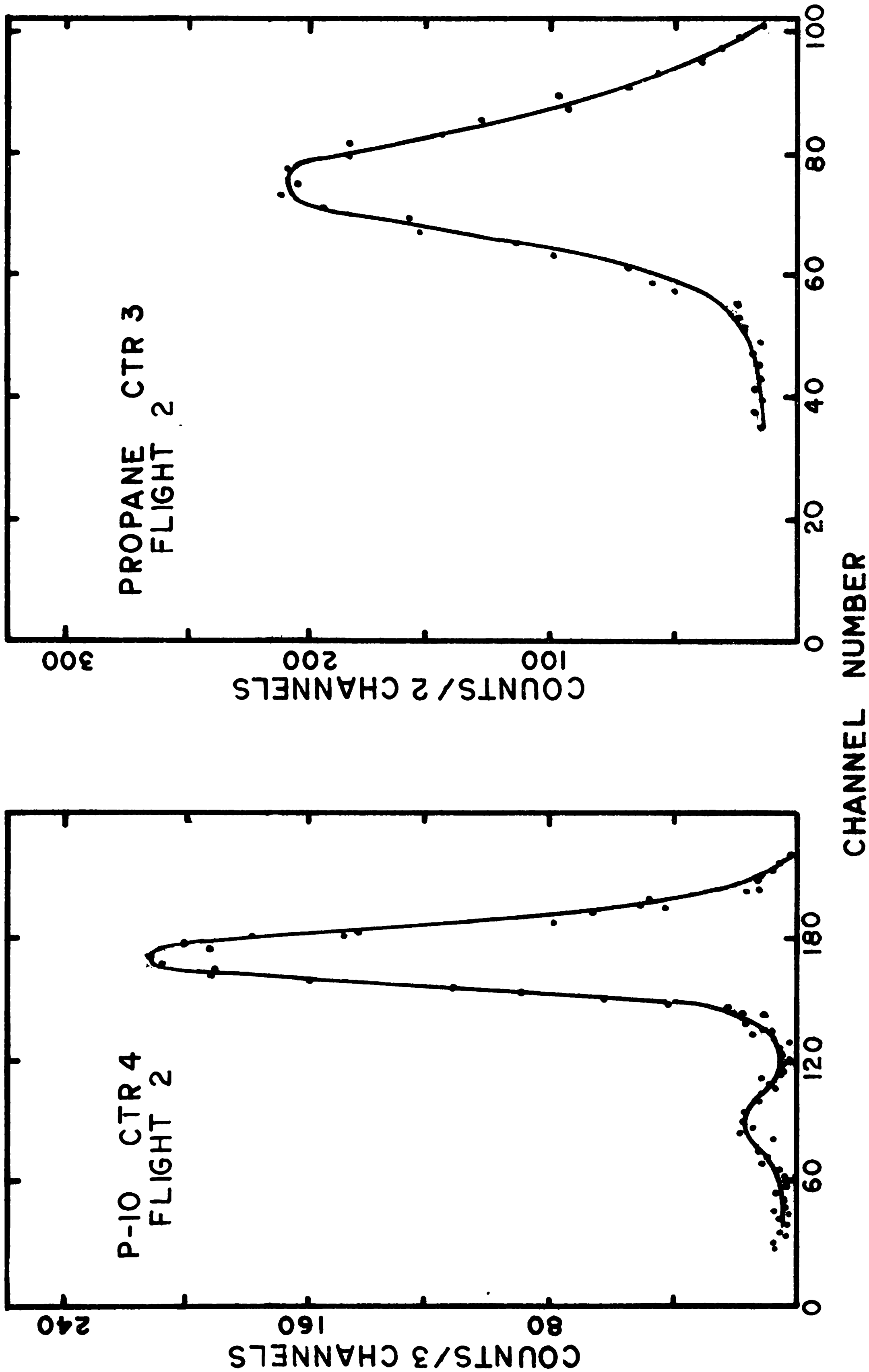
PROPANE CTR 3
FLIGHT 2
COUNTS/2 CHANNELS
300
200
100
0
20
40
60
80
100
P-10 CTR 4
FLIGHT 2
COUNTS/3 CHANNELS
240
160
80
0
60
120
180
CHANNEL NUMBER

instrument bakcground, primarily induced by cosmic rays, which at altitude havé a flux of approximately 1 $(cm^2\ s)^{-1}$. For typical path lengths in a cell of approximately 1" and an energy loss of 2 MeV $(g\ cm^2)^{-1}$, 2 and 9 keV are deposited by a minimum ionizing particle passing through the propane and P-10 counters respectively. Thus, without an effective veto system cosmic ray events would dominate the observed X-ray flux. With the veto system, however, the observed background rates in the propane counters, determined at altitudes of less than 100 km, amounted to 0.05 counts $(cm^2\ s\ keV)^{-1}$ at 0.15 keV and 0.01 counts $(cm^2\ s\ keV)^{-1}$ at 3 keV. Similar rates were observed in the P-10 counter.

Before flight 2, a preamplifier failure in counter 3, which could not be repaired in Australia, forced a change in the vetoing system of that counter. All four front cells of that counter were wired together, as were all back cells. Tests conducted at sea level have indicated that a vetoing system based on this arrangement is a factor of two less effective above 1 keV than the more sophisticated alternating system. However, these tests were not borne out by in-flight measurements which indicated only insignificant differences in the background rate.

Window material selection, like that of the counting gas, was predicated mainly by the energy range to be studied. A commercially available film, 0.0005" aluminized mylar, was used on the P-10 counter. Strong enough to hold up against a pressure differential of well over 800 torr, mylar has diffusion rates, unlike polypropylene, which are so low that the P-10 counter could be operated in flight as a sealed counter. Even so, 0.0005" mylar has very good transmission for X-rays above 2 keV. For the propane counters, much thinner 1.6 polypropylene coated with 15 μg $cm^{-2}$ of carbon was utilized. Polypropylene is a good choice for low energy detector windows not only because it retains strength when stretched to 160 μg $cm^{-2}$ (or thinner), but because it is a pure hydrocarbon ($C_3H_8$), which leads to good transmission properties. The pure carbon is needed to absorb stellar UV photons which the polypropylene transmits, and like the aluminization on the mylar to provide a ground plane for the front anode cells.

The propane counter windows were made by stretching commercially available 0.001" polypropylene sheet. Window stretching is a non-trivial art and considerable time was consumed in producing windows with uniform thickness throughout. The unstretched plastic was first firmly attached to a holding ring and placed over the end of a tube with diameter slightly smaller than the ring. After heating the polypropylene with a heat gun, the film can be stretched to the desired thickness by pulling down on the holding ring. (Note: The film may break at any point so avoid putting too much of _your_ weight on the ring.) Nylon netting, such as is used in women's hosiery, placed between the tube lip and the polypropylene sheet, prevented the polypropylene from sliding directly over the metal surface of the tube. The stretched sheets, which initially are quite elastic, were attached to aluminum rings using "double-sticky" tape and allowed to age for several days before being epoxied onto the metal window frames used during flight. Epoxied windows were dipped into a colloidal suspension of micron-sized carbon particles. By pulling the window out of the suspension at a fixed rate, a uniform carbon layer can be deposited. After drying, carbon was removed on the side of the window which was to be away from the counter gas.

Calibration of the polypropylene windows was carried out at four energies using $K_\alpha$ X-rays of carbon, fluorine, oxygen, and aluminum, which were fluorescently produced using Polonium-210 alpha particles (Table A.2). Transmission measurements were made at one inch intervals over the entire length of the window. Each measurement was of the transmission through a strip of polypropylene approximately 1" wide and over the entire 4.5" width of the window. For spectral determinations, a two-thickness model was fit to the average transmission at the four energies of the calibrations, e.g., the data was fit to the functional form

$$T(E) = A\, e^{-\mu(E)\rho_1} + (1 - A)\, e^{-\mu(E)\rho_2} \qquad (A.1)$$

where $\mu(E)$ were the mass absorption coefficients of polypropylene as given by Henke and Elgin (1970), $\rho$ are the surface densities, and A is the fraction of the window with surface density $\rho_1$. This model tends to fit the trans-data much better than a single thickness model due to the fact that the window is not really of uniform thickness,

Table A.2

WINDOW CALIBRATION RESULTS FOR POLYPROPYLENE WINDOWS USED IN AUSTRALIA

| | Counter | Window Transmission (%) | | | | | A | $\rho_1$ | $\rho_2$ | $\chi^{2+}_{min}$ |
|---|---|---|---|---|---|---|---|---|---|---|
| | | Carbon | Oxygen | Mg | Fe | Al | | ($\mu g\ cm^{-2}$) | ($\mu\ cm^{-2}$) | |
| Flight 1 | | | | | | | | | | |
| | 1 | 71.1±0.2 | 19.6±0.3 | 84.6±0.5 | 39.8±0.9 | 87.6±0.9 | 0.38 | 104 | 217 | 14.2 |
| | 2 | 70.5±0.2 | 20.4±0.3 | 85.2±0.5 | 40.8±0.4 | 88.1±0.9 | 0.32 | 82 | 224 | 9.9 |
| | 3 | 69.9±0.2 | 19.3±0.3 | 82.7±6.5 | 39.0±0.4 | 88.3±0.9 | 0.30 | 82 | 228 | 6.6 |
| Flight 2 | | | | | | | | | | |
| | 1 | 68.5±0.3 | 18.8±0.3 | 83.4±0.5 | 39.4±0.4 | 88.3±0.9 | 0.64 | 124 | 320 | 4.0 |
| | 2 | 70.6±0.3 | 19.2±1.6 | 84.0±0.6 | 41.0±0.5 | 89.4±1.0 | 0.80 | 140 | 332 | 0.3 |
| | 3 | 70.3±0.2 | 19.6±0.3 | 83.7±0.5 | 39.6±0.4 | 89.1±0.9 | 0.42 | 102 | 239 | 3.2 |

\+ There are only 2 degrees of freedom.

both due to the carbon deposition on the surface and due to intrinsic surface density variations in the stretched polypropylene.

Unlike the P-10 counters, an active gas-control system was required for the propane counters. In fact, two systems were used, primarily for purposes of redundancy, as indicated in Figure A.6. As had been the case on previous flights, gas pressure to propane counters 2 and 3 was maintained using a high quality Bellofram pneumatic regulator which maintained an ambient pressure differential of 150 torr. Manufacture specifications state that these regulators will maintain pressure to 1 part in $10^5$, from flow rates of 0 to 70 liters per minute. For counter 3, a transducer-solenoid system was installed. After turn-on, this system maintained pressure in the counter equal to that of a sealed reference volume. Unfortunately, this system was a fill-only system, e.g., did not reduce the pressure in the counter if it exceeded that of the reference volume. Because polypropylene windows are permeable to $O_2$ and $H_2O$, which will rapidly destroy counter resolution, in-flight purges of the propane counters was a requirement. This was accomplished in both gas control systems by opening a motorized valve, which allowed gas to escape through a calibrated leak. At the end of the flushing period, however, pressure in the counter 3 exceeded 150 torr by a small amount for reasons which are not fully understood. The end result, however, was that the solenoid system did not regulate gas pressure in counter 3 throughout the entire flight, resulting in the decreased gain discussed earlier. Due to the fact that the pneumatic regulators

Figure A.6

A schematic representation of the gas control system used in Australia on the Caltech payload. The transducer controls only the solenoid of counter 3, whereas the solenoids for counter 4 were externally activated and used for pre-flight filling of the P-10 counter.

# GAS CONTROL SYSTEM

LEGEND:

- CTR Counter
- GB Gas bottle
- F Air filter
- HP Conax high pressure regulator
- B Bellofram low pressure regulator
- T Transducer
- MV Motorized valve
- CS Circle Seal valve
- C Check valve
- PO Pop-off
- S Solenoid valve
- O Controlled orifice
- EF External flush line
- V Vent to atmosphere

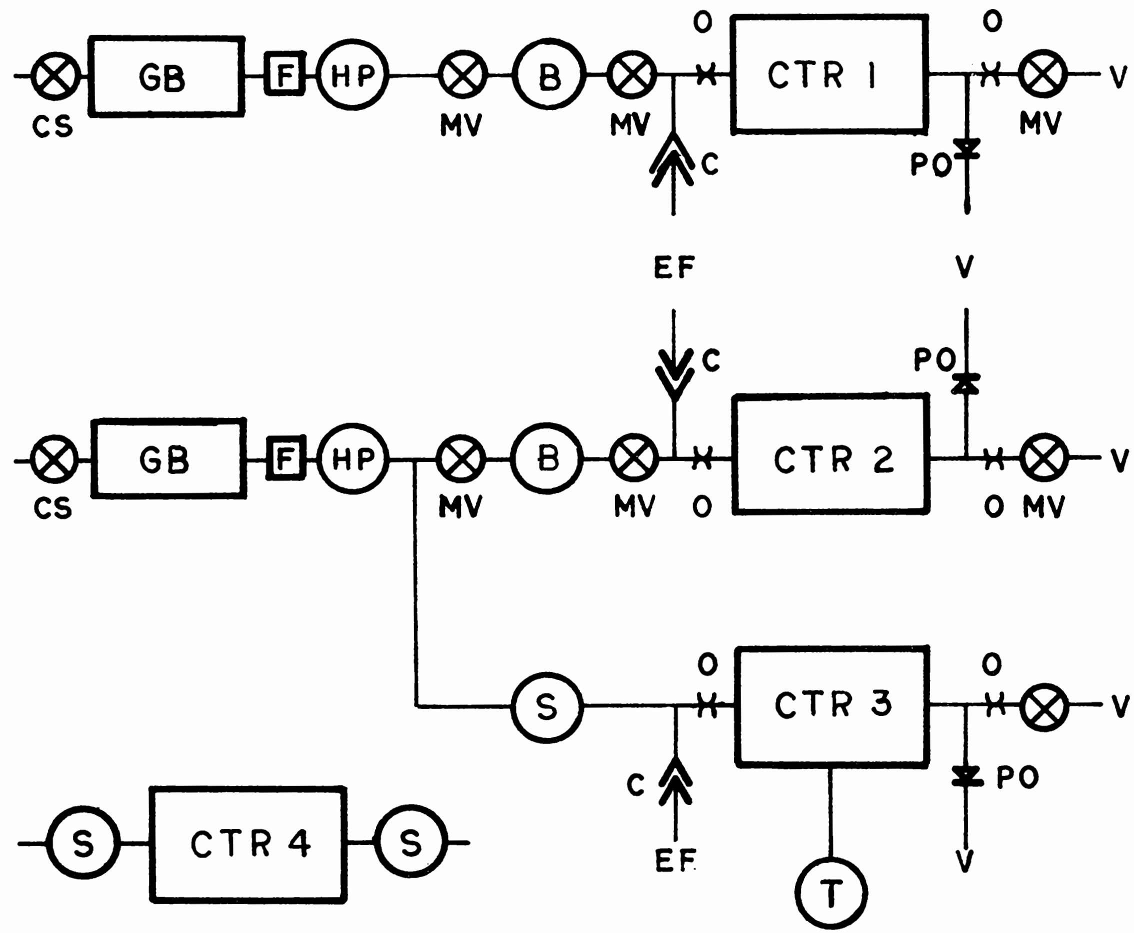

will "back bleed" if excess pressure develops, they are safeguarded against this problem. Note that simple pressure sensitive valves, "pop-offs", prevented a pressure greater than 200 torr from building up on the polypropylene windows during launch.

A block diagram, showing the on-board electronic processing used on the Australian flights, appears in Figure A.7. During the flight when an event occurred, it was energy analyzed and recorded as a good event (1) if no other event in the entire counter had occurred or did occur within 1 μs, and (2) if no previous good event in the given data channel had not yet been telemetered to the ground. The data channels were each read out 625 $s^{-1}$. The veto criterion introduced very little deadtime into the system. A typical deadtime correction of 10% was associated with the telemetry-rate criterion. (The deadtime correction follows from the number of times per second in which no good event was found in the data channel.) An electronic failure caused a loss of 1/2 of the data of counter 1 on flight 1 but did not compromise the veto system but does explain why the area of counter 1 was twice as large on flight 2 as on flight 1.

Data from the experiment was telemetered to three ground stations and recorded on magnetic tape. Telemetry dropouts at one or more ground stations occurred at various times during the flights; however, all data were recorded successfully on at least one ground station during the flights, except for one 15 second period on flight 2 of the transmitter carrying data from counters 2 and 3. Data from the

Figure A.7

A schematic representation of onboard data processing for 1 counter. There are four such circuits in the payload.

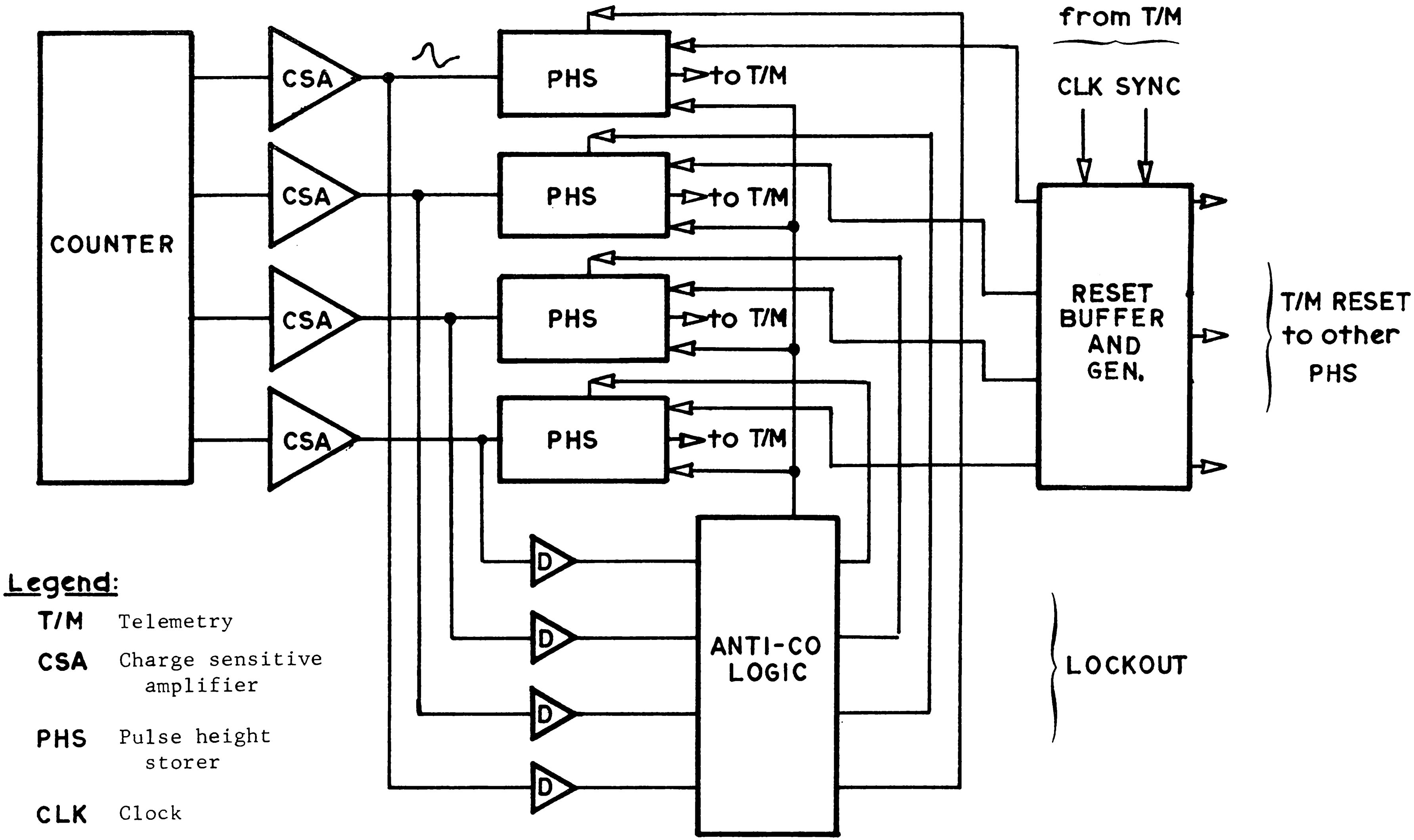
from T/M
CLK SYNC
COUNTER
CSA
CSA
CSA
CSA
PHS
PHS
PHS
PHS
to T/M
to T/M
to T/M
to T/M
RESET BUFFER AND GEN.
T/M RESET to other PHS
D
D
D
D
ANTI-CO LOGIC
LOCKOUT
Legend:
T/M Telemetry
CSA Charge sensitive amplifier
PHS Pulse height storer
CLK Clock

various ground stations were melded together using the maneuver voltages, which were also telemetered to the ground, as fiducials.